Drug Encapsulated Aerosolized Microspheres as a Biodegradable, Intelligent Glioma Therapy

Julee Alaina Floyd

A dissertation
submitted in partial fulfillment of the
requirements for the degree of

Doctor of Philosophy

University of Washington

2015

Reading Committee:

Buddy D. Ratner, Chair

Suzie H. Pun

Shaoyi Jiang

Program Authorized to Offer Degree:

Chemical Engineering

University of Washington

Abstract

Drug Encapsulated Aerosolized Microspheres as a Biodegradable, Intelligent Glioma Therapy

Julee Alaina Floyd

Chair of the Supervisory Committee:

Professor Buddy D. Ratner

Departments of Bioengineering and Chemical Engineering

The grim prognosis for patients diagnosed with malignant gliomas necessitates the development of new therapeutic strategies for localized and sustained drug delivery to combat tumor drug resistance and regrowth. Here we introduced the novel formulation of **dr**ug **e**ncapsulated **a**erosolized **m**icrospheres as a **b**iodegradable, **i**ntelligent **g**lioma therapy (DREAM BIG Therapy) that is applied post-resection. DREAM BIG Therapy consists of three types of microspheres [poly(lactic acid) (PLA), poly(lactic-co-glycolic acid) (PLGA), and poly(ε-caprolactone) (PCL)] containing various encapsulated chemotherapeutics, suspended in a degradable, aqueous poly(*N*-isopropylacrylamide) (PNIPAM) solution. The thermoresponsive PNIPAM solution is capable of suspending drug encapsulated microspheres at room temperature which can be "sprayed on" the post-surgical site. The physiological temperature of the treatment site (37°C) would cause PNIPAM solution to solidify and form an adherent gel layer with entrapped microspheres, providing intimate contact with remaining tumor cells. Over time, PLGA (rapid degradation), PLA (medium speed degradation), and then PCL (slow degradation) microspheres would break

down, releasing their drug payloads in a sequential, multi-drug release directly to the tumor site, addressing cancerous regrowth and tumor drug resistance. This dissertation will address the development of DREAM BIG Therapy, from microsphere formulation to pilot *in vivo* studies.

Initial work focused on developing blank and drug encapsulated microspheres using emulsion techniques. Preliminary studies utilized rhodamine B as a model drug for encapsulation in PLGA, PLA, and PCL particles and optimized formulation parameters to achieve a high encapsulation. Then, gefitinib, IgG, and lomustine were encapsulated in PLGA, PLA, and PCL microspheres, respectively, achieving encapsulation efficiencies greater than 80% and drug loadings greater than 0.3%. The *in vitro* release of gefitinib and IgG were also studied. Gefitinib released from PLGA microspheres over 40 days while the release of IgG from PLA microspheres was slower, over a year long period.

The microsphere-PNIPAM system was tested for aerosolized application *ex vivo*. The aqueous PNIPAM solution suspended the microspheres and was aerosolized before phase transitioning to an adherent gel layer on the tissue, entrapping the microspheres on the tissue surface. Finally, when tested *in vivo*, the gefitinib encapsulated PLGA microspheres entrapped in PNIPAM slowed the tumor volume growth of a subcutaneous C6 glioma in comparison to blank PLGA microspheres entrapped in PNIPAM. Overall, this research confirms the potential of DREAM BIG therapy for future use with multiple chemotherapeutics and microsphere types to combat gliomas at a localized site.

Acknowledgements

This work would not have been possible without the support and guidance of my advisor, Dr. Buddy Ratner. I am grateful to him for giving me the chance to work in his lab and on a project from the concept stage progressing to the point of *in vivo* studies. Whenever I went down a rabbit hole, Dr. Ratner was there with advice that would put me back on track. I would also like to thank my committee members, Dr. Shaoyi Jiang, Dr. Suzie Pun, and Dr. Pierre Mourad. Your guidance, expertise, and belief in my project's potential were vital throughout the PhD process. Thanks are given to my collaborators in the Department of Neurological Surgery, Dr. Rohan Ramakrishna and Dr. Robert Rostomily, who with Dr. Ratner, originally came up with the concept of the DREAM BIG Therapy. I would also like to acknowledge the National Science Foundation Graduate Research Fellowship No. DGE-0718124, UWEB21, and the Michael and Myrna Darland Endowment for their generous funding that made this work possible.

The Ratner lab group, both past and present, are thanked for providing insightful and helpful discussions throughout this project. Specific thanks are given to Dr. Anna Galperin, my fellow collaborator and polymer chemist who was always there to listen and give technical advice and troubleshooting tips. This project would not have progressed so far without your help! Thanks are also given to Colleen Irvin who provided vital assistance in all the *in vivo* work, listened to my rants, and provided several sanity-checking moments. The undergraduate researcher Douglas Chung is acknowledged for his rhodamine B encapsulation work and for teaching me what it means to be a mentor.

Outside of the lab, thanks are given to Susan Fredendall who listened to all my lab stories and practice talks and who had the guts to read this entire dissertation, to my old Clemson lab member, Joshua Barringer, who was there with ice cream to perk me up, and to Jason Murray, my master statistician who taught me more than I ever wanted to know about t tests. Special thanks are given to Dr. Michael Kilbey who first introduced me to research as an undergraduate at Clemson University and who kept tabs on me throughout my entire PhD career. Your advice for choosing a graduate school and project were spot on and I would not be here without your guidance and enthusiasm for science.

To my friends, thank you for making sure I had a life outside of research, for randomly cooking me dinners, and for making sure I had a memorable Seattle experience. Special thanks are given to Salle Auriol Seattle and Magnolia Ridge Training Center for giving me opportunities to de-stress, whether it was hitting someone with a metal stick or playing with horses. Finally, to my family, thank you yet again for supporting me as I pursued another scientific endeavor. I would not have survived without your continued encouragement and support throughout these studies.

Table of Contents

List of Abbreviations

5-FU	5-fluouracil
ATRP	Atomic transfer radical polymerization
BCNU	Bis-chloroethylnitrosourea
CED	Convection enhanced delivery
Cl-PCL-CL	Poly(caprolactone) based di-functional macroinitiator
CT	Computed tomography
CuCl	Copper chloride
DCM	Dichloromethane
DI	Deionized
DL	Drug loading
DMEM	Dulbecco's Modified Eagle Medium
DMF	Dimethylformamide
DMSO	Dimethyl sulfoxide
DREAM BIG	Drug encapsulated aerosolized microspheres as a biodegradable, intelligent glioma therapy
EE	Encapsulation efficiency
EGFR	Epidermal growth factor receptor
EHDA	Electrohydrodynamic atomization
EU	Endotoxin Unit
FBS	Fetal bovine serum
FDA	Food and drug administration
GB	Gefitinib
GB-PLGA	Gefitinib encapsulated PLGA microspheres
GB-PLGA-PNIPAM	Gefitinib encapsulated PLGA microspheres in PNIPAM
GBM	Glioblastoma multiforme
H&E	Hematoxylin and eosin
HCl	Hydrochloric acid
HPLC	High performance liquid chromatography
IACUC	Institutional animal care and use committee
IC_{50}	Half maximal inhibitory concentration
IgG	Immunoglobulin G
IgG-PLA	Immunoglobulin G encapsulated PLA microspheres
ISO	International Organization of Standardization
IUdR	5-iodo-2'-deoxyuridine
LCST	Lower critical solution temperature
LMT	Lomustine
LMT-PCL	Lomustine encapsulated PCL microspheres
M	Molar

Me_6TREN	Tris[2-(dimethylamino)ethyl]amine
$MgSO_4$	Magnesium sulfate
MRI	Magnetic resonance imaging
MTT	3-(4,5-dimethylthiazol-2-yl)-2,5-diphenytltetrazolium bromide
Mw	Molecular weight
$NaBH_4$	Sodium borohydride
$NaHCO_3$	Sodium bicarbonate
NaOH	Sodium hydroxide
NIPAM	*N*-isopropyl acrylamide
NMR	Nuclear magnetic resonance
O	Oil phase of an emulsion
O/W	Oil in water
PBS	Phosphate buffered saline
PCL	Poly(ε-caprolactone)
PCL diol	Poly(ε-caprolactone) diol
PF-4/CTF	C-terminal fragment of platelet factor 4
PLA	Poly(lactic acid)
PLGA	Poly(lactic-go-glycolic acid)
PMM 2.1.2	Poly(methylidene malonate 2.1.2)
PNIPAM	Poly(*N*-isopropylacrylamide)
PVA	Poly(vinyl alcohol)
Q%	Frequency distribution of the particle size
RAFT	Reversible addition fragmentation transfer
RB	Rhodamine B
RT	Room temperature
SEM	Scanning electron microscopy
Std Dev	Standard deviation
TEA	Triethylamine
TGP	Thermo-reversible gelation polymer
THF	Tetrahydrofuran
TREN	Tris(2-aminoethyl)amine
UV-vis	Ultraviolet-visible
v/v	Volume by volume
W1	Inner water phase of an emulsion
W2	Outer water phase of an emulsion
W/O/W, W1/O/W2	Water in oil in water
w/v	Weight by volume
w/w	Weight by weight

List of Figures

List of Tables

List of Equations

1 Introduction

1.1 Glioma Survival and Diagnosis

Malignant tumors that originate in the brain and spinal cord will be diagnosed in over 20,000 men and women in the United States in 2015 [1, 2]. Over half of these will prove fatal to the patient. The fastest growing and most common malignant tumors originate in the glial or support cells of the brain. These include astrocytomas, oligodendrogliomas, ependymomas, and the most common and aggressive type, glioblastoma multiforme (GBM) [2, 3]. After diagnosis of a GBM, a 12-15 month survival period is expected despite maximal therapy [4, 5]. The median survival is age dependent, with a five year survival rate of 17%, 6%, and 4% for 20-44, 45-54, and 55-64 year olds, respectively [2]. Even benign or non-cancerous tumors are cause for concern. If left untreated, they can continuously grow, destroying normal brain tissue until it becomes a life-threatening illness. While risk factors include family history, radiation exposure, and immune disorders, there are no known causes for brain cancer and thus cannot be prevented.

Currently, there are no widely practiced methods to screen for brain tumors. Common indicative symptoms include blurred visions, balance problems, headache, nausea, seizures, vomiting, numbness in parts of the body, and changes in speech, hearing, personality, or moods [2, 6]. After performing neurological exams to test the central nervous systems, doctors can order several different tests to image the brain, looking for abnormal tissue. The most commonly used are magnetic resonance imaging (MRI) and computed tomography (CT) [2, 6]. MRIs utilize radio waves and strong magnetic fields to image and differentiate between soft tissues of brain, providing detailed images of the location and growth of abnormal tissue. However, they do not look at bones or in this case, the skull, and require lengthy scans while the patient is confined in

a narrow tube. CTs, on the other hand, use x-rays to map out the soft tissue and bones of a patient. While the image is not as detailed as an MRI, they take less time and patients are less confined. Unfortunately, these imaging tests only tell that there may be a tumor present, but not what type of tumor (benign or malignant). Therefore, a biopsy procedure entailing the physical removal of a piece of the tumor tissue is performed and the sample tested to diagnose tumor type. Other possible tests include a positron emission tomography scan as an imaging aide and lumbar punctures to test for tumor cells in the cerebrospinal fluid.

1.2 Surgical Excision, Radiation Therapy, and Chemotherapy

After diagnosis of a brain tumor, treatment options include a combination of tumor resection, radiation therapy, and both systemic and localized chemotherapy. If the tumor location is operable, the first step is usually tumor resection. The surgeon removes as much of the tumor as possible without causing a loss of brain function to the patient. While some types of brain tumors like ependymomas and gangliogliomas are operable and may be cured from surgery alone, astrocytomas, oligodendrogliomas, and GBMs are infiltrative and cannot be fully removed without causing brain damage [2]. If left unchecked, the tumor remnants eventually grow back. In general, tumor reoccurrence is within 2 cm of the primary tumor site due to this issue [7]. Side effects of tumor resections include loss of brain function, general weakness and headaches, and the possibility of infection and brain swelling [2, 6]. Yet, these risks are considered minor when compared to the benefit of a reduced tumor mass.

Radiation therapy is another common treatment applied after tumor resection or as the main treatment if the tumor is inoperable. High-energy rays are concentrated on the tumor location to

kill tumor cells over several sessions [2, 6]. While radiation therapy targets the tumor cells, it can also be harmful to normal cells. Side effects include brain function loss, irritability, fatigue, nausea, and vomiting. In addition, there is a risk that the radiation can cause a second tumor due to damage of normal cell genes. Like tumor resection, these risks are balanced by the possibility of killing tumor cells and needing less chemotherapy.

Chemotherapy is the third common treatment for tumors and requires the application of drugs to kill cancer cells. This can be done systemically, either orally or intravenously, or locally at the tumor site. The treatments can be done alone or in combination with tumor resection and radiation therapy [2, 6, 8]. While there are many types of anti-cancer drugs, there are only a few that are able to reach the brain when applied systemically due to the blood brain barrier. This barrier consists of small blood vessels with tight junctions that surrounds and protect the brain, maintaining metabolic balance. However, the characteristic tight junctions and selectivity of this barrier makes it difficult for most drugs to penetrate from the blood stream to the brain. Therefore, drug options are limited. A few of the currently used drugs include cisplatin, temozolomide, vincristine, procarbazine, etoposide, carmustine, and carboplatin [2]. Common side effects of chemotherapeutics applied intravenously include loss of appetite, headaches, nausea, vomiting, fevers, weakness, infections, bruising, weakness, tiredness, hair loss, and mouth sores [2, 6]. These side effects are due to the drugs indiscriminately targeting all rapidly dividing cells which not only include tumor cells but also bone marrow, hair follicles, and the lining of the mouth and intestines. When applied systemically, these drugs get the chance to impact all of these cell types, lowering the overall quality of life for the patient. In addition, these

drugs are given in cycles that last for a few weeks, necessitating the patient to come into the clinic several times to receive treatment.

The only FDA approved intracerebral or localized therapy is the application of Gliadel® wafers to the site of tumor resection. Over a period of approximately two to four weeks, these wafers degrade and release the anti-cancer drug, carmustine, in a controlled delivery to tumor remnants. These wafers limit the severe side effects typical of systemic delivery by releasing their drug at a localized site, which by-passes the blood brain barrier and reduces the total amount of drug needed to reach therapeutic levels. The wafers are composed of a degradable, polymeric matrix of 1,3-bis(p-carboxyphenoxy)propane and sebacic acid in a 20 to 80 molar ratio loaded with 7.7 mg carmustine [9]. Combined with tumor resection and radiation therapy, the GLIADEL® wafers increased patient survival by approximately two months and are a current standard of care for brain tumor patients [10]. Drawbacks may include the risk of infection, seizures, and brain edemas [11].

1.3 Limitations of Current Therapies

Even when surgical excision, radiation therapy, and chemotherapy are applied in combination and maximal treatment is given, the survival still remains poor at 12-15 months [4, 5]. The bleak survival rate is attributed to such factors as tumor drug resistance, intracellular drug metabolism, and limited drug uptake, in part due to the major obstacle of the blood brain barrier, and tumor regrowth [12-15]. For example, consider the current gold standard of care for GBMs, which includes the application of Gliadel® wafers after tumor excision. When implanted, these dime sized wafers provide a controlled release to remaining tumor cells that could not be surgically

removed without causing loss of brain function. However, the wafers are not necessarily impacting all the tumor cells. Due to the convoluted morphology of the brain and the tumor resection cavity, these rigid, planar wafers are in poor surface contact with the brain tissue. As shown in Figure 1.1, there are obvious areas where the wafers are not in contact with the tissue, allowing tumor remnants to remain untreated.

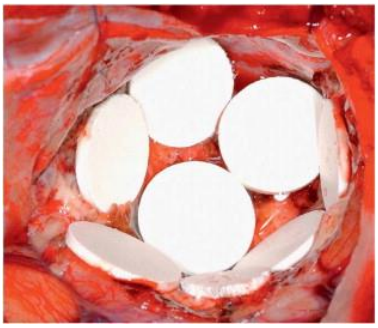

Figure 1.1: Gliadel® wafers applied to a brain tumor resection cavity, showing sub-optimal contact of the tissue and wafers [16]. Reprinted from Journal of Controlled Release, 159/1, Wolinsky et al., Local drug delivery strategies for cancer treatment: Gels, nanoparticles, polymeric films, rods, and wafers, 14-26, 2012, with permission from Elsevier.

Radiation therapy is also applied in combination with these wafers. However while radiation therapy can cure some brain cancers such as medulloblastomas and germinomas, it will only provide a limited control for astrocytomas, oligodendrogliomas, and ependymomas [17]. In addition, there is the issue of drug resistance. Tumors can either develop a resistance to chemotherapeutics or can be resistant to a range of anti-cancer drugs before chemotherapy is even applied [15]. The drug encapsulated in the wafer, carmustine, has a potential resistance mechanism through changes in O6-methylguanine-DNA methyltransferase, reduced glutathione/glutathione-S-transferase, and protein kinase. Therefore, while the wafers may be effective initially, they may not be effective long term. Even temozolomide, a very common and popular chemotherapeutic applied systemically has a potential resistance mechanism through

changes in O6-methylguanine-DNA methyltransferase [15]. Greater drug sensitivity is achieved when the promoter regions of the gene encoding the enzyme is methylated [18]. Therefore, a multi-drug therapy is needed to overcome tumor drug resistance. However, the blood brain barrier severely limits which drugs can be utilized. This presents the need for a sustained, localized, multi-drug delivery system to overcome the blood brain barrier and the shortcomings of the current therapies.

1.4 Intracerebral Drug Delivery Strategies for Glioma Treatment

To target the tumor remnants left after tumor resection and to bypass the blood brain barrier, the scientific community has developed many different approaches for a localized drug delivery system applied intracerebrally. These include manual injections, convection-enhanced delivery, implantable reservoirs, and biodegradable drug carriers [5, 18-21]. While the manual injection of chemotherapeutics to the cavity site is a simplistic approach, high risks of infections, edema, and backflow limits it use today, especially with less invasive and more effective technique available [5, 21].

Implantable reservoirs, such as the Ommaya reservoir, have also been used for malignant gliomas. The Ommaya reservoir is a subcutaneous reservoir connected to a catheter that is connected to the tumor bed through the skull [5, 21]. By manually compressing the reservoir, chemotherapeutics are delivered through the catheter to the tumor bed. The risk of infection and the inconvenience of having to refill the reservoir limits the wide scale clinical application of this drug delivery device [21].

Biodegradable drug carriers such as the Gliadel® wafers have garnered much interest from the scientific community due to their lack of systemic side effects, localized controlled drug release, minimal complexity, and full biodegradation [19-21]. These carriers also include gels, microcarriers, and nanocarriers [21]. However, biodegradable drug carriers have the distinct drawback of a small penetration depth into the tissue from the site of injection, which coupled with a high rate of elimination from the body, limits the therapeutic effectiveness of this treatment [19, 21]. In addition, the biodegradable carrier size limits the amount of drug that can be delivered.

To overcome limited diffusion and drug dosage, research has looked at convection enhanced delivery (CED) [5, 19, 21, 22]. Using a pumping device connected to a stereotactically implanted catheter, a drug solution is pressure driven into the cavity. This results in a larger volume of drugs that can be "pumped" onto the brain that then spreads further, when compared to a traditional diffusion drug delivery device such as the biodegradable carriers. However, a degree of backflow is common in CED due to the pressure necessary to pump the fluid, up to 70 mmHg [19]. This backflow could cause the drug to spread too much and lead to chemical meningitis and neurotoxicity [5, 19, 22]. Other drawbacks include invasiveness, long infusion times, and high intracranial pressure. Even so, CED is considered a potential therapy for GBM since it can forcibly deliver drugs at high concentrations to the tumor and can easily be altered by the doctor as needed [19].

Both biodegradable carriers and CED are promising methods of delivery, each with their own drawbacks and advantages. As such, further research is still being conducted to overcome the

shortcomings discussed here and provide a therapy that can treat malignant gliomas and ultimately, provide a long-term cure.

1.5 Drug Encapsulated Aerosolized Microspheres as a Biodegradable, Intelligent Glioma Therapy

Even with the limited drug penetration depth, the biodegradable drug carriers such as the Gliadel® wafers are promising avenues for intracranial delivery because of their controlled drug release, minimization of systemic side effects by delivering to a localized site, bypassing the blood brain barrier, and the potential for increased patient compliance by using a single treatment that releases drug over several weeks to months. However, these wafers are only a two to four week therapy. Therefore, biodegradable, drug encapsulated polymeric microspheres with a longer, sustained release profile have received a lot of attention as an alternative type of drug delivery vehicle [23-65].

Polymeric microspheres are well known for controlled drug delivery and review articles are available [66-71]. Their implantation and degradation in the brain has been studied and confirmed as biocompatible with experiments ranging from small animal experiments to Phase II human trials [33, 34, 72-74]. As such, we will be utilizing microspheres as the vehicles for our drug delivery to gliomas. However, instead of the commonly used single polymer type microsphere, we will be utilizing three different, FDA recognized, biodegradable polymers: poly(lactic-co-glycolic acid) (PLGA), poly(lactic acid) (PLA), and poly(ε-caprolactone) (PCL) [75]. Each of these polymers has their own, unique degradation rate, resulting with a multi-staged, sequential drug release when applied in combination (Figure 1.2). PLGA, the fastest

degrading polymer, would release its encapsulated chemotherapeutic first. Then a second chemotherapeutic would be released from PLA and then a third chemotherapeutic from PCL. In this manner, the tumor can be hit by multiple chemotherapeutics to overcome tumor drug resistance and the sequential releases will result in a long term therapy with only a single application by the care provider to the patient.

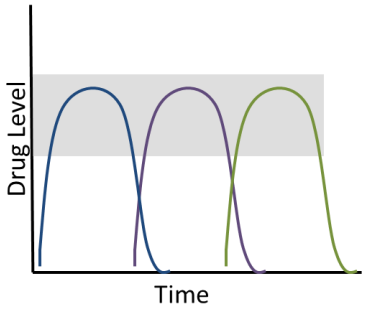

Figure 1.2: The release of chemotherapeutics from multiple microspheres: PLGA microspheres (blue) will release its pay load first, and then PLA (purple), and then PCL (green). The gray box indicates the therapeutic window, when the chemotherapeutics are effective in the body.

To address the poor surface contact of the Gliadel ® wafers with the tumor cells, we will use a poly(*N*-isopropylacrylamide) (PNIPAM) solution as a degradable, aerosolizable, thermoresponsive polymer carrier for the drug encapsulated microspheres. PNIPAM is an extensively studied polymer due to its sharp, reversible liquid-gel phase transition, demonstrating a lower critical solution temperature (LCST) of about 32 °C in deionized water [76]. Below the LCST, PNIPAM is a liquid, but above the LCST, PNIPAM phase transitions to a gel. As such, if drug encapsulated microspheres were suspended in the PNIPAM at room temperature, it would form a suspension. However, when applied as a spray to the tumor cavity at physiological conditions (37°C), the PNIPAM would phase transition and collapse, entrapping the microspheres at a localized site, conforming to the convoluted morphology of the brain and providing intimate contact with the remaining tumor cells. After the microspheres degrade and

release their payload, the PNIPAM would degrade, and hopefully, only cancer free tissue would remain.

Overall, the novelty of **dr**ug **e**ncapsulated **a**erosolized **mi**crospheres as a **b**iodegradable, **i**ntelligent **g**lioma therapy (DREAM BIG Therapy) is based on first, a multi-drug delivery system using polymeric microspheres for a sequential therapy that can combat tumor drug resistance; second, the PNIPAM transitions from an aerosolizable liquid to a conformal, adherent solid on contact with the brain, providing an easy application to a complex, irregular surgical site; and third, the entire system is fully biodegradable and only requires one application by the care giver to the patient.

1.6 Overview

The purpose of the studies presented here is to develop a topical, slow release, degradable, multi-drug delivery system applied post-surgically with the potential to significantly increase patient life expectancy. This system consists of drug encapsulated PLGA, PLA, and PCL microspheres suspended in a degradable, aerosolizable PNIPAM solution. At room temperature, the aqueous PNIPAM solution suspends the drug encapsulated microspheres that can be "sprayed on" the post-surgical site. The physiological temperature of the brain causes the thermoresponsive PNIPAM to solidify and form an adherent gel layer with entrapped microspheres, providing intimate contact with remaining tumor cells. Over time, PNIPAM degrades along with PLGA, PLA, and then PCL microspheres, releasing multiple chemotherapeutics at different rates directly to the tumor remnants to inhibit cancerous re-growth. Chapter 2 focuses on the formulation and characterization of the drug encapsulated polymeric microspheres in addition to

the synthesis of the degradable PNIPAM. Chapter 3 addresses the *in vitro* drug release from the formulated microspheres and the aerosolized delivery of PNIPAM to tissue at physiological temperature *ex vivo*. Chapter 4 focuses on a subcutaneous tumor model that was used to test the drug encapsulated PLGA microspheres entrapped in PNIPAM *in vivo*.

2 Formulation and Characterization of Blank and Drug Encapsulated Polymeric Microspheres and Synthesis of Degradable PNIPAM

2.1 Background

2.1.1 Motivation

There are numerous methods for formulating drug encapsulated polymeric microspheres and for synthesizing PNIPAM. In this chapter, the methods chosen to formulate drug encapsulated microspheres and to synthesize linear, degradable PNIPAM will be described and the results discussed. In subsequent chapters, the products of these methods will be used for *in vitro* and *in vivo* experiments.

2.1.2 Microsphere Formulation and Characterization

Polymeric microspheres for controlled drug delivery are well known and documented [66-68, 70, 77]. Their applications have ranged from the treatment of prostate cancer symptoms (Lupron Depot®) to the treatment of alcoholism (Vivitrol®) and acromegaly (Somatuline Depot®) [70]. In most cases, these drug encapsulated microspheres are injectable, achieving a slow, sustained release as the microsphere degrades. Unlike intravenous delivery where the drug is injected as a bolus dosage and can be rapidly cleared by the body, the sustained release profile of microspheres provides therapeutic levels long term, necessitating fewer treatments.

With the various applications of injectable microspheres achieving approval from the FDA for drug delivery, it is not surprising that polymeric microspheres are used as a potential vehicle for a localized, controlled release of chemotherapeutics for glioma therapy [23-65]. This type of

therapy has the advantage of being applied after tumor resection, overcoming the blood brain barrier and enabling the delivery of drugs that have not successfully penetrated the blood brain barrier. In addition, this type of therapy should have limited side effects when compared to systemic delivery as the chemotherapeutics are localized to the tumor site and not circulating throughout the entire body.

Some chemotherapeutics that have been successfully encapsulated in polymeric microspheres include 5-fluoruracil (5-FU), bis-chloroethylnitrosourea (BCNU), camptothecin, carboplatin, doxorubicin, imatinib mesylate, 5-iodo-2'-deoxyuridine (IUdR), mitoxantrone, paclitaxel, temozolomide, C-terminal fragment of platelet factor 4, hemopexin, and antisense oligonucleotides. The most common technique for formulating these drug encapsulated microspheres is emulsion methodology [27-32, 37, 43-49, 78], while other options include coacervation [38-40, 50] and spraying techniques [24, 51-54]. Since emulsion methodologies are widely used for microspheres targeted for glioma therapy and are relatively simple to design and carry out, they were used to create the drug encapsulated microspheres presented in this work. The spraying techniques were not tested due to the necessary specialized equipment e.g. spray dryers. Coacervation was as an alternative if the emulsion technique proved unsuccessful.

The emulsion methodology can either involve a single or a double emulsion depending on the drug to be encapsulated. For hydrophobic chemotherapeutics, the single emulsion or oil in water (O/W) emulsion is commonly used [27-30]. As shown in Figure 2.1, the polymer to form the microsphere, PLGA or PLA for example, is dissolved in an organic solvent, usually methylene chloride, along with the drug to be encapsulated. This "oil" solution is added to an aqueous

solution containing a stabilizer, e.g. poly(vinyl alcohol) (PVA), and homogenized, creating an O/W emulsion. The organic solvent is then removed by evaporation before the polymeric microspheres are dried and recovered. A variation of the single emulsion can use an acetone/mineral oil emulsion instead of the organic and water system [31].

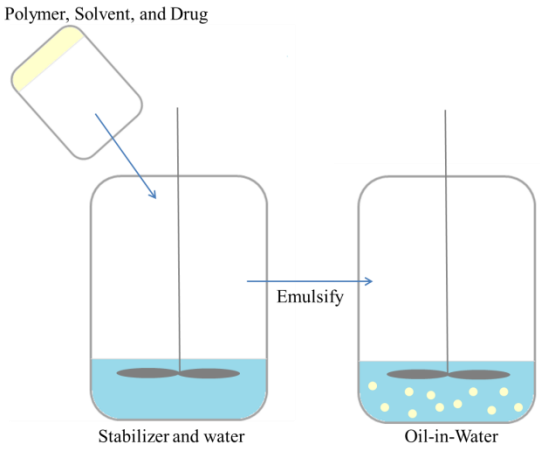

Figure 2.1: Schematic of the oil in water solvent evaporation technique for microsphere formation.

For water soluble chemotherapeutics, the double emulsion or water in oil in water (W/O/W) emulsion is utilized [43, 46, 49, 78]. As shown in Figure 2.2, an extra phase is utilized when compared to the single emulsion. Instead of dissolving the drug in the oil phase, the drug is dissolved in water that is then added to the oil phase and homogenized, creating the first O/W emulsion. This primary emulsion is then added to the aqueous solution containing a stabilizer and homogenized, creating a W/O/W emulsion. The organic layer acts as a barrier, preventing the hydrophilic drug from diffusing from the internal, aqueous phase to the external, aqueous phase [37]. Then, the organic solvent is evaporated and the microspheres recovered.

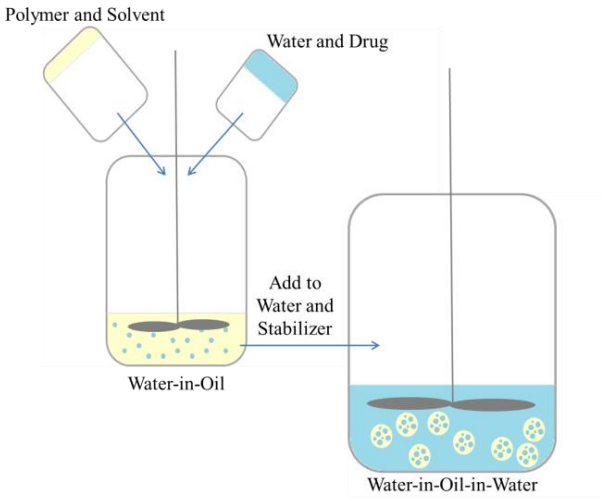

Figure 2.2: Schematic of the water in oil in water (W/O/W) solvent evaporation technique for microsphere formation.

One of the chief methods for characterizing drug encapsulated microspheres is by scanning electron microscopy (SEM) [28, 30]. As shown in Figure 2.3a, SEM visualizes shape, surface morphology, and size distribution of the drug loaded microspheres. Typically, samples are mounted on a metal stub and coated with a conductor, either platinum or gold [28, 30, 31, 47]. SEM can also be used to study cross sections of microspheres, showing the inner structure of the microsphere along with the possibility of drug crystals [31]. The cross sections of microspheres have also been characterized with confocal microscopy. As shown in Figure 2.3b, this technique provides a visual method for determining drug distribution within the microsphere, showing piroxicam located in the PLGA microsphere interior [79]. Aside from SEM, particle size can also be measured by laser diffraction [30, 36, 37, 78], sieving and weighing the fractions [31], and a coulter counter [41, 43-46].

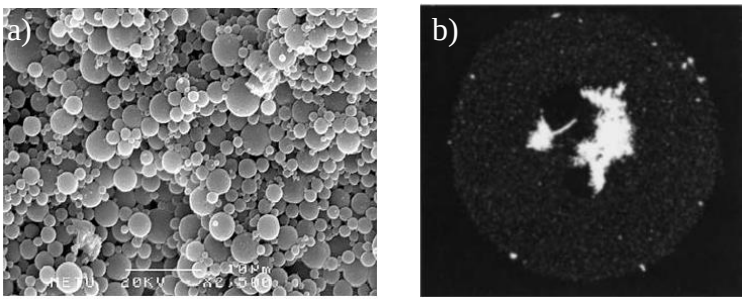

Figure 2.3: Physical characterization of microspheres: a) SEM micrograph of mitoxantrone encapsulated PLGA microspheres, b) confocal micrograph of a midline cross section of piroxicam loaded PLGA microspheres [78, 79] Reprinted from Neurosurgery, 59/6, Yemisci et al., Treatment of malignant gliomas with mitoxantrone-loaded poly (lactide-co-glycolide) microspheres, 1296-1302, 2006, with permission from Wolters Kluwer and reprinted from Pharmaceutical Research, 20/7, Berkland et al., PLG Microsphere Size Controls Drug Release Rate Through Several Competing Factors, 1055-1062, 2003, with kind permission from Springer Science and Business Media.

The emulsion methodologies allow for a tunable particle size distribution by altering the speed of homogenization. For example, Zhang et al. demonstrated that manipulating the emulsion speed from 400 to 800 rpm caused a 24% decrease in microparticle size, from 71.7 to 54.3 µm, respectively, for temozolomide encapsulated PLGA microspheres [28]. This decrease in particle size was due to the greater shear rates at the higher speeds. Reza et al. also showed the same trend for IUdR loaded PLGA microspheres, where an increase in stirring rate from 300 to 1,000 rpm decreased the mean particle size from 89.8 to 38.2 µm, respectively [37].

Drug loading, a measurement of how much drug is present compared to the polymer carrier, and encapsulation efficiency, a measurement of how much drug is encapsulated, can also be tuned using the emulsion techniques. For example, Chen et al. used the single emulsion technique to create carboplatin encapsulated PLGA microspheres [31]. They demonstrated that an increase in polymer concentration from 6 to 8% (w/v) increased drug loading from 9.6 ± 0.2% to 10.5 ±

0.2%. This increase in drug loading can be due to the more viscous polymer concentration that hinders the diffusion of carboplatin to the external aqueous phase. However, a critical point was reached where a further increase in concentration did not yield a higher drug loading. The solution became viscous enough to encapsulate the maximum amount of drug and a further increase in polymer concentration would cause a decrease in drug loading.

Similarly, Gil-Alegre et al. showed that there is a limit to the drug/polymer ratio for increasing the drug loading of BCNU loaded PLGA microspheres [30]. When the ratio was increased from 0.2 to 0.4, the drug loading doubled and the encapsulation efficiency remained the same. However, for an increase to a 0.8 ratio, the drug loading did not change; instead, a decrease in encapsulation efficiency resulted. This indicates that there is a solubility limit that must be considered when encapsulating drugs with the emulsion techniques.

Another way to increase encapsulation efficiency and drug loading is to saturate the external, aqueous phase with the drug of interest, lowering the concentration gradient between the phases. For example, saturating the PVA aqueous phase for temozolomide encapsulated PLGA microspheres more than doubled the encapsulation efficiency from 30% to as high as 85% [28]. Typically, optimized drug loadings for the emulsion system can range from 0.1% to 20% based on the drug and formulation parameters [25, 26, 30, 43-45]. Encapsulation efficiencies can range from 15-100% [23, 27, 41, 46, 51, 52].

Overall, the emulsion system provides a relatively simple methodology for formulating drug encapsulated polymeric microspheres. By changing parameters such as emulsion speed, polymer

concentration, drug concentration, etc., we can formulate microspheres with tunable properties such as particle size, encapsulation efficiency, and drug loading.

2.1.3 Chemotherapeutic Choice

With the wide range of chemotherapeutics that are available to encapsulate by using the emulsion techniques, it was left to our collaborator, Dr. Rohan Ramakrishna (University of Washington Department of Neurological Surgery), to determine which chemotherapeutics should be utilized. Three chemotherapeutics were identified: gefitinib, bevacizumab, and lomustine.

Gefitinib (Iressa®) is an epidermal growth factor receptor tyrosine kinase inhibitor that prevents uncontrolled cell proliferation. This drug is approved for use on non-small cell lung cancers and is studied for other types of cancer [80]. Bevacizumab (Avastin®) is an antibody that prevents angiogenesis by blocking the vascular endothelial growth factor A. It is approved for treatment of colorectal, non-small cell lung, kidney cancer, and GBM [81]. Lomustine (CeeNU ®) is an alkylating nitrosourea compound, which prevents cell replication, triggering cell death. It is approved for the treatment of brain cancer due to its ability to readily penetrate the blood brain barrier, Hodgkin's disease, lung cancer, melanomas, and various solid tumors [82-84].

Gefitinib has been delivered orally for metastatic brain tumors with positive results [85-87]. Bevacizumab is applied intravenously for glioblastoma multiforme and is shown to help slow the re-growth of certain brain tumors such as GBM; however, its effect on survival is still unclear [2]. Lomustine is an FDA approved, oral drug for the treatment of brain tumor in patients who have already had surgery or radiation therapy [88].

To date, gefitinib has been encapsulated in PCL microcapsules for use in subcutaneous drug delivery, achieving capsules approximately 200 to 240 μm in size and a seven day release *in vitro* [89]. Gefitinib has also been encapsulated in PLGA nanoparticles for the treatment of lung and skin carcinoma [90]. Bevacizumab has been encapsulated in PLGA nanoparticles, liposomes, and poly(ethylene glycol)-*b*-poly(D,L-lactic acid) microspheres for the treatment of age-related macular degeneration [91-93]. However, neither gefitinib nor bevacizumab have been encapsulated in polymeric microspheres for intracranial tumor therapy.

Lomustine has already been encapsulated in liposomes for the intravenous treatment of gliomas, in chitosan nanoparticles for the treatment of human lung cancer, in PLA microspheres for leukemia treatment, and in PLA microspheres acting as an embolic agent, causing obstruction in arteries leading to the tumor and allowing for lomustine release [82, 83, 94, 95]. However, reports of lomustine encapsulated in PCL microspheres or a long term release of lomustine greater than three days were not found in the literature.

2.1.4 Degradable PNIPAM

PNIPAM, a biostable polymer, has been synthesized by numerous polymerizations techniques ranging from atom transfer radial polymerization (ATRP) to surface-initiated, photoiniferter-mediated photopolymerization to reversible addition fragmentation transfer (RAFT) [76, 96, 97]. However, for the synthesis of a biodegradable PNIPAM, there are only limited reports [98, 99]. In one study, a degradable PNIPAM hydrogel was synthesized using UV polymerization of the monomer NIPAM with a benzo-2-methylene-1,3-dioxepen in the presence

of poly(ethylene glycol-co-glycolic acid) diacrylate. This created a hydrogel with degradable ester bonds in both the backbone of the PNIPAM and crosslinking sites [98, 99].

Previously, our lab has reported the synthesis of a degradable, linear PNIPAM via ATRP [99]. ATRP was utilized to create a polymer with a controlled, tunable molecular weight of the parent polymer and its degradation products. To create a degradable PNIPAM, a bi-functional, degradable initiator containing PCL was incorporated in the polymer. The use of the bi-functional initiator allowed the polymer chains to grow on both sides of the initiator at the same rate. Therefore, when the polymer cleaves at the PCL linker, the polymer molecular weight should be roughly halved. This was shown for a 2.29 x 10^4 g/mol PNIPAM that had degradation products of 1.38 x 10^4 g/mol [99]. This linear PNIPAM also demonstrated an LCST of 30.8 °C, ideal for our application of a room temperature microspheres suspension to an adherent layer at physiological temperature and will be used in the work presented here.

2.2 Hypothesis

It is hypothesized that:

(1) Polymeric microspheres with a smooth morphology and a tunable particle size distribution can be achieved using the emulsion techniques

(2) Gefitinib, bevacizumab (or a model of bevacizumab), and lomustine can be encapsulated in PLGA, PLA, and PCL, microspheres, respectively

    a. An encapsulation efficiency greater than 60% and a drug loading greater than 0.1% can be achieved for all three polymeric microspheres

(3) Degradable PNIPAM can by synthesized using ATRP that demonstrates a thermoresponsive phase transition

2.3 Materials and Methods

2.3.1 Materials

2.3.1.1 Materials for Microsphere Formulation

Dichloromethane (DCM; EMD, HPLC grade), tetrahydrofuran (THF; EMD), hydrochloric acid (HCl; EMD, 12.1 M), sodium hydroxide (NaOH; Mallinckrodt Chemicals), poly(lactic acid) (PLA; gift to Ratner Lab, Mw unknown and Evonik Industries, Mw 58,000), poly(ε-caprolactone) (PCL; Aldrich, Mn 70,000-90,000), poly(lactic-co-glycolic acid) 50:50 (PLGA; Evonik Industries, Mw 60,000), poly(vinyl alcohol) (PVA; Sigma Aldrich, 98% hydrolyzed, Mw 13,000-23,000), rhodamine B (RB; Sigma), fluorescein (Fluka), gefitinib (GB; Fisher, free base >99%), immunoglobulin G from sheep serum (IgG; Sigma, ≥95%, lyophilized powder), and lomustine (LMT; Enzo Life Sciences) were used as received.

2.3.1.2 Materials for PNIPAM Synthesis

Acetonitrile (EMD), chloroform (Sigma), diethyl ether (Sigma), dimethylformamide (DMF; Sigma, anhydrous), dichloromethane (DCM; EMD, HPLC grade), formaldehyde solution (Fisher), tetrahydrofuran (THF; EMD, anhydrous), acetic acid (Fisher, glacial), hydrochloric acid (HCl; EMD, 12.1 M), sodium hydroxide (NaOH, EMD), *N*-isopropyl acrylamide (NIPAM; Sigma), poly(caprolactone diol) (PCL diol; Sigma, Mn ~530), triethylamine (TEA; Sigma, 99.5%), copper chloride (CuCl; Sigma, ≥99%), sodium bicarbonate ($NaHCO_3$; Fisher), magnesium sulfate ($MgSO_4$; J.T. Baker, anhydrous), 2-chloropropionyl chloride (Sigma), tris(2-

aminoethyl) amine (TREN, Sigma, 96%), sodium borohydride (Sigma), and aluminum oxide (Fluka) were used as received.

2.3.2 Microsphere Formulation

PLGA, PLA, and PCL microspheres were produced by either a double or single emulsion, solvent evaporation technique. Unless otherwise stated, the following steps were used to produce microspheres by the double emulsion method. A total of 1.75 g of PLGA, PLA, or PCL was dissolved in 35 mL of DCM (organic phase, O) and 0.5 g of PVA was dissolved in 50 mL of deionized water (external water phase, W2). After dissolution, the organic phase was iced for 30 minutes to prevent solvent evaporation during emulsification. Then, 1500 µL of deionized water, with or without the drug (inner water phase, W1), was added to the organic phase and homogenized at 6000 rpm for two minutes using an Arrow 6000 electric stirrer and a five blade, circular impeller. Seven mL of this oil in water solution was added to the PVA solution and homogenized for one minute at a given speed (Table 2.1 and Table 2.2) creating a W1/O/W2 emulsion. This W1/O/W2 evaporated overnight before being stirred for 2 hours for further DCM evaporation. The solution was then centrifuged (3000 g, 4 °C) for 15 minutes with three wash cycles of deionized water before being filtered through two filters (Whatman Filter No. 4) to remove spheres less than 10 µm in diameter. The remaining spheres were dried under vacuum and stored in vials out of direct light. A schematic representation of this process is shown in Figure 2.2.

To produce microspheres using the single emulsion technique, the double emulsion methodology was used, with a few adaptations. The polymer was dissolved in 33.5 mL of DCM and the 1500

µL of deionized water with or without the drug was replaced with 1500 µL DCM (with or without the drug). Otherwise, all steps remained the same. The conditions studied for each polymer type and model drug or chemotherapeutic are listed in Table 2.1 and Table 2.2.

Table 2.1 List of formulation conditions for blank microsphere.

Polymer Type	Emulsion Type	Impeller Speed Setting	Other Conditions
PLA	Double	2800	
			3% PVA
		3560	
			3% PVA
PCL	Double	2800	
			3% PVA
			5% PVA
			2.25 g PCL, 3% PVA
			2.25 g PCL, 5% PVA
			2.5 g PCL, 5% PVA
		3240	
		3560	
			3% PVA
			1 % PVA in W1, 3% PVA
			Only 5 mL of W1/O, 3% PVA
			2.5 g PCL, 5% PVA
			3 g PCL, 5% PVA
	Single	2800	
		3240	
		3560	3% PVA
PLGA	Double	2000	
		2800	
	Single	2000	3% PVA
			2.5 g PLGA, 3% PVA
		2800	3% PVA

Table 2.2 List of formulation conditions for drug encapsulated microspheres.

Polymer	Drug	Emulsion Type	Impeller Speed Setting (rpm)	Initial Drug Loading (mg)	Other Conditions
PLGA	Rhodamine B	Double	2000	1.5	
				1.5	3% PVA, 1 mg RB in W2
			2800	1.5	3% PVA, 5 mg RB in W2
	Fluorescein	Double	2800	1.5	
	Gefitinib	Double	2000	1.5	
		Single	2000	1.5	3% PVA
				3	3% PVA
				4.5	3% PVA
				15	2.5 g PLGA, 3% PVA
			2800	1.5	3% PVA
			5600	15	2.5 g PLGA, 3% PVA
PLA	Rhodamine B	Double	2800	1.5	3% PVA
				3	3% PVA
			3560	1.5	3% PVA
	Fluorescein	Double	2800	1.5	
	IgG	Double	1260	7.5	30 mL W2, 10 mg IgG in W2, 5% PVA
			2800	3	3% PVA
				15	3% PVA
				3	30 mL W2, 5% PVA
				12	30 mL W2, 5% PVA
				3	30 mL W2, 5 mg IgG in W2, 5% PVA
				7.5	30 mL W2, 5 mg IgG in W2, 5% PVA
				7.5	30 mL W2, 10 mg IgG in W2, 5% PVA
				3	2 g PLA, 3% PVA
				15	2 g PLA, 3% PVA
PCL	Rhodamine B	Double	2800	1.5	
				3	
				6	
				1.5	2.25 g PCL, 3% PVA
				6	2.25 g PCL, 5% PVA
				6	5% PVA, 10 mg RB in W2
			3240	1.5	
		Single	2800	1.5	
				6	
			3240	1.5	
	Fluorescein	Double	2800	1.5	
	Lomustine	Single	2800	1.5	3% PVA
				3	3% PVA
				6	3% PVA
				9	3% PVA
				15	3% PVA
				15	5 mg LMT in W2, 3% PVA
				3	30 mL W2, 5% PVA
				15	30 mL W2, 5% PVA
				3	30 mL W2, 5 mg LMT in W2, 5% PVA
				15	30 mL W2, 5 mg LMT in W2, 5% PVA
				3	2.5 g PCL, 5% PVA
				15	2.5 g PCL, 5% PVA
			3560	3	3% PVA

2.3.3 Microsphere Characterization

2.3.3.1 Microscopy Characterization

Microsphere shape, size, and fluorescence were determined using a Nikon E800 Upright Microscope with fluorescence capabilities. Samples were prepared by placing 5 µL of an aqueous solution of suspended microspheres on a glass slide and drying under vacuum prior to analysis. Both bright field and fluorescence images were taken. The cubes included UV/DAPI (Ex: 360/40, Em: 460/50, DM: 400LP), FITC (Ex: 480/40, Em: 535/50, DM: 505LP), and TRITC (Ex: 540/20, Em: 620/60, DM: 565LP). Microsphere morphology and size were determined using a FEI Sirion XL30 scanning electron microscope. Samples were prepared by placing 10 µL of an aqueous solution of microspheres on a silicon chip and drying under vacuum. The chips were then placed on double sided tape and sputter coated with gold-palladium for 30 to 50 seconds prior to imaging.

2.3.3.2 Particle Sizing

Particle size was determined using a Partica LA-950 Laser Diffraction Particle Size Distribution Analyzer. The surfactant Triton 10X was added to an aqueous solution of microspheres. Then the resulting dispersion was placed in the sample chamber for determination of the equivalent spherical diameter. Three measurements were taken per sample to confirm particle size distribution.

2.3.3.3 Encapsulation Efficiency and Drug Loading

Microsphere encapsulation efficiency (EE) and drug loading (DL) were determined using a Shimadzu UV-1601 ultraviolet-visible (UV-vis) spectrophotometer. Initially, a full spectrum of the drug (or model drug) was taken to determine the wavelength with the highest absorbance

(Table 2.3). These wavelengths were used to create a standard curve of drug concentration versus absorbance by measuring the absorbance of known concentrations of the drug dissolved in a solvent. These curves are shown in Appendix 1.

The amount of drug in the microsphere samples were calculated by dissolving a known amount of dried, drug encapsulated microspheres in the solvent and measuring the absorbance. The same steps were repeated for "blank" spheres (sphere with no drug but same formulation conditions) to produce a baseline absorbance. This baseline absorbance was subtracted from the drug absorbance reading. From this corrected absorbance value, the amount of drug in the microsphere samples could be calculated from the standard curves.

The theoretical amount of drug initially added for microsphere formation was determined with a similar method. A known amount of the solution resulting from the first homogenization, the W1/O for a double emulsion and the O for a single emulsion, was allowed to evaporate to remove DCM before adding a known amount of the solvent. The absorbance of this solution was measured and the "blank" solution absorbance from a drug-free emulsion subtracted out. The initial, theoretical drug amount was then calculated from the standard curves. All measurements were performed in triplicate with error to one standard deviation and statistical significance analyzed with an unpaired t test. The following equations were used to determine encapsulation efficiency and drug loading.

Equation 2.1 Encapsulation efficiency

$$EE(\%) = \frac{weight\ of\ drug\ encapsulated\ (mg)}{weight\ of\ theoretical\ drug\ encapuslated\ (mg)} * 100$$

Equation 2.2 Drug loading

$$DL(\%) = \frac{weight\ of\ drug\ encapsulated\ (mg)}{total\ weight\ of\ microsphere\ sample\ (mg)} * 100$$

Table 2.3 Wavelengths used for absorbance readings.

Molecule	Wavelength (nm)	Solvent
Rhodamine B	536	THF-1 M HCL 90-10 (v/v)
Gefitinib	333	THF-1 M HCL 90-10 (v/v)
Immunoglobulin G	283	1 M NaOH
Lomustine	396	DCM

2.3.4 Polymer Spin Coating and Contact Angle Measurements

PLGA, PLA, and PCL were dissolved in DCM at 2.5% w/v. Using an EC101 Series Photo Resist Spinner, approximately 70 µL of the polymer solution was spin-dropped at 4000 rpm for 20 seconds on glass substrates (Gold Seal Microscope Cover Glasses, 15 mm diameter, #2 thickness).

Water contact angles were acquired using a FTA200 goniometer. Advancing contact angles were measured and analyzed using FTA32 Analysis Software. Four measurements were completed for each polymer sample.

2.3.5 Synthesis of Linear PNIPAM [99]

2.3.5.1 Synthesis of the Di-functional Macroinitiator

Five grams of PCL diol (Mw~530, 9.4 x 10^{-3} mol) and 6.5 mL of TEA (0.047 mol) were dissolved in 150 mL of anhydrous THF. This solution was cooled in an ice bath to 4°C before 2.3 mL of chloropropionyl chloride (0.024 mol) was added drop-wise while maintaining an inert, nitrogen atmosphere. The reaction mixture was stirred for 18 hours at room temperature. The resulting white precipitate was removed by vacuum filtration and the remaining solvent removed with a Büchi rotary evaporator. This material was then dissolved in DCM and washed with saturated $NaHCO_3$ three times to remove acids, twice with 1 N HCl solution to remove TEA, and once with deionized water to remove salts. The organic phase was dried over $MgSO_4$, filtered, and rotovapped to produce a dark yellow oil. A schematic representation of this synthesis is shown in Figure 2.4.

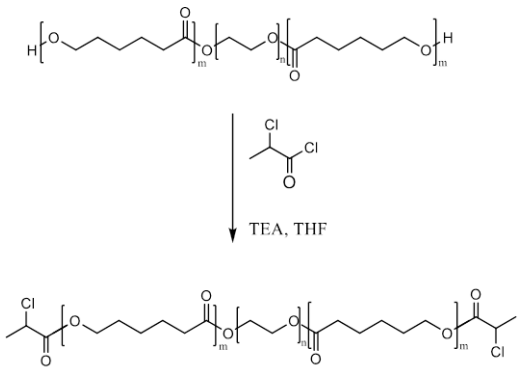

Figure 2.4: Synthesis of the degradable, di-functional macroinitiator.

2.3.5.2 Synthesis of the Ligand Tris[2-(dimethylamino)ethyl]amine (ME_6TREN)

Three mL of TREN (19.9×10^{-3} mol) and 135 mL acetic acid were combined together to produce a white solid. Then, 6000 mL of acetonitrile was added to dissolve the solid. After dissolution, 40 mL of aqueous formaldehyde (37% w/v, 660×10^{-3} mol) was added and stirred at room temperature for one hour. Then, the reaction mixture was placed in an ice bath before 10 g of sodium borohydride (13.4×10^{-3} mol) was slowly and carefully added. This mixture was then allowed to stir for 48 hours at room temperature. The solvent was removed with a rotary evaporator to obtain a yellow solid. The solid was dissolved in 3 M NaOH with a final pH of 11. This product was extracted three times with DCM, dried over $MgSO_4$, filtered, and rotovapped to obtain a yellow, viscous, oil-like liquid. This oil was vacuumed for 12 hours and centrifuged at 4000 g, 4°C, for 10 minutes to remove any possible solids and then stored at 4°C. A schematic representation of the synthesis is shown in Figure 2.5.

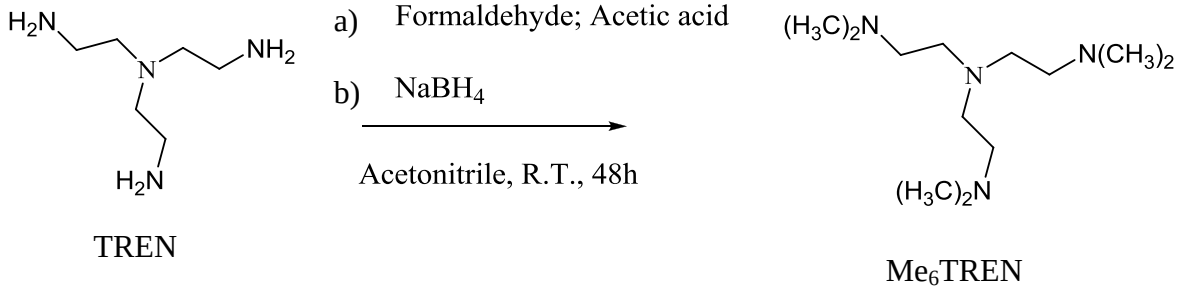

TREN Me_6TREN

Figure 2.5: Synthesis of the ligand ME_6TREN.

2.3.5.3 Synthesis of Linear PNIPAM (20k)

One gram of NIPAM (0.009 mol) and 36 mg of the macroinitiator CL-PCL-Cl (5×10^{-5} mol) were dissolved in 1 mL DMF and purged with nitrogen for one hour while, in parallel, 0.115 g of

Me_6TREN (0.0005 mol) was also purged. These solutions were transferred to a glove box before 50 mg of CuCl (0.0005 mol) was added to the DMF solution and dissolved by stirring. Then, the Me_6TREN was added and stirred at room temperature overnight, forming a viscous solution. The solution was then diluted with THF (1:1 THF:DMF v/v). The resulting THF solution was passed through an alumina column until a clear solution was obtained. The resulting solution was rotovapped to remove the solvent, producing a white-yellow solid. This solid was dissolved in a minimal amount of chloroform before being precipitated in a cold diethyl ether three times, with a centrifugation of 4000 g, 4°C, for 5 minutes between each precipitation. The resulting powder was dried under vacuum, dissolved in water, and lyophilized before storage. A schematic representation of this synthesis is shown below in Figure 2.6.

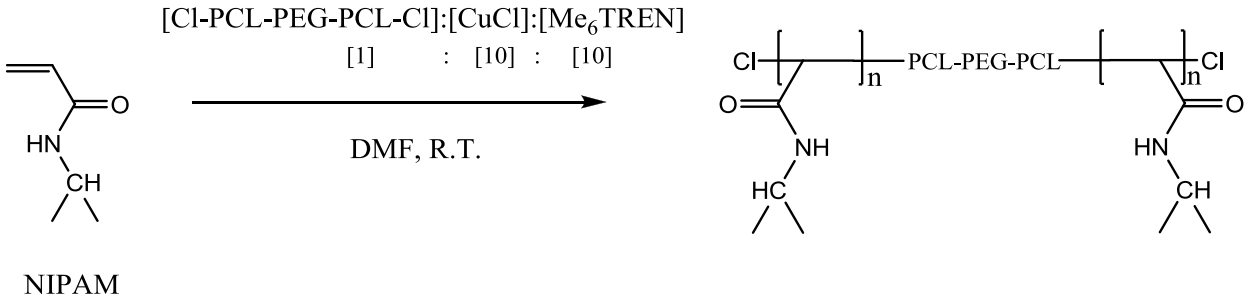

Figure 2.6: Synthesis of linear PNIPAM.

2.3.6 Analysis of Macroinitiator, Ligand, and PNIPAM

The di-functional macroinitiator, ligand, and PNIPAM were characterized using a Bruker AV-300 nuclear magnetic resonance (NMR) spectrometer. ^{1}H NMR spectra were obtained in solution of chloroform-d with chemical shifts expressed in parts per million downfield from the tetramethylsilane internal standard.

2.3.7 Testing Thermoresponsiveness of PNIPAM

The ability of the degradable PNIPAM based formulation to form a stable gel for entrapping microspheres at physiological temperatures was tested as follows. The PNIPAM was dissolved in PBS over night at 4°C at a concentration of 2.5% W_{PNIPAM}/V_{PBS}. To 1 mL of the aqueous PNIPAM solution at RT, 15 mg of RB-PLGA microspheres were added and suspended. Then, the suspension was placed at 37°C to trigger gelation. After gelation, the vial was removed and the transition from a gel to a liquid observed. This was also repeated for PNIPAM without the presence of microspheres.

2.4 Results

2.4.1 Non-encapsulated Polymeric Microsphere Formulation

Non-encapsulated or "blank" PLGA, PLA, and PCL microspheres were initially formulated using the double emulsion, solvent evaporation technique. Representative SEM images are presented in Figure 2.7. As a starting point, the goal of these formulations was a smooth, spherical, non-porous microsphere approximately 50 μm in diameter. SEM images of preliminary attempts are shown in Appendix 2, where flattened, non-spherical particles were produced dependent on the impeller type used in the emulsions.

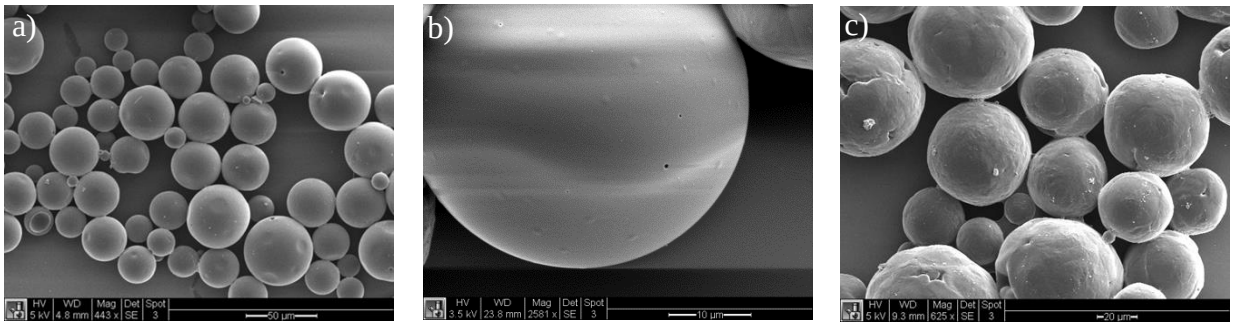

Figure 2.7: SEM micrographs of blank polymeric microspheres: a) PLGA at 2000 rpm, scale bar 50 µm, b) PLA at 2800 rpm, scale bar 10 µm, and c) PCL at 3240 rpm, scale bar 20 µm.

Two stirring speeds were used during the secondary emulsion to produce two distinct particle size distributions. The results are summarized in Table 2.4. An example particle size distribution is shown in Figure 2.8 for PLGA microspheres formulated at 2000 and 2800 rpm. The diameters of blank microspheres corresponding with the optimized gefitinib-PLGA, IgG-PLA, and lomustine-PCL microspheres are also listed in Table 2.4.

Table 2.4 Particle size distribution for blank microspheres.

Polymer	**Conditions**	**Average Diameter (µm)**	**Standard Deviation (µm)**
PLGA	2000 rpm, double emulsion	35	14
	2800 rpm, double emulsion	25	9
	2000 rpm, 3% PVA, single emulsion	22	8
	2800 rpm, 3% PVA, single emulsion	15	6
	2000 rpm, 2.5 g PLGA, 3% PVA, single emulsion	40	24
PLA	2800 rpm, double emulsion	37	13
	3560 rpm, double emulsion	29	10
	1260 rpm, 30 mL W2, 5% PVA	28	12
	2800 rpm, 30 mL W2, 5% PVA	11	8
PCL	2800 rpm, double emulsion	49	17
	3240 rpm, double emulsion	44	18
	2800 rpm, 30 mL W2, 5% PVA, single emulsion	30	12

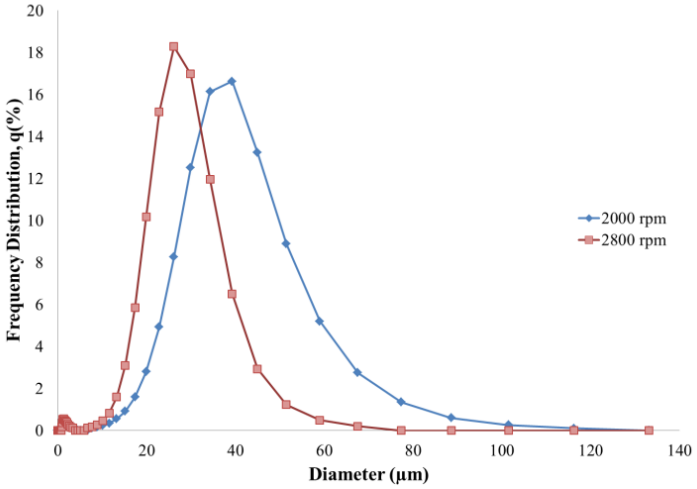

Figure 2.8: The particle size distribution of blank PLGA microspheres formulated at 2000 rpm (35 ± 14 µm) and 2800 rpm (25 ± 9 µm).

2.4.2 Rhodamine B Encapsulated Polymeric Microspheres

Rhodamine B (RB) is a commercially available, hydrophilic dye that was used as a model drug for initial testing of encapsulation. Due to its hydrophilicity, the double emulsion technique was utilized. Encapsulation potential was tested on all three polymeric microspheres with full characterization including microscopy, encapsulation efficiency, and drug loading. The presence of rhodamine B was determined with fluorescence microscopy, shown in Figure 2.9 for PLGA, PLA, and PCL microspheres. Representative SEM images are shown in Figure 2.10 and the particle size distributions are listed in Table 2.5. Two stirring speeds at the secondary emulsion stage were utilized to create two particle size distributions.

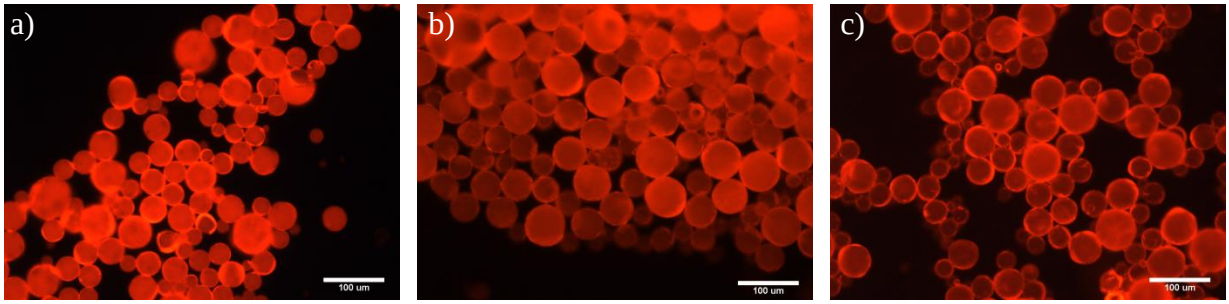

Figure 2.9: Fluorescence micrographs of rhodamine B encapsulated microspheres: a) PLGA microspheres at 2000 rpm, b) PLA microspheres at 2800 rpm, and c) PCL microspheres at 3240 rpm at an initial rhodamine B loading of 1.5 mg.

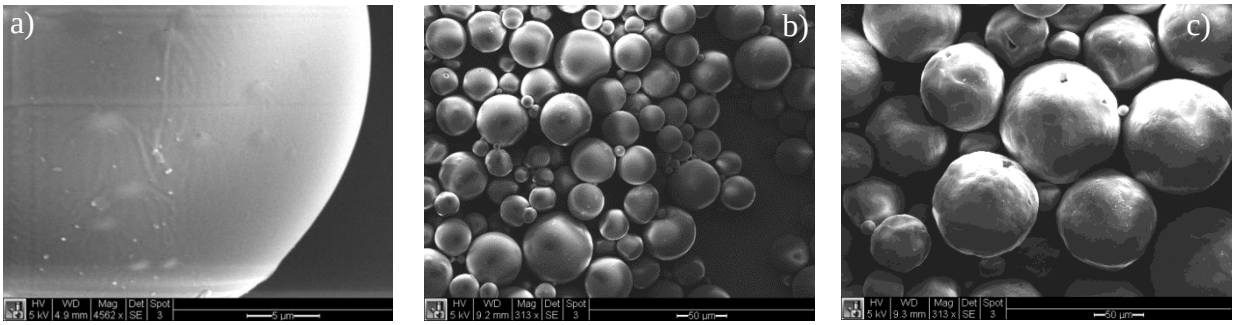

Figure 2.10: SEM micrographs of rhodamine B encapsulated polymeric microspheres: a) PLGA at 2000 rpm, scale bar 5 µm, b) PLA at 2800 rpm, scale bar 50 µm, and c) PCL at 3240 rpm, scale bar 50 µm.

Table 2.5 Particle size distribution for rhodamine B encapsulated microspheres.

Polymer	Conditions	Average Diameter (µm)	Standard Deviation (µm)
PLGA	2000 rpm, 1.5 mg RB	42	15
	2800 rpm, 1.5 mg RB	23	8
PLA	2800 rpm, 1.5 mg RB	37	11
	3560 rpm, 1.5 mg RB	27	10
PCL	2800 rpm, 1.5 mg RB	52	20
	3240 rpm, 1.5 mg RB	51	20

The encapsulation efficiency (EE) and drug loading (DL) of the rhodamine B encapsulated polymeric microspheres were also determined. Figure 2.11 and Figure 2.12 shows the differences between selected encapsulation efficiencies and drug loadings for different formulation parameters of the three polymeric microspheres. Appendix 3 and 4 quantitatively defines the encapsulation efficiencies and drug loadings for all formulations studied, respectively.

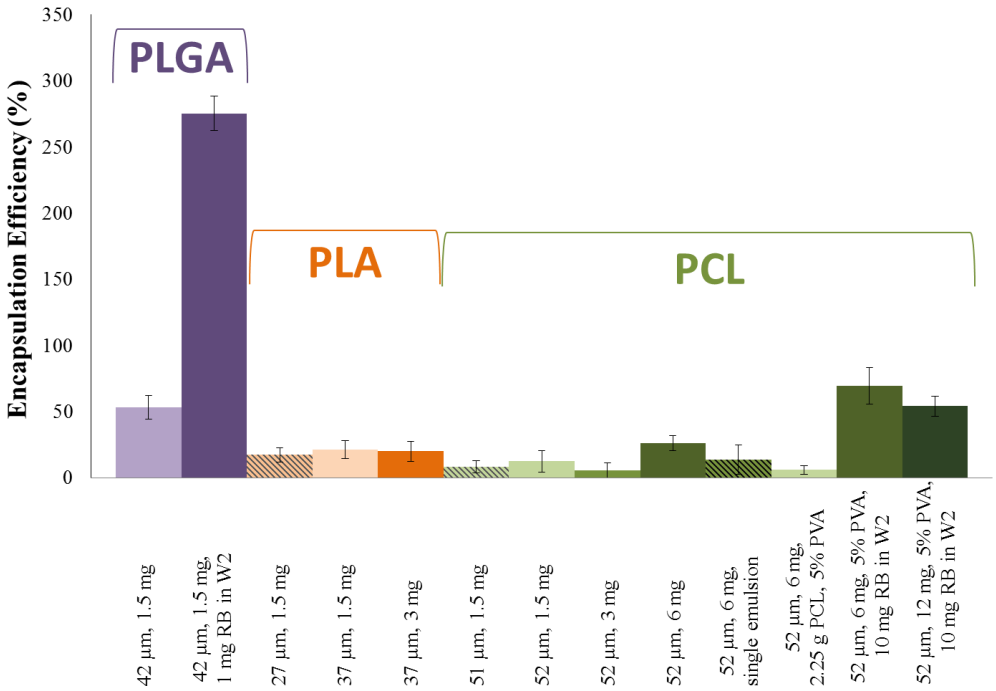

Figure 2.11: The encapsulation efficiency of rhodamine B encapsulated PLGA, PLA, and PCL microspheres.

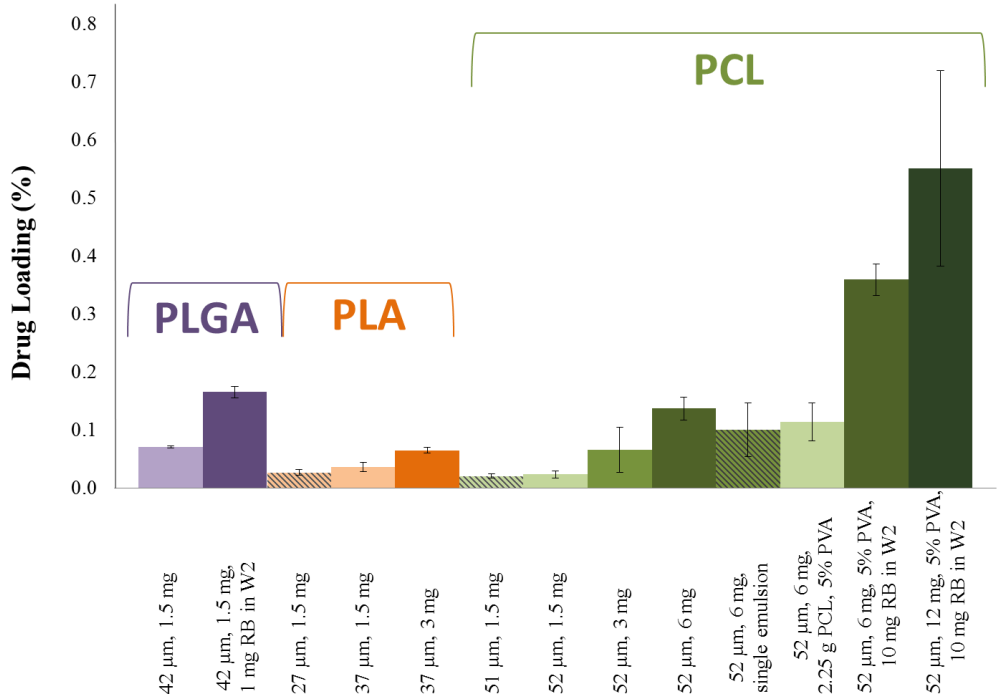

Figure 2.12: The drug loading of rhodamine B encapsulated PLGA, PLA, and PCL microspheres.

2.4.3 Fluorescein Encapsulated Polymeric MicrospheresThe hydrophobic dye fluorescein was used to test the encapsulation potential of PLGA, PLA, and PCL microspheres created using the double emulsion technique. Only fluorescence micrographs (Figure 2.13) were taken since more detailed characterization would occur for the chemotherapeutics and this encapsulation was only a proof of principle.

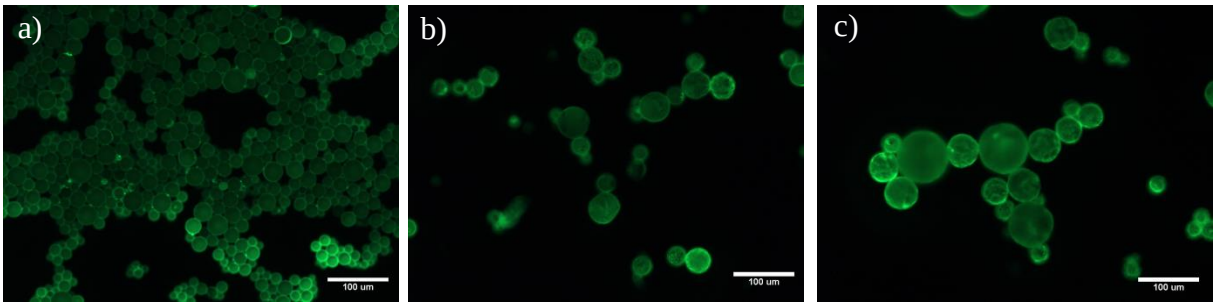

Figure 2.13: Fluorescence micrographs of fluorescein encapsulated microspheres: a) PLGA microspheres at 2800 rpm, b) PLA microspheres at 2800, and c) PCL microspheres at 2800 rpm at an initial fluorescein loading of 1.5 mg.

2.4.4 Gefitinib Encapsulated PLGA Microspheres

Gefitinib (GB) was the first chemotherapeutic encapsulated during the course of this dissertation research. Based on the similar ring structure and molecular weight to rhodamine B, this drug was chosen to be encapsulated in PLGA. After preliminary testing, single emulsions were used to encapsulate this drug due to its higher hydrophobicity. Figure 2.14a and b shows the fluorescence and SEM images of the gefitinib encapsulated PLGA microspheres (GB-PLGA). Table 2.6 lists the different particle sizes achieved and Figure 2.15 shows particle size distribution tuning based on increasing impeller speed. Figure 2.16 and Figure 2.17 describe the encapsulation efficiency and drug loading of gefitinib in PLGA, respectively. Quantitative numbers on encapsulation efficiency, drug loading, and the total amount of drug encapsulated are in Appendix 5, 6, and 7, respectively.

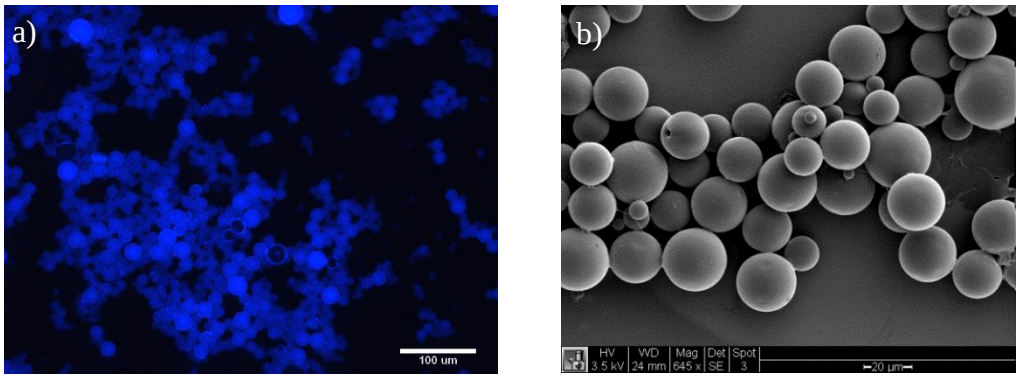

Figure 2.14: Characterization of gefitinib encapsulated PLGA microspheres: a) fluorescence micrograph of microspheres formulated at 2800 rpm (19 ± 8 µm) and b) SEM image of microspheres formulated at 2000 rpm (23 ± 8 µm), scale bar 20 µm.

Table 2.6 Particle size distribution for gefitinib encapsulated PLGA microspheres.

Polymer	**Conditions**	**Average Diameter (µm)**	**Standard Deviation (µm)**
PLGA	2000 rpm, 3% PVA, 1.5 mg GB	23	8
	2800 rpm, 3% PVA, 1.5 mg GB	19	8
	2000 rpm, 3% PVA, 15 mg GB, 2.5 gr PLGA	28	11
	4100 rpm, 3% PVA, 15 mg GB, 2.5 gr PLGA	17	6
	5600 rpm, 3% PVA, 15 mg GB, 2.5 gr PLGA	10	5

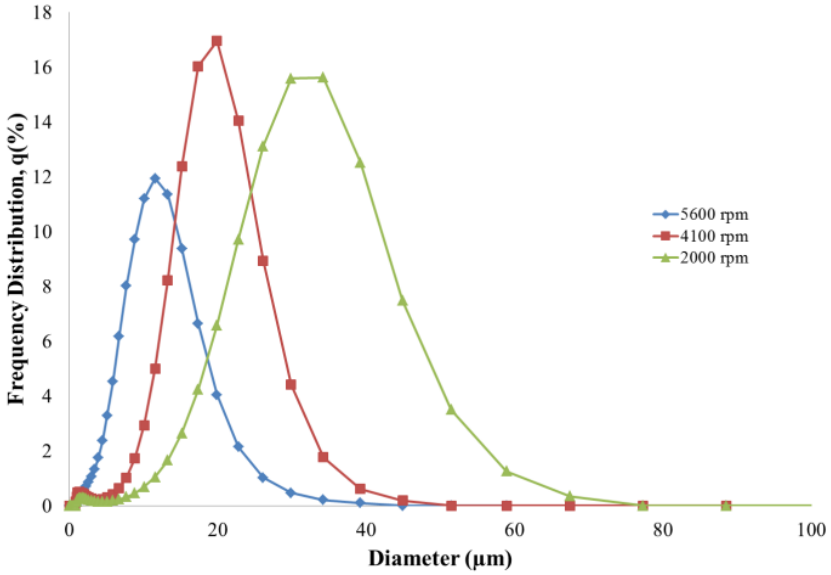

Figure 2.15: The particle size distribution of gefitinib encapsulated PLGA microspheres formulated at 2000, 4100, and 5600 rpm.

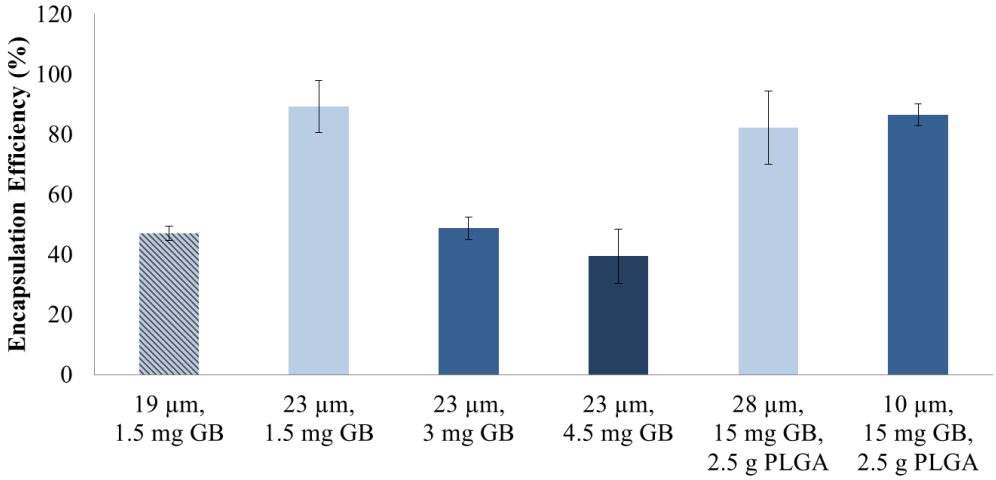

Figure 2.16: The encapsulation efficiency of gefitinib encapsulated PLGA microspheres.

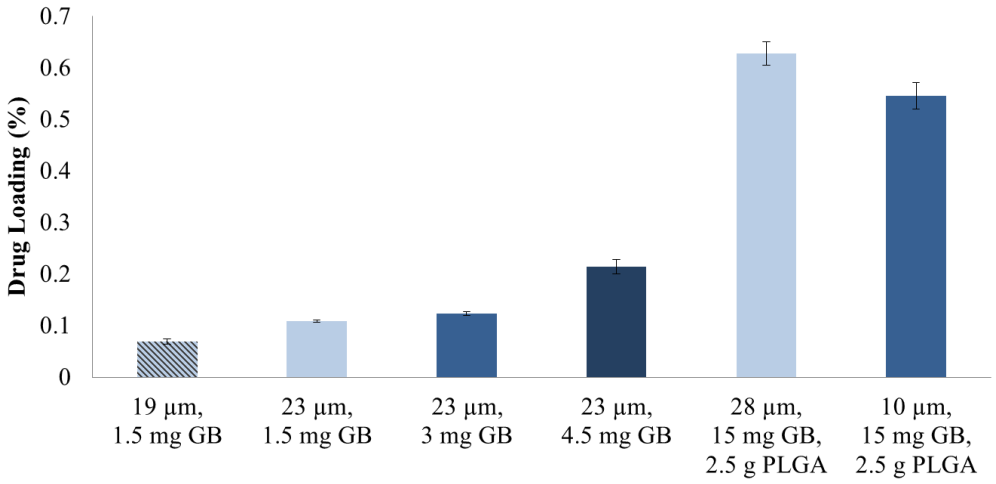

Figure 2.17: The drug loading of gefitinib encapsulated PLGA microspheres.

2.4.5 IgG Encapsulated PLA Microspheres

Bevacizumab was the second chemotherapeutic to be encapsulated in the microspheres using the double emulsion technique. However, due to the high cost of this chemotherapeutic, the model antibody immunoglobulin G (IgG) was used. Fluorescence and SEM micrographs of IgG encapsulated PLA microspheres (IgG-PLA) are shown in Figure 2.18. Table 2.7 lists the particle sizes of IgG-PLA at the optimal condition (2800 rpm, 7.5 mg IgG, 30 mL W2, 10 mg IgG in W2, 5% PVA) and at a larger sphere size, using the same formulation parameters. Figure 2.19 describes the encapsulation efficiency while Figure 2.20 describes the drug loading. For quantitative numbers on encapsulation efficiency, drug loading, and the total amount of drug encapsulated, see Appendix 8, 9, and 10, respectively.

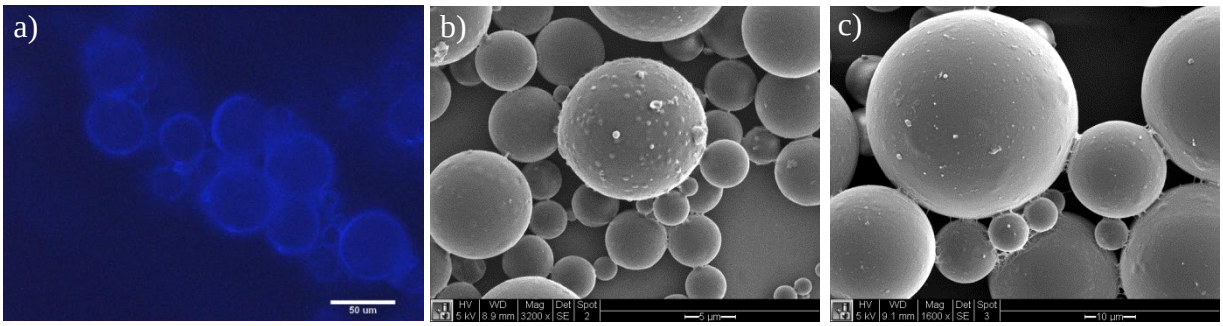

Figure 2.18: Characterization of IgG encapsulated PLA microspheres a) fluorescence microscopy with microspheres formulated at 3 mg IgG initial loading at 2800 rpm and with 7.5 mg IgG initial loading and a 30 mL W2 phase containing 10 mg IgG at b) 2800 rpm, scale bar 5 µm and c) 1260 rpm, scale bar 10 µm.

Table 2.7 Particle size distribution for IgG encapsulated PLA microspheres.

Polymer	Conditions	Average Diameter (µm)	Standard Deviation (µm)
PLA	1260 rpm, 7.5 mg IgG, 30 mL W2, 10 mg IgG in W2, 5% PVA	43	25
	2800 rpm, 7.5 mg IgG, 30 mL W2, 10 mg IgG in W2, 5% PVA	11	7

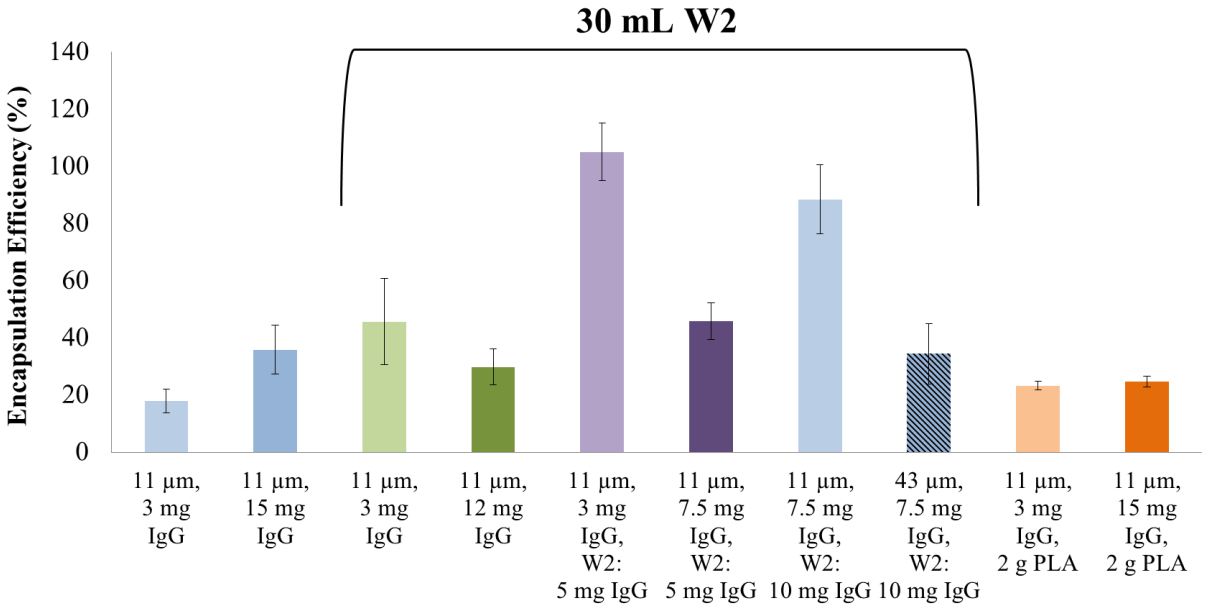

Figure 2.19: The encapsulation efficiency of IgG encapsulated PLA microspheres.

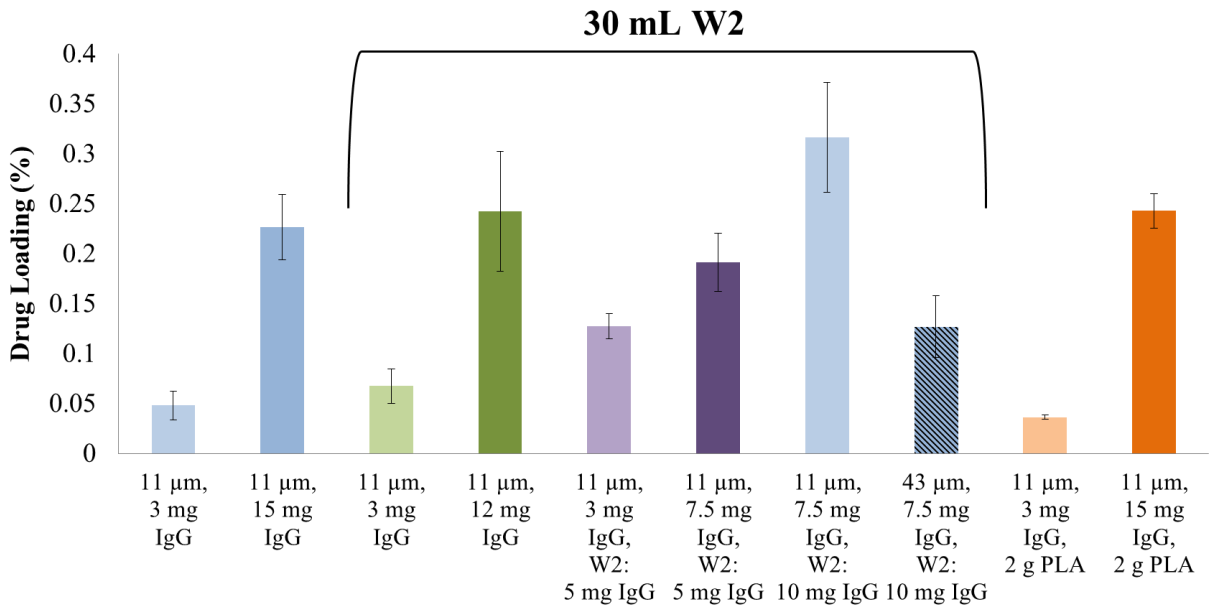

Figure 2.20: The drug loading of IgG encapsulated PLA microspheres.

2.4.6 Lomustine Encapsulated PCL Microspheres

Lomustine (LMT) was the third chemotherapeutic encapsulated during the course of this dissertation research. Due to its hydrophobicity [82], LMT was encapsulated in PCL microspheres. Figure 2.21 shows SEM micrographs of LMT encapsulated PCL microspheres (LMT-PCL). Fluorescence micrographs of LMT-PCL are not available due to the limitation of the available filter cubes on the microscope. Table 2.8 lists the particle size achieved for the optimal parameters and Figure 2.22 and Figure 2.23 describe the encapsulation efficiency and drug loading, respectively. For quantitative numbers on encapsulation efficiency, drug loading, and the total amount of drug encapsulated, see Appendix 11, 12, and 13, respectively.

Table 2.8 Particle size distribution of lomustine encapsulated PCL microspheres.

Polymer	Conditions	Average Diameter (µm)	Standard Deviation (µm)
PCL	2800 rpm, 15 mg LMT, 30 mL W2, 5 mg LMT in W2, 5% PVA	31.1	12.1

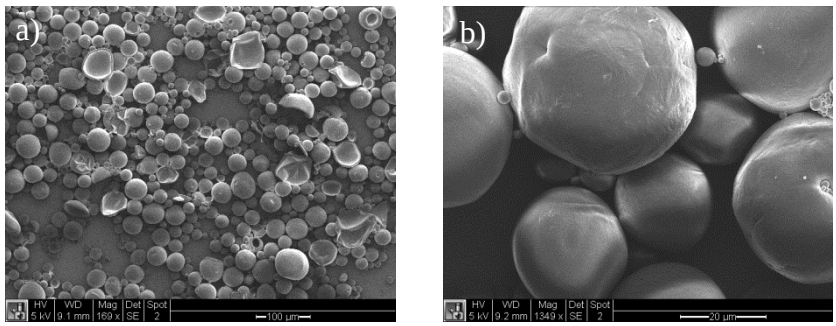

Figure 2.21 Characterization of lomustine encapsulated PCL microspheres formulated at 2800 rpm, with an initial loading of 15 mg LMT and 30 mL for W2 containing 5 mg LMT, a) scale bar 100 µm, b) scale bar 20 µm.

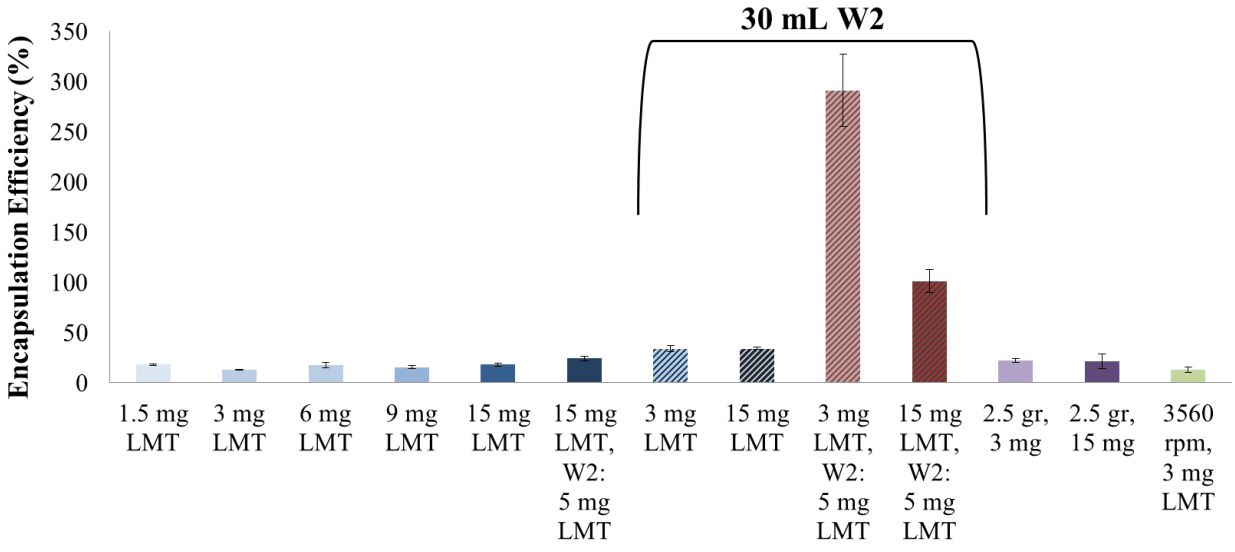

Figure 2.22 The encapsulation efficiency of lomustine encapsulated PCL microspheres. All formulations are at 2800 rpm, unless otherwise noted.

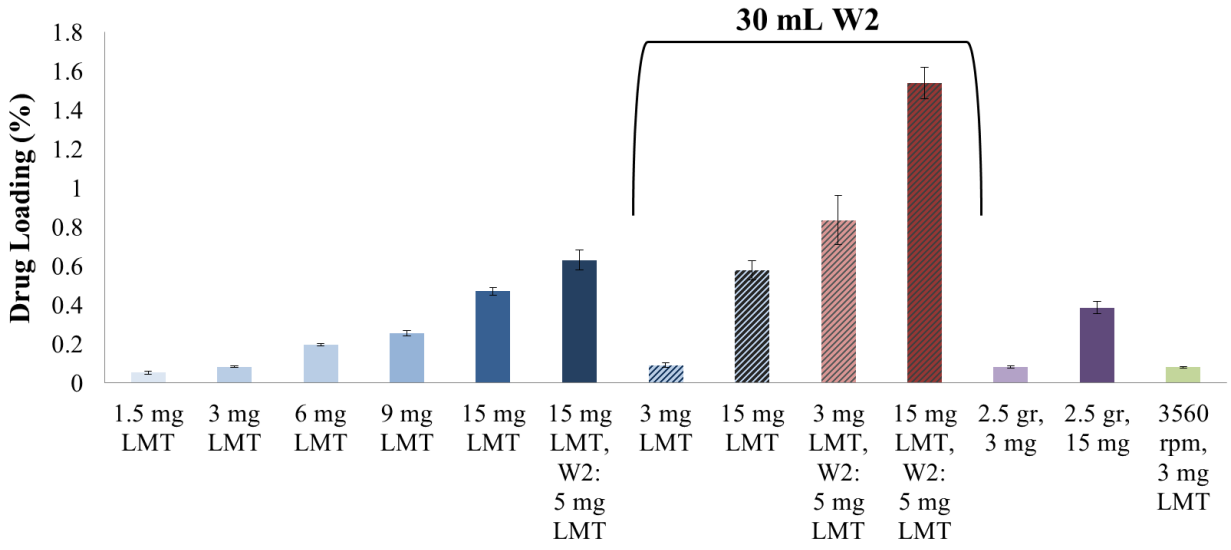

Figure 2.23 The drug loading of lomustine encapsulated PCL microspheres. All formulations are at 2800 rpm, unless otherwise noted.

2.4.7 Contact Angle Measurements of PLGA, PLA, and PCL

The advancing contact angle measurements for the three polymers are listed in Table 2.9.

Table 2.9 Contact angle measurements of PLGA, PLA, and PCL.

	Average Contact Angle	**Standard Deviation**
PLGA	70.8	1.5
PLA	74.7	1.3
PCL	75.5	0.8

2.4.8 Analysis of Macroinitiator, Ligand, and PNIPAM

2.4.8.1 Di-functional Macroinitiator

^{1}H NMR spectra in $CDCL_3$ is as follows: δ 1.30 (m, -$COOCH_2CH_2C\underline{H_2}CH_2CH_2COO$-), 1.52 (m, -$COOCH_2C\underline{H_2}CH_2CH_2CH_2COO$- and $ClCH(C\underline{H_3})COO$-), 2.35

(m, -COOCH$_2$CH$_2$CH$_2$CH$_2$C<u>H$_2$</u>COOCH$_2$CH$_2$O-), 3.75 (m, -COOC<u>H$_2$</u>CH$_2$-O-CH$_2$C<u>H$_2$</u>COO-), 4.0-4.6 (m, -COOCH$_2$CH$_2$CH$_2$CH$_2$CH$_2$COOC<u>H$_2$</u>CH$_2$O- and ClC<u>H</u>(CH$_3$)COO-).

2.4.8.2 Ligand (Me_6TREN)

^{1}H NMR spectra in CDCL$_3$ is as follows: δ 2.2 (s, 18H, -C<u>H$_3$</u>), 2.32 (m, 6H, -NC<u>H$_2$</u>CH$_2$N(CH$_3$)$_2$), and 2.60 (m, 6H, -NCH$_2$C<u>H$_2$</u>N(CH$_3$)$_2$).

2.4.8.3 PNIPAM

^{1}H NMR spectra in CDCL$_3$ is as follows: δ 1.14 (-CONHCH(C<u>H$_3$</u>)$_2$-), 1.4-2.4 (-C<u>H$_2$</u>C<u>H</u>CO-) 4.03 (-CONHC<u>H</u>(CH$_3$)$_2$-).

2.4.9 Thermoresponsiveness of PNIPAM

The ability of degradable, aqueous PNIPAM (20,000 g/mol) to form a stable gel and to entrap RB-PLGA microspheres is shown in Figure 2.24a and Figure 2.24b, respectively.

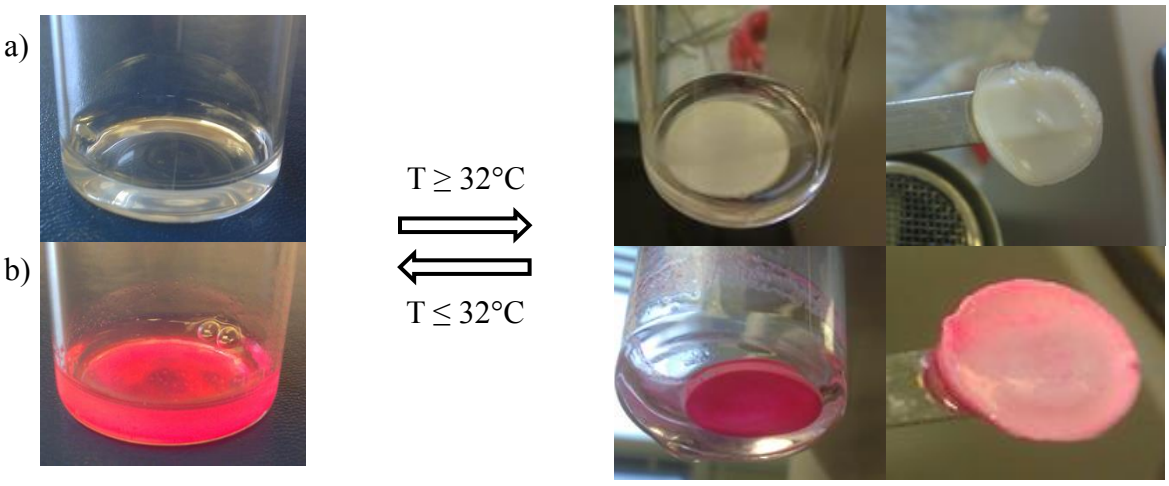

Figure 2.24: The thermoresponsiveness of an aqueous solution of degradable PNIPAM in PBS (2.5% W_{PNIPAM}/V_{PBS}) without a) and with b) RB-PLGA microspheres at room temperature and 37°C.

2.5 Discussion

In this chapter, we have formulated blank and encapsulated PLGA, PLA, and PCL microspheres. Initial studies were focused on creating blank or non-encapsulating microspheres using the well-established emulsion technique [26, 33-37, 41]. After optimization of impeller type, smooth, spherical, non-porous microparticles were produced from both double and single emulsions (Figure 2.7). It was observed that the speed of the impeller during the secondary emulsion had an impact on particle size; the faster impeller speed and the resulting greater shear forces produced smaller microspheres compared to a slower speed (Table 2.4). As an example, Figure 2.8 shows the particle size distribution of blank PLGA microspheres emulsified at 2000 and 2800 rpm with diameters of 35 ± 14 μm and 25 ± 9 μm, respectively.

The model drug rhodamine B was chosen to test the encapsulation potential of the microsphere system. This hydrophilic dye was used previously as a model drug for encapsulation in PLGA and poly(sebacic anhydride) microspheres [79, 100, 101]. In addition, rhodamine B has a molecular weight similar to one of the chosen chemotherapeutics, gefitinib, with a molecular weight of 479 and 447 g/mol, respectively, and is easy to quantify using UV-vis spectroscopy. Initial encapsulation and characterization of PLGA, PLA, and PCL microspheres demonstrated that rhodamine B was part of the polymeric microsphere due to the microsphere's fluorescence and that the dye was not localized to the surface, as demonstrated by the lack of surface dye crystals when viewed with SEM (Figure 2.9 and Figure 2.10). If a large amount of rhodamine B was not encapsulated but localized at the surface, it would be visible with SEM as demonstrated by Berkland et al. in Figure 2.25b [101]. The pits that are visible on the microsphere surfaces are assumed to be due to DCM evaporation as the microspheres are drying [102].

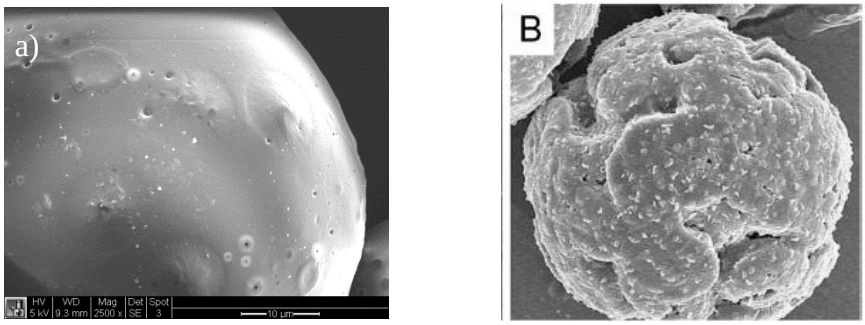

Figure 2.25 A comparison of rhodamine B encapsulated microspheres: a) PLA microspheres without surface localized rhodamine B and b) poly(sebacic acid) microspheres with surface localized rhodamine B [101]. Reprinted from Journal of Controlled Release, 94/1, Berkland et al., Microsphere size, precipitation kinetics and drug distribution control drug release from biodegradable polyanhydride microspheres, 129-141, 2004, with permission from Elsevier.

The particle sizes of the rhodamine B encapsulated microspheres were also determined at two different impeller speeds, matching the same formulation conditions of the blank microspheres (Table 2.4 and Table 2.5). It was found that the particle size did not significantly change due to encapsulation, but remained within one standard deviation of the blank particle measurements. This indicates that, for the rhodamine B system, blank microspheres can be used to test formulation conditions to produce a selected particle size without testing multiple drug loaded microspheres.

When encapsulation efficiencies and drug loadings were calculated, there was a strong correlation between the values and polymer type (Figure 2.11 and Figure 2.12). Initial formulations at an emulsion speed of 2000 rpm (PLGA) or 2800 rpm (PLA, PCL) and a 1.5 mg initial rhodamine B loading resulted in PLGA microspheres having the statistically greatest encapsulation efficiency and drug loading at 53 ± 9% and 0.08 ± 0.007%, then PLA at 21 ± 7% and 0.04 ± 0.008% and PCL at 13 ± 8% and 0.02 ± 0.006%, respectively ($p < 0.05$). The crystallinity of these polymers can provide some insight into why this happens. PCL and PLA

are semi-crystalline polymers with an approximate 40% crystallinity for PCL and 37% crystallinity for PLA [103, 104]. The crystalline phase of these polymers is relatively impermeable to water, so the drug entrapment of the water soluble rhodamine B will most likely occur in the amorphous region of the polymer, as demonstrated by Huatan et al., Kim et al., and Youan et al., where an increase in the amorphous region of the polymer and decrease in polymer crystallinity increased the encapsulation efficiency [105-107]. Therefore, PLGA 50:50, characterized as an amorphous or non-crystalline polymer [108], would have the greatest encapsulation efficiency, as we showed, and PLA and PCL would be lower. The contact angle measurements of these polymers provide further insight to the encapsulation efficiency of the microspheres, with PLGA having the smallest angle at 70.8 ± 1.5°, indicating its greater hydrophilicity when compared to PLA at 74.7 ± 1.3°and PCL at 75.5 ± 0.8°. Therefore, rhodamine B, a hydrophilic dye, would be more readily retained within a PLGA microsphere. When encapsulated in PLA or PCL, rhodamine B would preferentially diffuse to the external aqueous phase (W2) and wash out of the microspheres during formulation.

Even so, there are ways to overcome a low encapsulation efficiency and drug loading. For example, Chen et al. increased the PLGA polymer concentration during emulsification from 6 to 18% w/v to increase carboplatin drug loading [31]. The polymer solution became more viscous, reducing the amount of drug that leached out during the sphere hardening phase. This modestly increased the drug loading from 9.6 ± 0.15 to 10.5 ± 0.2%. Another option was demonstrated by Zhang et al. for temozolomide encapsulated PLGA microspheres using the single emulsion method [28]. To overcome a low encapsulation efficiency, the external aqueous phase was

saturated with the drug in addition to having the drug in the internal, oil phase. This more than doubled the efficiency from 30% to as high as 85%.

Increasing the initial drug loading can also have an impact on drug loading and encapsulation efficiency. As demonstrated by Gil-Alegre et al., increasing the drug/polymer ratio from 0.2 to 0.4 doubled the drug loading, maintaining the same encapsulation efficiency [30]. However, for an increase to a 0.8 ratio, the drug loading did not change; instead, a decrease in encapsulation efficiency resulted. This indicates that there is a solubility limit that must be considered when encapsulating drugs using the emulsion techniques.

Following these examples, PCL, having the lowest encapsulation efficiency, was subjected to changes in initial drug loading, polymer amount, and rhodamine B in both the internal (W1) and external (W2) aqueous phases. The best and highest encapsulation efficiencies and drug loadings were achieved when rhodamine B was present in both the internal and external water phases, lowering the concentration gradient and significantly increasing the encapsulation efficiency to 70 ± 14% from 13 ± 8% and drug loading to 0.35 ± 0.024% from 0.02 ± 0.003% ($p < 0.05$). Increasing the initial drug loading from 1.5 mg to 6 mg increased the encapsulation efficiency to 26 ± 6% and drug loading to 0.14 ± 0.02% while changes from double to single emulsion and increasing the polymer concentration did not impact the encapsulation efficiency and drug loading.

Following these results, PLGA was optimized by placing rhodamine B in the external, aqueous phase (W2). In an initial test, 5 mg of rhodamine B were used in W2 (10%, w/v), increasing

encapsulation efficiency to 439% ± 16. This greater than 100% efficiency is from part of the rhodamine B in W2 being encapsulated in the microsphere during emulsification, approximately 27 ± 1%. To reduce the amount of drug, 1 mg of rhodamine B in W2 was used (2% w/v) with a resulting efficiency of 274% ± 13 and a drug loading of 0.23 ± 0.010%. Approximately 47% of the rhodamine B in the external phase was encapsulated. PLA was not optimized because of limited polymer amounts. However, it is assumed that similar optimization would be possible.

Fluorescein, a hydrophobic dye, was also used as a model drug to test the encapsulation capability of the microsphere system. It was encapsulated in all three polymer types and present when viewed with fluorescence microscopy (Figure 2.13). A full characterization of encapsulation efficiency and drug loading was not conducted since gefitinib, a hydrophobic chemotherapeutic, would be used instead.

The first chemotherapeutic to be encapsulated was gefitinib, utilizing the single emulsion technique due to its poor water solubility, less than 1 mg/mL [109]. PLGA was chosen to encapsulate gefitinib since rhodamine B, with a similar molecular weight and ring structure, best encapsulated in this polymer. Initial characterization showed that the gefitinib encapsulated microspheres were UV fluorescent, indicating gefitinib was located somewhere on or in the microspheres (Figure 2.14a). As a control, blank PLGA microspheres were also examined and were not UV fluorescent. When imaged with SEM, the gefitinib encapsulated microspheres were smooth and nonporous (Figure 2.14b). Surfaced localized drug crystals were not present, indicating gefitinib was encapsulated inside the microspheres. The gefitinib encapsulated PLGA microspheres demonstrated a tunable particle size distribution based on impeller speed, as shown

in Table 2.6 and Figure 2.15, with sizes ranging from 28 ± 11 μm in diameter at a low impeller speed to 10 ± 5 μm in diameter at a high speed.

In initial experiments, encapsulation efficiency was high at 90 ± 2% for a 1.5 mg initial gefitinib loading and 2000 rpm impeller speed (Figure 2.16). However, as shown in Figure 2.17, the drug loading was low at this condition (0.11 ± 0.002%). Further increases in initial gefitinib loading from 1.5 mg to 3 and 4.5 mg actually caused a decrease in encapsulation efficiency, indicating a limit to the drug/polymer ratio, as previously discussed. Therefore, the polymer concentration was increased by changing the PLGA amount from 1.75 g to 2.5 g and the initial gefitinib loading increased to 15 mg. The resulting increase in polymer viscosity and initial gefitinib loading significantly increased the drug loading to 0.63 ± 0.023% and the amount of drug present from 0.2 ± 0.02 mg to 1.9 ± 0.21 mg ($p < 0.05$). Encapsulation efficiency remained high at 82 ± 9%. This formulation was considered optimal since reported *in vivo* studies have a drug dosage from 15 μg to 1 mg for intracranial tumor bearing mice and rats [30, 36, 43-45]. The increase in PLGA and initial gefitinib loading had a minimal effect on particle size, causing an increase from 23 ± 8 μm to 28 ± 11 μm. This could be attributed to the more viscous oil phase present with the higher concentration of PLGA. Of note is that the same, optimal formulation parameters but at a faster impeller speed (5600 versus 2000 rpm) resulted in smaller microspheres, 10 ± 5 μm, while maintaining a comparable encapsulation efficiency at 87 ± 12% and drug loading at 0.55 ± 0.026%. This indicates that a robust set of optimized formulation parameters was achieved for the gefitinib-PLGA microspheres, allowing for particle size (and subsequent drug release) tuning without the need for repetitive optimization.

The second chemotherapeutic to be encapsulated was the antibody, bevacizumab. However, due to the high cost of this chemotherapeutic, the commercially available antibody, immunoglobulin G (IgG), was used instead. PLA was chosen to encapsulate IgG due to its slightly higher hydrophilicity, as determined by contact angle (Table 2.9). The double emulsion technique was selected for encapsulation because it was used to successfully encapsulate other non-small molecules such as hemopexin and C-terminal fragment of platelet factor 4 (PF-4/CTF) for glioma treatment and to formulate bevacizumab encapsulated PLGA and poly(ethyleneglycol)-*b*-poly(D,L-lactic acid) microspheres for the treatment of age-related macular degeneration [43, 44, 91].

Following similar basic formulations conditions of gefitinib-PLGA, IgG was encapsulated at 2800 rpm with an initial IgG loading of 3 mg IgG. Preliminary characterization showed that the IgG encapsulated PLA microspheres were UV-fluorescent (Figure 2.18a), indicating that IgG was present on or in the microspheres. However, the encapsulation efficiency was low at 18 ± 4% (Figure 2.19). While increasing the initial IgG loading to 15 mg IgG increased efficiency to 36 ± 9%, this was still considered too low. Therefore, the PLA amount was increased to 2 grams, resulting in an efficiency of 23 ± 2% for a 3 mg IgG initial loading. The low encapsulation efficiency could be due to the hydrophilicity of IgG; IgG would preferentially diffuse to the external aqueous phase with a low IgG concentration from the high IgG concentration in the internal aqueous phase. Therefore, the next step was to reduce the amount of the external aqueous phase from 50 mL to 30 mL. This reduction would hopefully reduce the driving force of IgG to the external phase. The IgG that did diffuse out would result in a higher concentration of IgG because of the lower volume. While this modestly improved the efficiency to 46 ± 15%, it

was not at our goal of 60%. Therefore, following the previous work with rhodamine B and PCL, 5 mg IgG (17% w/v) was loaded into the reduced, external phase. This increased encapsulation efficiency to 105 ± 10% with an initial IgG loading of 3 mg; however, the drug loading was still considered low at 0.13 ± 0.013% (Figure 2.20). The initial IgG loading was then increased to 7.5 mg IgG and the external phase concentration increased to 33% (w/v), resulting with an optimized encapsulation efficiency of 88 ± 12% and a drug loading at 0.32 ± 0.055%, significantly higher than the first attempt ($p < 0.05$). These same conditions were used to produce larger microspheres 43 ± 25 µm in diameter. However, the encapsulation efficiency was low at 34 ± 11% for this larger size. This lowered encapsulation efficiency could be due to the precipitation kinetics of polymer microspheres. As described by Berkland et al., there are two competing factors affecting encapsulation efficiency during the time that the microspheres "harden" from a DCM enriched polymer phase to a "hard" polymer phase with no DCM [101]. First, larger microspheres have a decreased amount of drug that successfully diffuses out of the sphere because of the large, physical size of the polymer the drug must diffuse through. On the other hand, larger spheres take longer for the DCM to evaporate and "harden", allowing more time for the drug to diffuse before being entrapped by the hard polymer. Specifically, Berkland et al. describes a minimum in encapsulation efficiency for 50 µm microspheres, where the rate of entrapment and sphere hardening is slower than the drug diffusion, as compared to microspheres approximately 10 µm in diameters [101]. Our larger microspheres set at 43 ± 25 µm and smaller microsphere set at 11 ± 7 µm with the resulting low and high encapsulation efficiencies, would support this hypothesis.

These two particles size sets of IgG-PLA were also imaged with SEM, showing that spherical particles were produced (Figure 2.18b and c). However, the microspheres were not as smooth as the gefitinib-PLGA microspheres. The smaller diameter microspheres had outward protruding bumps on the surface while the larger diameter microspheres had material present at the surface. Following the hypothesis of the precipitation kinetics described above, the bumps on the smaller sized microspheres could be pockets of IgG that were diffusing towards the external aqueous phase that were entrapped as the sphere hardened. These bumps are not present on the larger microsphere set due to the longer time of sphere hardening, allowing the IgG to fully diffuse and result in a lower encapsulation efficiency. Instead, the material that is seen via SEM could be residual IgG from the external aqueous phase that was not fully washed off during microsphere formulation. While the spheres are not perfectly smooth when compared to the blanks, these microspheres are still spherical and considered an acceptable product.

The third chemotherapeutic to be encapsulated was lomustine, a hydrophobic, small molecule drug already approved for the treatment of gliomas [82-84]. Lomustine (LMT) was chosen to be encapsulated in PCL, the most hydrophobic of the three polymers (Table 2.9). Early formulations were similar to GB-PLGA and IgG-PLA formulations, with an initial LMT loading of 1.5 mg LMT at 2800 rpm. As can be seen in Figure 2.22, the encapsulation efficiency was low at 18 ± 0.7% and remained low despite increasing the initial LMT loading to 3, 6, 9, and 15 mg LMT. Increasing the oil viscosity by increasing the PCL amount from 1.75 g to 2.5 g did not have a significant impact on encapsulation efficiency, causing an increase to 22 ± 2% ($p < 0.05$). Following a similar protocol to RB-PCL and IgG-PLA, 5 mg of LMT was loaded in the external aqueous phase (10% w/v). However, this only modestly increased the encapsulation efficiency to

24 ± 2%. Therefore, the external aqueous phase volume was reduced to 30 mL. Without any LMT present in the external aqueous phase, LMT encapsulation efficiency remained low at 34 ± 3%. However, with LMT in the external phase at 10% w/v, the encapsulation efficiency significantly increased to 291 ± 36% for an initial LMT loading of 3 mg ($p < 0.05$). Similar to RB and IgG, this means that PCL was encapsulating part of the LMT in the external aqueous phase (~ 25%). The next step was to increase the initial LMT loading to 15 mg, which would hopefully increase the overall drug loading in the microspheres. As seen in Figure 2.22 and Figure 2.23, this reduced the encapsulation efficiency to 102 ± 12% and increased drug loading to 1.54 ± 0.08%. The amount of drug initially loaded into the microsphere was fully encapsulated by reducing the concentration gradient between the internal and external aqueous phase. Other formulations that were tried without success to increase encapsulation include immediately stirring the microspheres after emulsification to increase the rate of sphere hardening and decrease the diffusion time, rinsing the microspheres once to remove excess drug, and formulating the microspheres in the dark, due to light sensitivity of LMT.

The particle size of the optimized formulation parameters (2800 rpm, 15 mg initial LMT loading, 30 mL W2 with LMT 10% w/v) was 31 ± 12 µm in diameter. This is comparable to blank PCL microspheres formulated at similar conditions, with a particle size of 30 ± 12 µm in diameter. The microspheres produced were, for the most part, smooth and spherical, as shown by the SEM images in Figure 2.21a and b. The presence of "flattened" microspheres seen in Figure 2.21a may indicate that some PCL microspheres being hollow, demonstrating the same sunken shape of hollow spheres reported in the literature [110-112]. In nanoparticle mini-emulsions, these hollow spheres arise from phase separation inside the particles between the hydrophobic material

and polymer [110, 113]. Since these "hollow" spheres are minimally present, these microspheres are still considered an acceptable product.

The synthesis of the di-functional macroinitiator, ligand, and PNIPAM were characterized by NMR, comparing detected peaks to reported values [99]. In the case of PNIPAM, the ^{1}H-NMR spectra showed the disappearance of the peaks related to the vinyl protons (at 5.5 ppm and 6.2 ppm) of the NIPAM monomer and showed the characteristic PNIPAM peaks at 1.14, 1.4-2.4, and 4.03 ppm.

The thermoresponsiveness of aqueous PNIPAM was demonstrated when a 2.5% W_{PNIPAM}/V_{PBS} solution was exposed to room temperature (25°C) and physiological temperature (37°C). As shown in Figure 2.24a, at room temperature below the LCST of PNIPAM, the solution was a liquid. However, after exposure above the LCST at 37°C, the solution solidified, forming an opaque gel. Figure 2.24b shows that the presence of rhodamine B encapsulated PLGA microspheres did not hinder this phase transition. Instead it shows that the PNIPAM was capable of entrapping the microspheres, demonstrating PNIPAM's capability as a carrier for drug encapsulated microspheres. It is important to note that the gelation phenomenon is reversible. Once allowed to cool back to room temperature, the PNIPAM reverted back to liquid form, releasing the microspheres.

2.6 Conclusions

The first part of this work was focused on formulating blank and drug encapsulated polymeric microspheres. Smooth, spherical, non-porous microparticles were produced from both double

and single emulsions with the size dependent on the impeller speed during emulsification. The model drugs rhodamine B and fluorescein were successfully encapsulated in PLGA, PLA, and PCL microspheres. For rhodamine B encapsulation, PLGA microspheres had the highest encapsulation efficiency and drug loading, then PLA, and then PCL. However, by altering the formulation parameters, high encapsulation efficiencies and drug loadings were achieved.

Gefitinib encapsulated PLGA microspheres, IgG encapsulated PLA microspheres, and lomustine encapsulated PCL microspheres were also successfully produced using the emulsion techniques. All three drug and microsphere combinations were optimized with a high encapsulation efficiency, greater than 80%, and drug loading, greater than 0.3%. These optimized particles were spherical and mostly smooth, with particle size dependent on impeller speed during emulsification.

The second part of this work was focused on synthesizing a linear, degradable PNIPAM. PNIPAM with a 20,000 g/mol molecular weight was successfully synthesized and an aqueous solution of PNIPAM demonstrated a reversible, temperature dependent phase transition that was capable of entrapping microspheres.

3 Evaluation of the *In Vitro* Drug Release

3.1 Background

3.1.1 Motivation

Chapter 2 demonstrated that polymeric microspheres were capable of encapsulating both model drugs and chemotherapeutics. While the microspheres were characterized for particle size, surface morphology, and drug encapsulation, the release rate *in vitro* has not yet been elucidated. The release rates determined *in vitro* are the first steps to understanding the drug release rate *in vivo* and for deciding the amount of microspheres necessary for a therapeutic dosage. In this chapter, the methods used to determine the release rates of rhodamine B, gefitinib, IgG, and lomustine will be described and the results discussed. Linear, degradable PNIPAM will also be tested for an aerosolized application on tissue at physiological temperature.

3.1.2 In Vitro Release of Drugs from Polymeric Microspheres

The release of chemotherapeutics from polymeric microspheres is dependent on several factors including particle size, drug type, polymer type and molecular weight, fabrication technique, drug loading content, stabilizer concentration, the use of additives to control porosity, etc. [24, 27, 41, 51, 52, 55, 56]. For example, a typical release of 5-FU from PLGA microspheres has a biphasic profile: an initial burst phase in the first day or two followed by a sustained release for 18 days, as shown in Figure 3.1 [36, 72]. However, as demonstrated by Fournier et al., this release can be extended by changing several formulation factors [41]. First, the polymer type was changed from PLGA to the slower degrading poly(methylidene malonate 2.1.2) (PMM 2.1.2). Then, a higher polymer concentration and molecular weight was used, resulting with a more viscous organic phase that prevented the diffusion of the drug crystals to the surface of the

particles. Last, a shorter emulsion time was used, which provided less time for the 5-FU crystals to escape to the external phase, resulting with a higher drug loading and again, fewer crystals localized along the peripheral of the sphere that can release at early time points. With this type of formulation parameter tuning, a 65% initial burst at 24 hours followed by an ongoing release 43 days later was achieved.

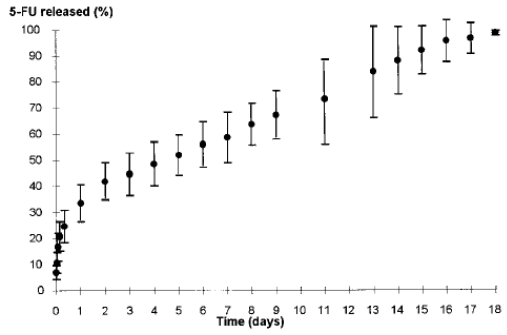

Figure 3.1: *In vitro* release profile of 5-fluorouracil from PLGA microspheres [72]. Reprinted from Cancer, 86/2, Menei et al., Local and sustained delivery of 5-fluorouracil from biodegradable microspheres for the radiosensitization of glioblastoma, 325-330, 1999, with permission from Wiley.

Lin et al. also demonstrated that the choice of polymeric carrier has a significant effect on the release of the chemotherapeutic, doxorubicin, using PLGA and PLGA-PLA composite microspheres [52]. In the first part of the study, doxorubicin was loaded into PLGA microspheres with differing ratios of the lactide and glycolide copolymers. The more hydrophobic PLGA composition with the higher lactide content (85:15) had a slower drug release and lower initial burst (by 10%) compared to the more hydrophilic composition with a higher glycolide content (65:35) (Figure 3.2). The particle size also attributed to the greater initial burst and faster release for the more hydrophilic PLGA (65:35) spheres due to its smaller sphere size, 2.91 ± 0.53 μm versus 3.74 ± 0.17 μm. The most noticeable effect on burst release was detected in the second

part of the study, comparing doxorubicin loaded PLGA and PLGA-PLA composite microspheres, with a burst release decrease from 60-75% to 36-48%, respectively. It was suggested that the protective PLA layer prevented the rapid release of the drug from the polymeric carrier, resulting in a more promising release profile.

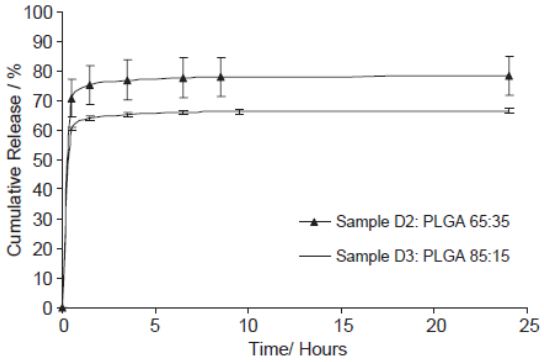

Figure 3.2: Release profiles of doxorubicin from two different PLGA copolymer compositions [52]. Reprinted from Biomaterials, 26/21, Lin et al., In vitro study of anticancer drug doxorubicin in PLGA-based microparticles, 4476-4485, 2005, with permission from Elsevier.

A clearer example on the role of particle size in drug release was demonstrated by Berkland et al. using precisely sized, mono-disperse, piroxicam (anti-inflammatory) encapsulated PLGA microspheres [100]. As shown in Figure 3.3a, the smaller diameter microspheres (10 μm) released fastest when compared to the larger microsphere sets (50 and 100 μm). This is due to smaller microspheres having a higher surface area to volume ratio when compared to larger microspheres. Berkland et al. then mixed the mono-disperse microspheres together to achieve a linear release profile, shown in Figure 3.3b. This linear release profile was an intermediate between the two individual microsphere release profiles and could be tuned to release faster by adding more of the smaller microspheres or to release slower by adding more of the larger microspheres.

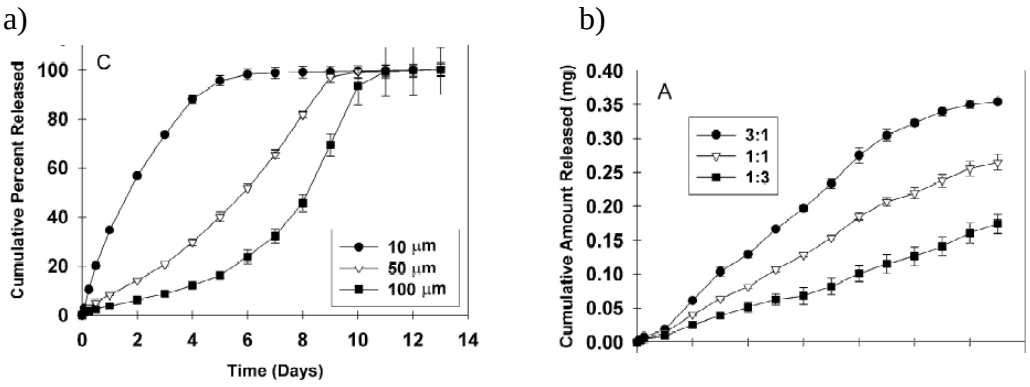

Figure 3.3: The effect of particle size on drug release: a) mono-disperse piroxicam encapsulated PLGA microspheres at a 15% theoretical loading and b) mixing the 10 and 50 μm piroxicam-PLGA spheres at a 3:1, 1:1, and 1:3 ratio (w/w)[100]. Reprinted from Journal of Controlled Release, 82/1, Berkland et al., Precise control of PLG microsphere size provides enhanced control of drug release rate, 137-147, 2002, with permission from Elsevier.

The typical release profile from PLGA microspheres is biphasic, as demonstrated by Chen et al. using carboplatin encapsulated PLGA microspheres [31]. During the first ten days, there was a slow release due to diffusion and then from days 12-22, a faster release attributed to diffusion and bulk degradation of the microspheres. Yemisci et al. encapsulated mitoxantrone in PLGA microspheres and detected the same biphasic release behavior, with a release of 55% at day 21, followed by a near linear release through day 70, attributed to diffusion of the drug and then degradation and solubilization of the PLGA matrix [78]. If a significant burst is present, the release profile can become tri-phasic: burst, diffusion, and degradation. This was demonstrated by Zhang et al. for temozolomide loaded PLGA microspheres [23].

Ozeki et al. studied a system similar to what is proposed in this work, using camptothecin encapsulated PLGA microspheres that were contained in a non-degradable, injectable, thermo-reversible gelation polymer (TGP) hydrogel composed of PNIPAM, poly(n-butyl methacrylate), and poly(ethylene glycol) [47, 57]. The *in vitro* release profile lasted 30 days with an

approximate 80% release. Dispersing the microspheres in the TGP resulted in a slightly slower but similar release, indicating the release from PLGA was the rate limiting step instead of an effect of the TGP.

3.1.3 Aerosolized PNIPAM

Thermoresponsive PNIPAM has been used in many different applications ranging from scaffolding for tissue engineering [99], cell release from surfaces using low temperature lift-off [114], as a thermo-sensitive glue for retinal implants [115], microgels for biosensing [116],and vehicles for drug delivery including hydrogels, liposomes, and nanoparticles [117-119]. To the best of our knowledge, PNIPAM has not been applied in an aerosolized form as a vehicle for drug delivery. The closest example to our application is a non-degradable, thermo-reversible gelation hydrogel containing PNIPAM in addition to poly(*n*-butyl methacrylate) and poly(ethylene glycol) applied as an injectable formulation for a localized camptothecin, doxorubicin, or vincristine encapsulated PLGA microsphere delivery[47, 48, 57, 61]. Therefore, this will be the first time that PNIPAM applied as an aerosol to tissue at 37°C will be tested and reported.

3.2 Hypothesis

It is hypothesized that:

(1) Rhodamine B will be released from PLGA microspheres *in vitro* following a diffusion, degradation regime of approximately one month

(2) Gefitinib will be released from PLGA microspheres *in vitro* following the same diffusion, degradation regime with a delay in release due to its hydrophobicity. Release is hypothesized to take approximately two months

(3) Immunoglobulin G will release *in vitro* for approximately six months, following a diffusion and degradation regime

(4) Lomustine will have an accelerated release from PCL microspheres over 5 days by using 5M NaOH

(5) When combined and released together, gefitinib will release first from PLGA microspheres then IgG from PLA microspheres

(6) PNIPAM will not significantly hinder the *in vitro* release of any of the model drugs or chemotherapeutics

(7) Aqueous PNIPAM can be applied as an aerosol to tissue at physiological temperature and will entrap drug encapsulated microspheres in a conformal layer on the tissue

3.3 Materials and Methods

3.3.1 Materials

3.3.1.1 Materials for In Vitro Drug Release

Microspheres and PNIPAM used in this section were formulated or synthesized in Chapter 2. Phosphate buffered saline (PBS; Sigma), sodium carbonate (Fisher Scientific, anhydrous), sodium bicarbonate (Fisher Scientific), citric acid monohydrate (Sigma), sodium phosphate dibasic (Sigma, anhydrous), MES sodium salt (Sigma,) hydrochloric acid (HCl; EMD, 12.1 M), sodium hydroxide (NaOH; Mallinckrodt Chemicals), dimethyl sulfoxide (DMSO; EMD),

rhodamine B (Sigma), gefitinib (Fisher, free base >99%), immunoglobulin G from sheep serum (IgG; Sigma, ≥95%, lyophilized powder), and lomustine (LMT; Enzo Life Sciences) were used as received.

3.3.2 Buffer Preparation

Buffers at pH 4, 6, 7.4, and 10 were prepared as described in Table 3.1 [120]. Small amounts of hydrochloric acid and sodium hydroxide were added to the buffer solutions to adjust pH level within ±0.1 of the target pH.

Table 3.1 Preparation of buffer solutions

pH	Component 1	mL component 1	Component 2	mL component 2
4	citric acid monohydrate, 0.1 M	61.45	sodium phosphate dibasic, 0.2 M	38.55
6	MES sodium salt, 0.01 M	100	N/A	-
7.4	PBS packet, 0.01 M	100	N/A	-
10	sodium carbonate, 0.1 M	60	sodium bicarbonate, 0.1 M	40

3.3.3 In Vitro Drug Release

3.3.3.1 Release from Microspheres

The *in vitro* drug release of rhodamine B encapsulated PLGA microspheres in PBS was determined using a concentration of 30 mg dry microspheres per 5 mL PBS. The different microspheres and formulation conditions are listed in Table 3.2. The dry microspheres were added to PBS, sonicated for 5 minutes, and placed on a shaker at 300 rpm, 37 °C. At specified time points (Appendix 14), the sample was removed and centrifuged at 3000 g and 4°C for 5

minutes. The supernatant was removed for measurement while the pellet was re-suspended to the original concentration and placed back on the shaker. The supernatant was measured using a Shimadzu UV-1601 ultraviolet-visible spectrophotometer with the wavelength dependent on the drug being studied (Table 3.2). A "blank" drug release was also conducted as described above, with the blank absorbance values subtracted out of the drug values. The amount of drug was then calculated using a standard curve (Appendix 1).

The release of gefitinib from PLGA microspheres followed the same protocol with a few modifications. Before centrifugation of the sample, 1 M HCl was added to obtain a PBS-1 M HCL 90-10 (v/v) solution. This was to prevent the ring opening of gefitinib and to increase gefitinib solubility [121]. After centrifugation, the supernatant was allowed to equilibrate for two days before measurement and passed through a 0.2 μm cellulose acetate syringe filter before measurement. Note that the release of gefitinib from PLGA microspheres was subjected to a 2.4 correction factor. We hypothesize that this is due to non-soluble polymer fragments adsorbing gefitinib that is then caught in the syringe filter. A correction factor was not necessary for the PNIPAM release discussed next. We hypothesize this is due to the PNIPAM retaining the polymer fragments, preventing the adsorption and subsequent drug loss. We will test this hypothesis at a later time.

The release of IgG from PLA microspheres followed the same protocol listed for RB-PLGA microspheres with the addition of using a 0.2 μm cellulose acetate syringe filter before measurement. For the accelerated release, PBS was replaced with a buffered solution at pH 4, 6, or 10.

For the combined release of gefitinib from PLGA and IgG from PLA, the same protocol was followed with a few modifications. Both GB-PLGA and IgG-PLA were present at a concentration of 30 mg/5 mL solution. PBS was replaced with pH 10 buffered solution and before centrifugation, 1 M HCl was added to obtain a pH 10-1 M HCL 80-20 (v/v) solution. This was to enhance the solubility of gefitinib. A 0.2 μm cellulose acetate syringe filter was used before each measurement. Additional controls included the individual release of GB-PLGA and IgG-PLA under the same conditions. The total contribution of the gefitinib release at the IgG UV-vis peak (283 nm) was subtracted from the 283 nm peak measurement of the combined release. The contribution of the IgG release at the gefitinib UV-vis peak (333 nm) was also subtracted from the 333 nm peak of the combined release. This was an attempt to remove any peak contribution that was from the drug not being studied, i.e., gefitinib contributing to a higher estimate of IgG and vice versa.

The release of lomustine from PCL followed the same basic protocol of RB-PLGA. For release in PBS, DMSO was added to the supernatant after centrifugation for lomustine solubility, ending with a final ratio of PBS-DMSO 55-45 (v/v). For accelerated release, PBS was replaced with 5 M NaOH-DMSO 65-35 (v/v). A 0.2 μm polytetrafluoroethylene syringe filter was used before each measurement.

Table 3.2 details the conditions of release along with the microsphere formulation parameters. All measurements were performed in triplicate with error propagated through the cumulative release and statistical significance analyzed with an unpaired t test.

Table 3.2 Microsphere release conditions

Drug	Polymer	Final Solvent	Wavelength (nm)	Microsphere Conditions
Rhodamine B	PLGA	PBS	536	2000 rpm, 1.5 mg RB
				2800 rpm, 1.5 mg RB
Gefitinib	PLGA	PBS-1 M HCL 90-10 (v/v)	333	2000 rpm, 1.5 mg GB, 3% PVA
				2800 rpm, 1.5 mg GB, 3% PVA
IgG	PLA	PBS	283	1260 rpm, 7.5 mg IgG, 30 mL W2, 10 mg IgG in W2, 5% PVA
				2800 rpm, 7.5 mg IgG, 30 mL W2, 10 mg IgG in W2, 5% PVA
		pH 4		2800 rpm, 7.5 mg IgG, 30 mL W2, 10 mg IgG in W2, 5% PVA
		pH 6		2800 rpm, 7.5 mg IgG, 30 mL W2, 10 mg IgG in W2, 5% PVA
		pH 10		2800 rpm, 7.5 mg IgG, 30 mL W2, 10 mg IgG in W2, 5% PVA
Gefitinib and IgG	PLGA and PLA	pH 10-1 M HCL 80-20 (v/v)	283 and 333	IgG: 2800 rpm, 7.5 mg IgG, 30 mL W2, 10 mg IgG in W2, 5% PVA GB: 2800 rpm, 1.5 mg GB, 3% PVA
Lomustine	PCL	PBS-DMSO 55-45 (v/v)	396	2800 rpm, 15 mg LMT, 30 mL W2, 5 mg LMT in W2, 5% PVA
		5 M NaOH-DMSO 65-35 (v/v)	344	2800 rpm, 15 mg LMT, 30 mL W2, 5 mg LMT in W2, 5% PVA

3.3.3.2 Release from Microspheres Entrapped in PNIPAM

The *in vitro* drug release of rhodamine B encapsulated PLGA microspheres from PNIPAM in PBS was determined using a concentration of 15 mg dry microspheres /1 mL PNIPAM/2.5 mL PBS. Initially, the dry microspheres were added to a 2.5% W_{PNIPAM}/V_{PBS} solution, formulated in Chapter 2. This solution was placed in a water bath at 40°C, allowing the PNIPAM to form a gel. Then, PBS at 40°C was added and the sample placed on a shaker at 250 rpm, 37 °C. At specified time points (Appendix 14), the liquid surrounding the PNIPAM pellet was removed. The sample was centrifuged at 3000 and 4°C for 5 minutes, the supernatant removed for measurement, and the pellet re-suspended with PBS at 40°C and placed back on the PNIPAM. Then, the absorbance of the supernatant was measured at 536 nm. A "blank" drug release was also conducted. The blank absorbance values were subtracted from the drug absorbance values. The amount of drug was then calculated using a standard curve (Appendix 1).

For the release of gefitinib from PLGA microspheres entrapped in PNIPAM, the same steps were followed with a few modifications. Before centrifugation, 1 M HCl was added to the sample to obtain a 90:10 v/v PBS:1 M HCl solution. This was to prevent the ring opening of gefitinib and to increase gefitinib solubility. After the supernatant was removed, it was allowed to equilibrate for two days, passed through a 0.2 μm cellulose acetate syringe filter, and measured at 333 nm.

Table 3.3 details the conditions of release along with the microsphere formulation parameters. All measurements were performed in triplicate with error propagated through the cumulative release and statistical significance analyzed with an unpaired t test.

Table 3.3 Release conditions of microspheres entrapped in PNIPAM

Drug	Polymer	Solvent	Wavelength (nm)	Microsphere Conditions
Rhodamine B	PLGA	PBS	536	2000 rpm, 1.5 mg RB
				2800 rpm, 1.5 mg RB
Gefitinib	PLGA	PBS-1 M HCL 90-10 (v/v)	333	2800 rpm, 1.5 mg GB, 3% PVA

3.3.4 Ex Vivo Spray Application of Rhodamine B-PLGA Microspheres in PNIPAM

The spray application of PNIPAM and rhodamine B encapsulated PLGA microspheres was performed *ex vivo* on rats provided by the Animal Use Training Program at the University of Washington. First, dry rhodamine B encapsulated PLGA microspheres (1.5 mg initial loading, 44 ± 11 μm) were added to aqueous PNIPAM (2.5% W_{PNIPAM}/V_{PBS}) in a travel perfume bottle (Bartell Drugs) at a concentration of 30 mg microspheres/5 mL PNIPAM. Then, four "pumps" of the RB-PLGA-PNIPAM formulation was applied as an aerosol to the exposed rat brain (maintained at 37°C) and imaged. Images were taken with a SMZ15000 stereoscope with epi-

fluorescence capability (P-FL GFP-L; GFP long pass emission, Ex: 480 / 40, Em: 510 LP, Dichroic: 505) An additional 6 pumps were added for comparison. Finally, the PNIPAM was removed, first with tweezers to test adhesion and then with cold water. As controls, untreated exposed brain and a rat brain with four pumps of blank PNIPAM solution were imaged.

3.4 Results

3.4.1 In Vitro Release of Rhodamine B from PLGA Microspheres and PLGA Microspheres Entrapped in PNIPAM

The release profile of rhodamine B from PLGA microspheres was the only rhodamine B release studied due to PLGA's higher encapsulation efficiency when compared to PLA and PCL. Figure 3.4 shows the release of rhodamine B from two different sizes of PLGA microspheres suspended in PBS at 37°C. The release of rhodamine B from PLGA microspheres entrapped in PNIPAM was also determined (Figure 3.5). Figure 3.6 compares the release from free microspheres and microsphere entrapped in PNIPAM for the smaller microsphere set, 22.9 ± 8.0 µm in diameter. The comparison of the second, larger microsphere set is in Appendix 15.

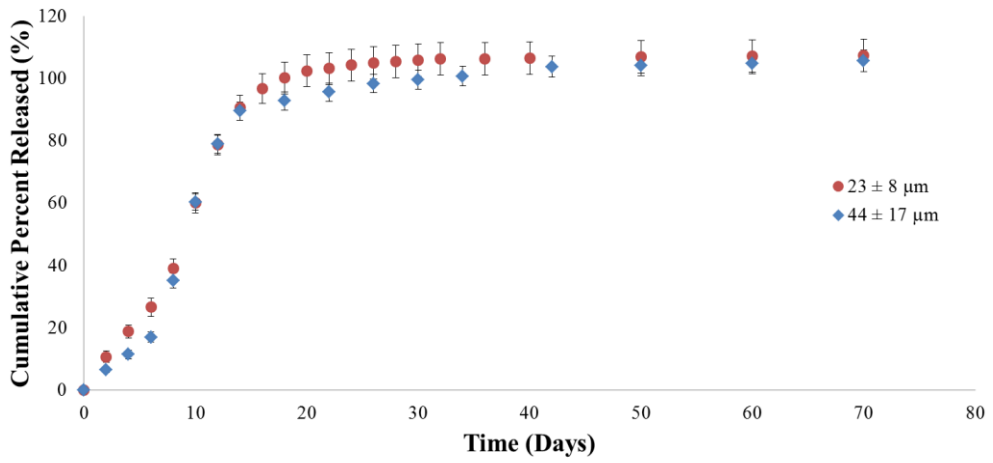

Figure 3.4: *In vitro* release of rhodamine B from PLGA microspheres suspended in PBS at 37°C and gently shaken, n=3.

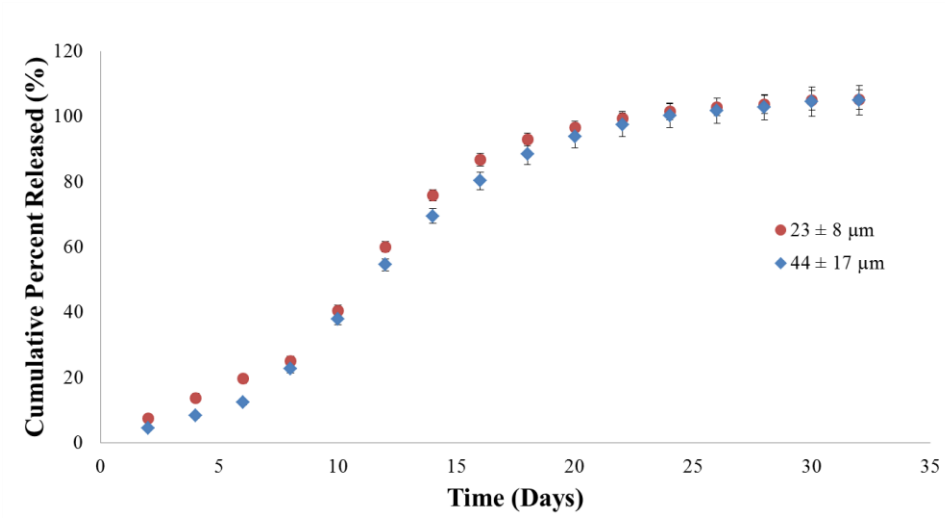

Figure 3.5: *In vitro* release of rhodamine B from PLGA microspheres entrapped in PNIPAM and suspended in PBS at 37°C and gently shaken, n=3.

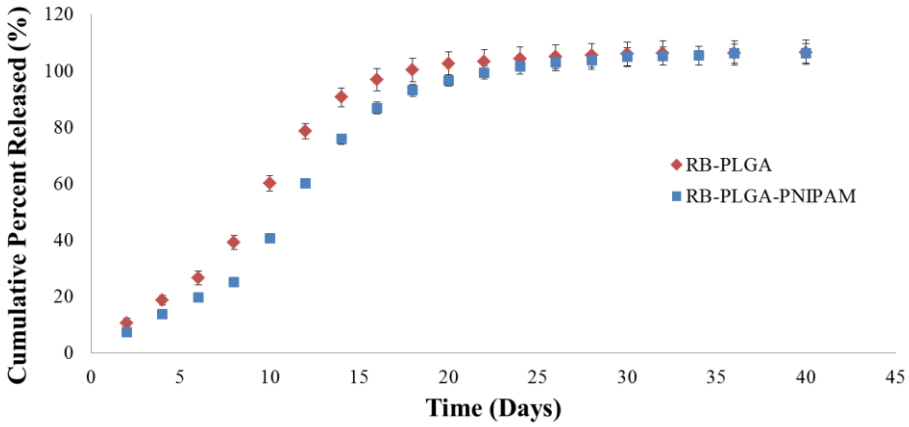

Figure 3.6: *In vitro* release of rhodamine B from PLGA microspheres and microspheres entrapped in PNIPAM, suspended in PBS at 37°C and gently shaken, n=3, diameter: 23 ± 8 µm.

3.4.2 In Vitro Release of Gefitinib from PLGA Microspheres and PLGA Microspheres Entrapped in PNIPAM

Gefitinib was the first chemotherapeutic to be encapsulated and the first drug to have its release elucidated. Figure 3.7 shows the release of gefitinib from PLGA microspheres suspended in PBS. Two different particle size distributions were studied.

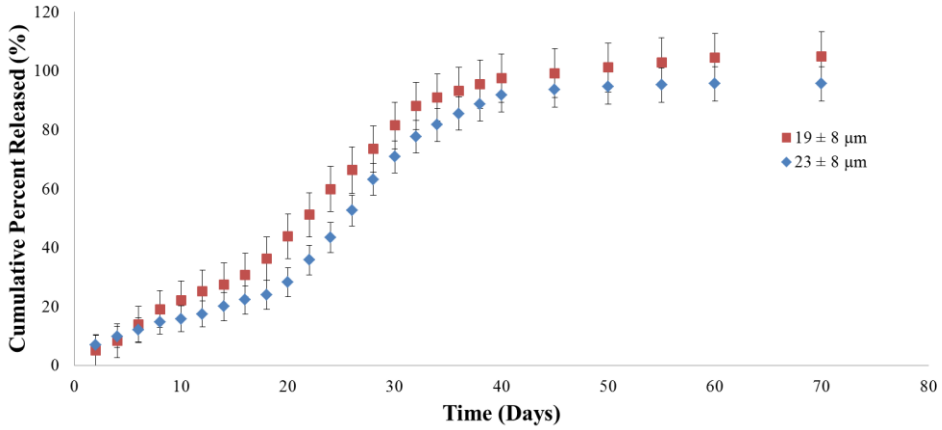

Figure 3.7: *In vitro* release of gefitinib from PLGA microspheres suspended in PBS at 37°C and gently shaken, n=3.

Figure 3.8 compares the release of microspheres and microsphere entrapped in PNIPAM for the smaller set of GB-PLGA microspheres (19 ± 8 µm). Only the smaller set was studied since a statistically significant difference was not seen between the two release profiles in Figure 3.7 ($p < 0.05$).

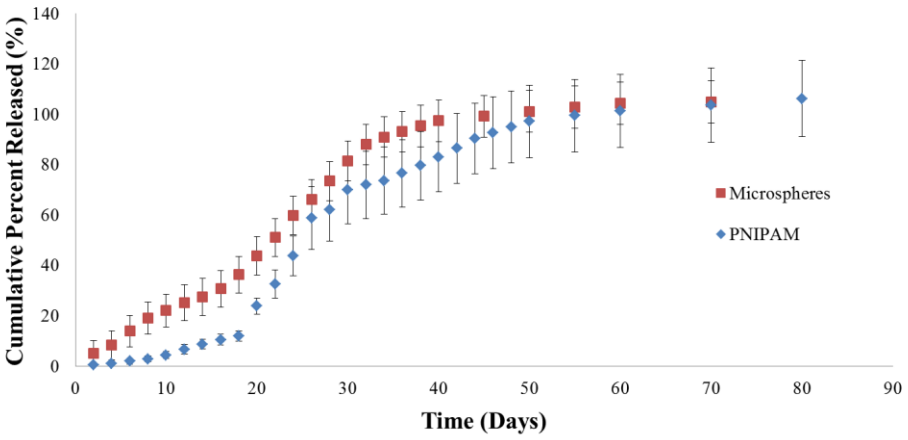

Figure 3.8 *In vitro* release of gefitinib from PLGA microspheres and microspheres entrapped in PNIPAM, suspended in PBS at 37°C and gently shaken, diameter: 19 ± 8 µm, n=3.

3.4.3 In Vitro Release of IgG from PLA Microspheres

The second drug to be encapsulated and studied for release was IgG, a model antibody for the chemotherapeutic, bevacizumab. Figure 3.9 shows the release of IgG from PLA microspheres suspended in PBS at 37 °C. Note that two distinct size sets of IgG-PLA were studied. Also, the error shown in Figure 3.9 is the error per day instead of the cumulative error as shown in previous release graphs. To see the release of IgG from PLA with cumulative error, refer to Appendix 16.

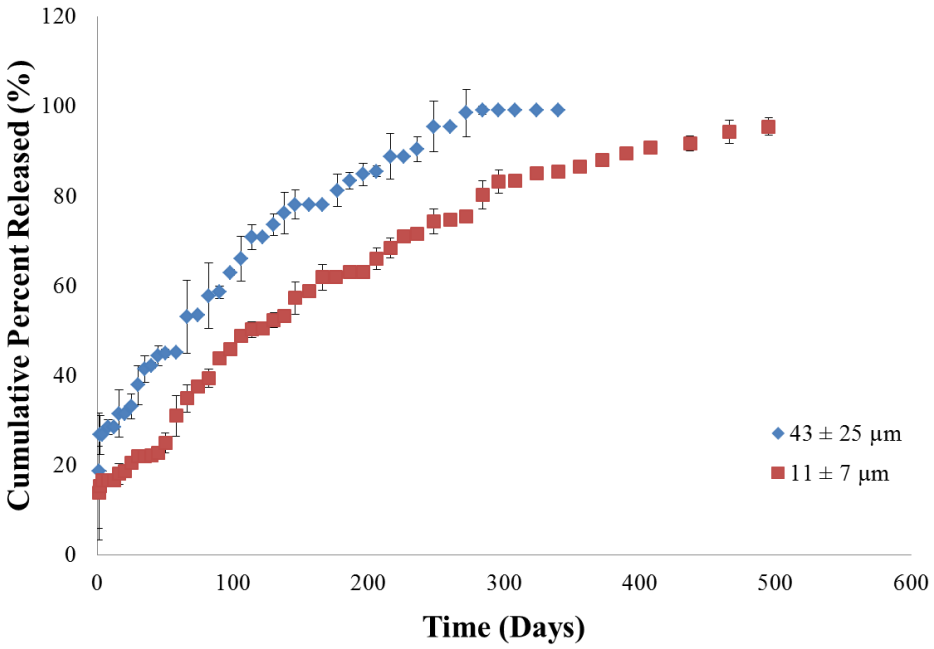

Figure 3.9 *In vitro* release of IgG from PLA microspheres suspended in PBS at 37°C and gently shaken, n=3. Error is per day.

Due to the release of IgG occurring over one year in PBS, release of IgG from PLA microspheres in various pH solutions was studied to determine which pH level caused the quickest release of IgG. Figure 3.10 shows the release of IgG from PLA microspheres at pH 4, 6, and 10 compared to IgG release at pH 7.4.

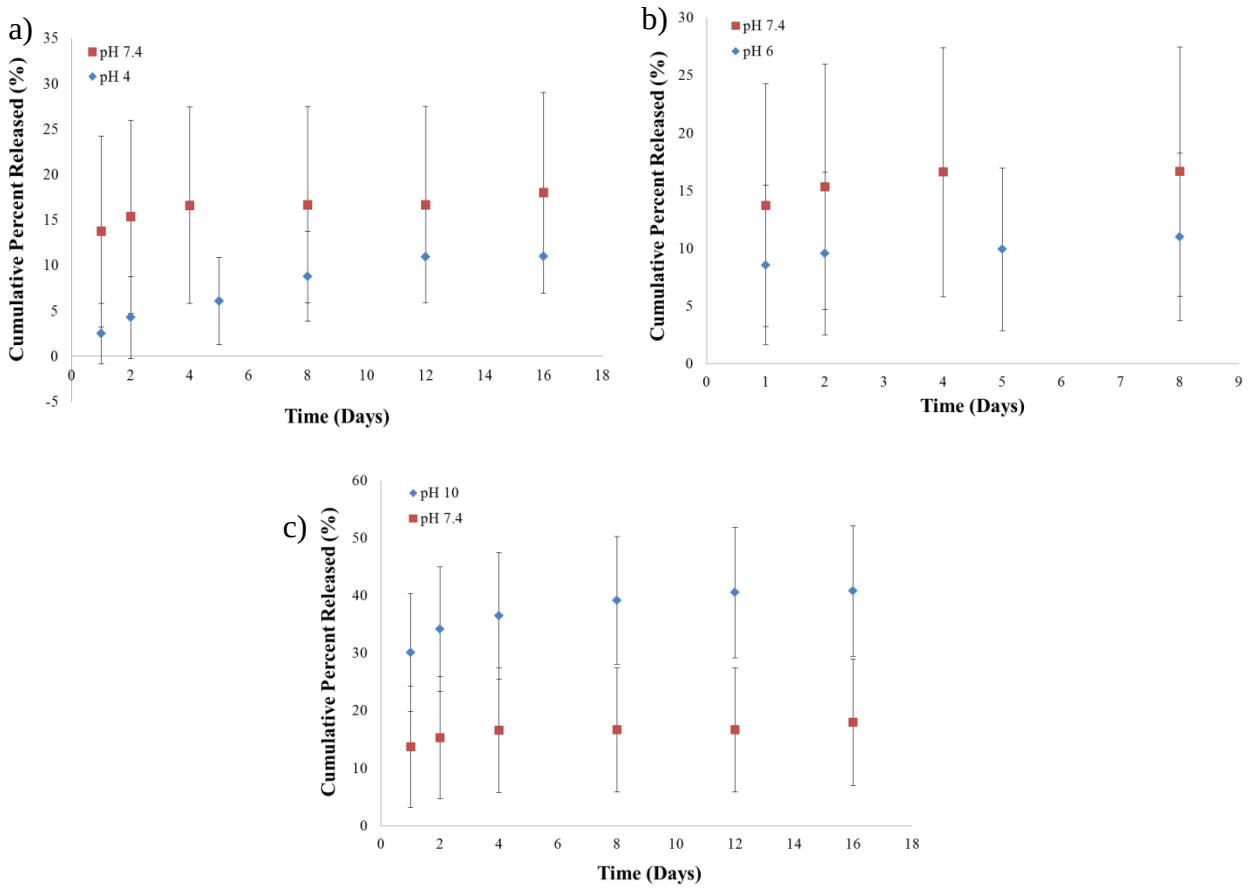

Figure 3.10 *In vitro* release of IgG from PLA microspheres suspended in pH 4, 6, 7.4, and 10 at 37°C and gently shaken: a) pH 4 and pH 7.4, b) pH 6 and 7.4, and c) pH 7.4 and 10, n=3.

3.4.4 Combined In Vitro Release of Gefitinib from PLGA microspheres and IgG from PLA Microspheres

To achieve a better understanding of the drug release that the overall DREAM BIG Therapy system would achieve, gefitinib encapsulated PLGA microspheres and IgG encapsulated PLA microspheres were combined together in pH 10 and their release studied (Figure 3.11). For comparison, separate releases of GB-PLGA and IgG-PLA in pH 10 were also elucidated to determine if the first drug release would significantly increase or inhibit the second drug release.

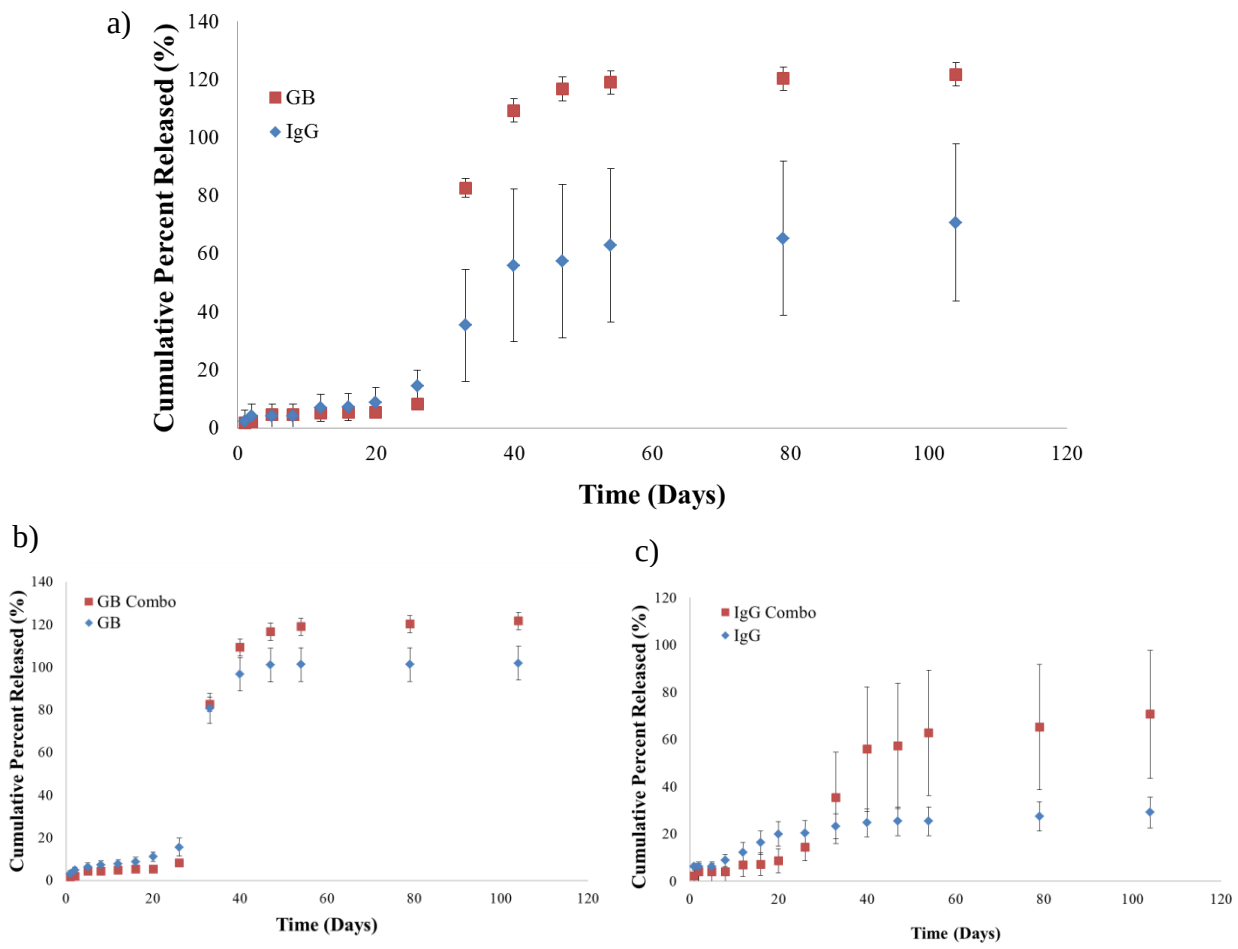

Figure 3.11 The combined *in vitro* release of gefitinib from PLGA and IgG from PLA at pH 10 maintained at 37°C and gently shaken: a) combined release of GB-PLGA and IgG-PLA, b) comparison of gefitinib release from the combination release and the single release of GB-PLGA at pH 10, and c) comparison of IgG release from the combination release and the single release of IgG-PLA at pH 10, n=3.

3.4.5 In Vitro Release of Lomustine from PCL microspheres

Lomustine was the last chemotherapeutic to be encapsulated and studied for release. To determine if the LMT-PCL microspheres had an initial burst release, a short term, four day release study in PBS was conducted. After four day, a negligible release of ~1% was achieved

for lomustine from PCL microspheres. Due to PCL's potential for long-term degradation, up to two to four years, an accelerated study was conducted using 5 M NaOH-DMSO 65-35 (v/v), as shown in Figure 3.13 [122-124]. Since lomustine degrades in aqueous solutions, the degradation rate of free lomustine in both PBS and 5 M NaOH-DMSO was determined (Figure 3.12) and applied as a correction to the release of lomustine from PCL microspheres.

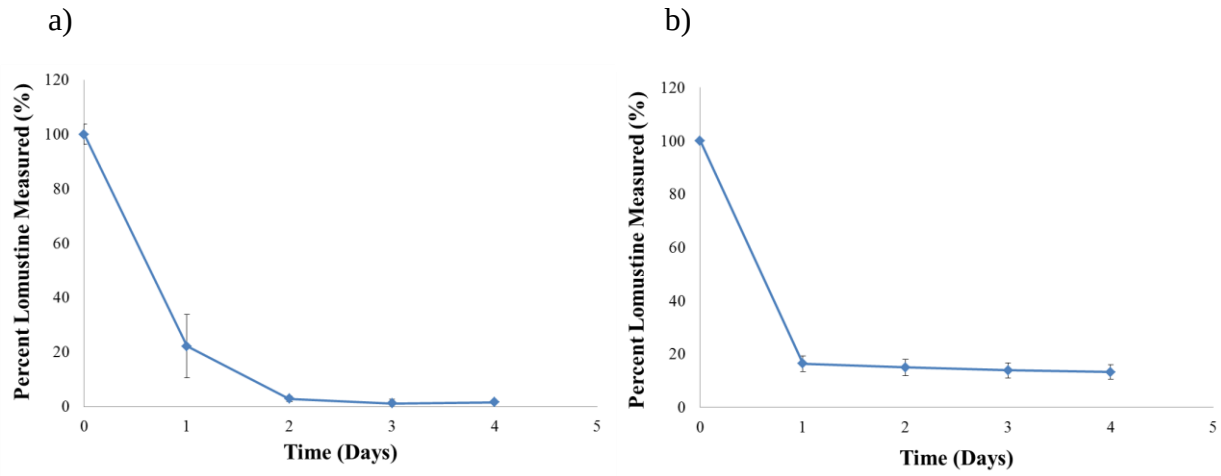

Figure 3.12 The degradation of lomustine in aqueous solutions a)PBS at 37°C and b) 5 M NaOH-DMSO 65-35 (v/v), n=3.

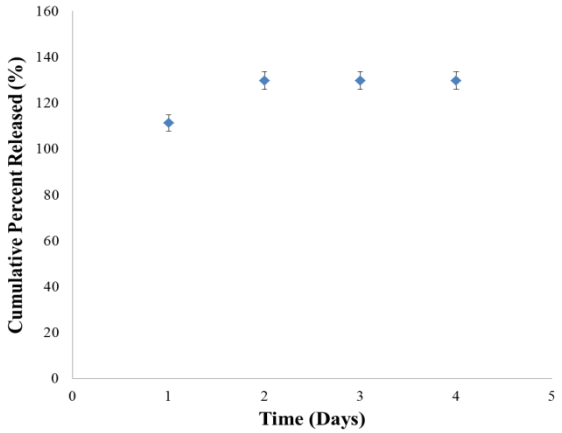

Figure 3.13 The *in vitro* release of lomustine from PCL microspheres in 5 M NaOH-DMSO 65-35 (v/v), n=3.

3.4.6 Aerosolized Application of Rhodamine B-PLGA Microspheres in Degradable PNIPAM

The aerosolized delivery of RB encapsulated PLGA microspheres formulated in degradable PNIPAM (2.5% W_{PNIPAM}/V_{PBS}) was tested *ex vivo* on rats maintained at physiological temperature. As a control, initial tests imaged non-treated brain tissue, both bright field and fluorescence, and blank PNIPAM applied to the tissue (no microspheres), shown in Figure 3.14a, b, and c, respectively. Then rhodamine B encapsulated PLGA microspheres were added to the PNIPAM solution and four pump sprays applied (Figure 3.15) before an additional 6 pumps were added (Figure 3.16). The PNIPAM layer was then physically removed with tweezers and in a second, separate sample, the top layer of an untreated, exposed brain was removed for comparison (Figure 3.17).

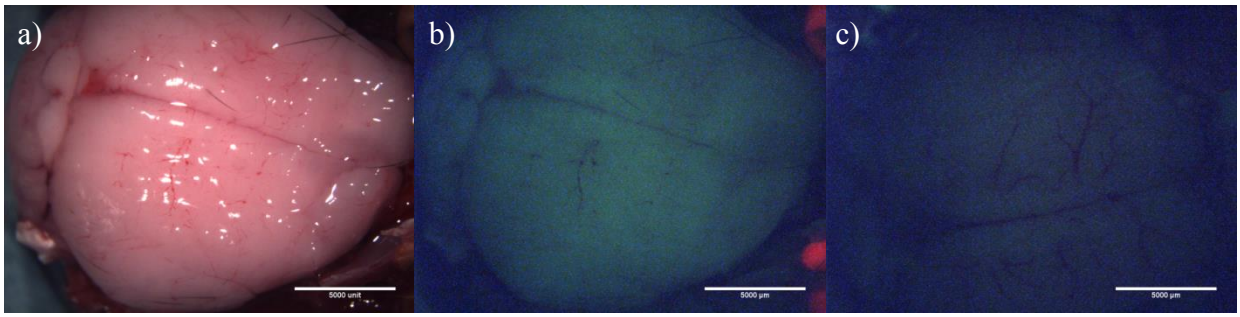

Figure 3.14: Images of an untreated rat brain: a) bright field and b) fluorescence microscopy and c) a rat brain with PNIPAM applied in spray form (4 pumps) imaged with fluorescence microscopy. Scale bar is 5000 µm.

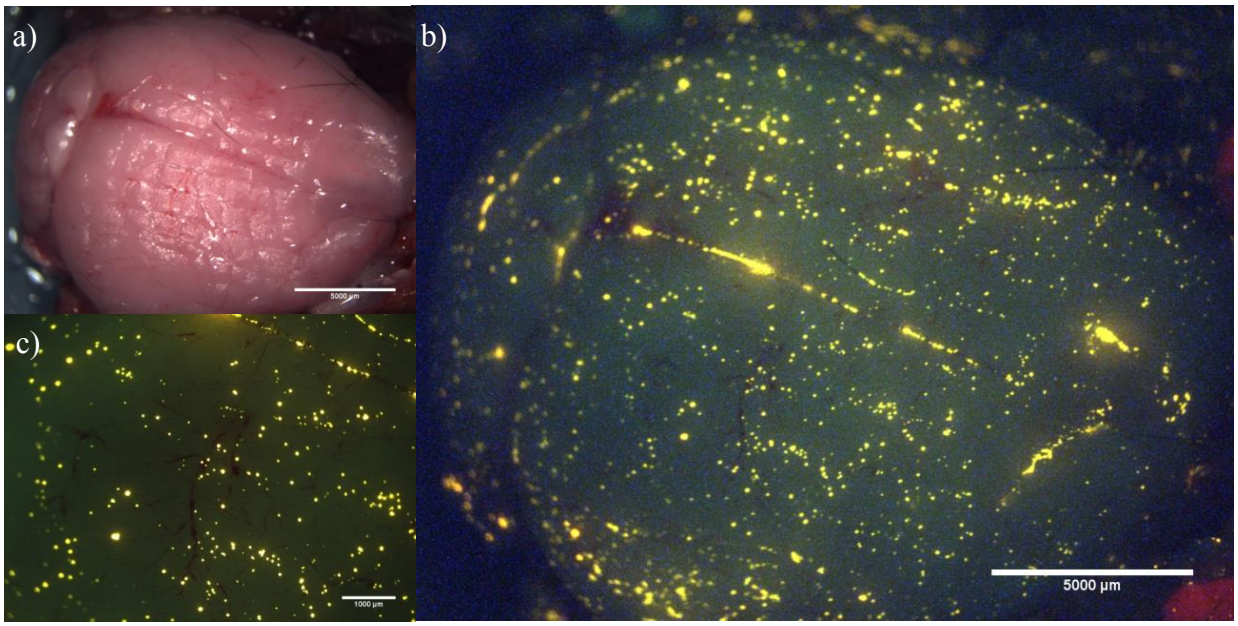

Figure 3.15: A rat brain sprayed with four pumps of rhodamine B encapsulated PLGA microspheres suspended in PNIPAM solution imaged with a) bright field (scale bar 5000 µm), b) fluorescence (scale bar 5000 µm) and c) fluorescence microscopy (scale bar 1000 µm).

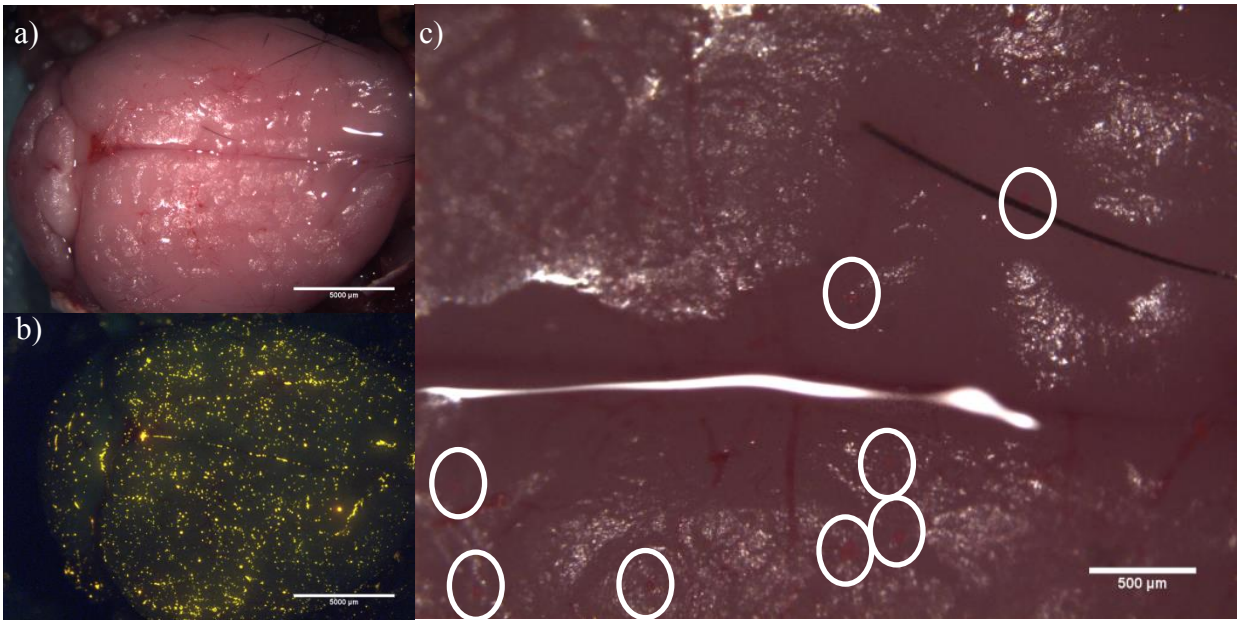

Figure 3.16: A rat brain sprayed with ten total pumps of rhodamine B encapsulated PLGA microspheres suspended in PNIPAM solution imaged with a) bright field (scale bar 5000 µm), b) fluorescence (scale bar 5000 µm) and c) bright field microscopy with visible microspheres circled (scale bar 500 µm).

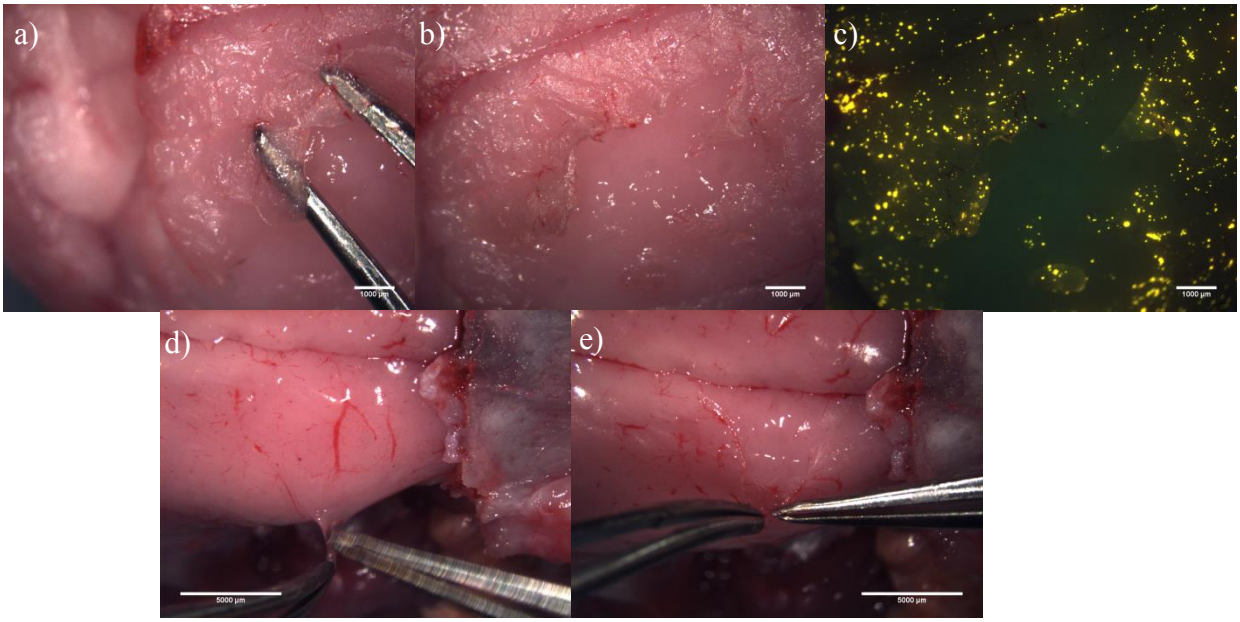

Figure 3.17: Removal of the exposed layer of a rat brain: a) ten total pumps of rhodamine B encapsulated PLGA microspheres suspended in PNIPAM being removed and showing the disruption in the PNIPAM layer with b) bright field and c) fluorescence microscopy, d) a rat brain without PNIPAM and the exposed layer being removed and e) demonstrating the thinness of the removed layer. Scale bar for a-c is 1000 µm and for d-e is 5000 µm.

3.5 Discussion

The studies detailed in Chapter 3 are focused on the *in vitro* release of a model drug, rhodamine B, and three chemotherapeutics from the polymeric microspheres developed in Chapter 2. For all studies, microspheres were suspended in solution at 37°C and gently shaken to simulate physiological conditions. The solution was completely removed and replaced at certain time points in an attempt to model the conditions of the cerebral spinal fluid, which has a net turnover of 3.7 times a day [125]. While this is a simplistic model, it is the standard for determining the *in vitro* release of chemotherapeutics from polymeric microspheres [27, 49, 51, 52].

Rhodamine B was the first molecule studied for release from PLGA microspheres. Only PLGA microspheres were studied due to its high rhodamine B encapsulation efficiency when compared to PLA and PCL (Figure 2.11). In addition, the polymer in use, PLGA 50/50, should have the shortest release time of approximately one to two months [126]. As can be seen in Figure 3.4, a 20 day release was achieved. This release can be broken down into two distinct regimes, passive diffusion and polymer degradation. From day 0 through day 6, there is an initial, moderate continuous release due to the microspheres becoming hydrated and the dye passively diffusing into PBS. After day 6, there is a significant increase in the release curve slope from the polymer bulk degrading via hydrolysis and the dye being released before the release curve plateaus off after day 18. This type of diffusion-degradation release profile has also been described by Zhang et al. and Yemisci et al. [23, 78].

During the six day diffusion phase, the smaller microspheres released significantly faster due to their larger surface area to volume ratio ($p < 0.05$). This demonstrates a method for tuning the release profile based on particle size. An initial burst release was not present, characteristic of several other types of polymeric microsphere systems [41, 42, 46, 52-54]. This initial burst is a concern; if too much drug is released at once, a toxic overdose could result. We hypothesize that the three wash steps conducted during microsphere formulation removes any of the surface localized dye (as shown with SEM in Figure 2.10) that would contribute to a burst release.

When the microspheres were entrapped in PNIPAM and then suspended in PBS, a similar biphasic profile was demonstrated (Figure 3.5). From day zero to day 8, a moderate release attributed to diffusion occurred before the release increased as the polymer bulk degraded from

day 8 to day 22. Again, the smaller microspheres released faster from day zero to day 6 of the diffusion phase due to their smaller diameters ($p < 0.05$). When the release through PNIPAM is compared to the release from free microspheres (Figure 3.6, Appendix 15), the PNIPAM is shown to delay rhodamine B release by approximately two days. This delay is statistically significant from day 4 to day 18 ($p < 0.05$). While this means that PNIPAM does present a barrier to the release of the dye from the microspheres, the main control for release tunability will be from the microsphere design.

Gefitinib was the first chemotherapeutic whose release rate was studied. As can be seen in Figure 3.7, the overall release time was roughly doubled for gefitinib when compared to rhodamine B. Yet, the biphasic release profile is still apparent. For the first 18 days, there was a slow, moderate release attributed to passive diffusion without an initial burst release. After day 18 through day 40, there was a sharp increase in the release of gefitinib as the PLGA bulk degraded before the release plateaued off through day 70. Since the particle size distributions of the two GB-PLGA sets were similar, a significant difference between the releases was not seen ($p < 0.05$).

There are several possible reasons why the gefitinib release was doubled when compared to the rhodamine B release. First, the PLGA microspheres that encapsulated gefitinib were made by the single emulsion methodology while the rhodamine B encapsulated PLGA microspheres were formulated using the double emulsion. The single emulsion microspheres could be denser and less porous internally due to the absence of an inner water phase that would create pockets in the oil of a double emulsion. This denser polymer microsphere would then slow the water penetration that would release the drug. To gain insight into the internal structure of the

microspheres, confocal microscopy or sectioning the microspheres and light microscopy could be used. Secondly and perhaps more importantly, gefitinib is more hydrophobic than rhodamine B, from < 1 mg/mL solubility for gefitinib in water to 50 mg/mL for rhodamine B [109, 127]. Therefore, based on solubility alone, rhodamine B should release sooner in PBS than gefitinib, all other factors remaining the same.

When gefitinib encapsulated PLGA microspheres were entrapped in PNIPAM (GB-PLGA-PNIPAM), a delayed release of approximately 6-8 days was demonstrated through day 24 (Figure 3.8). This longer delay in release of gefitinib when compared to rhodamine B's approximate two days is most likely from the hydrophobicity of gefitinib. The delay was statistically significant from day 10-24, the second half of the diffusion phase and the first few days of the degradation phase ($p < 0.05$). We hypothesize this comes from the gefitinib remaining in the microsphere and PNIPAM as long as possible before the microsphere significantly degraded and gefitinib was released into the aqueous solution. After day 24 of the degradation phase, there is no longer a statistical difference in the release from the free microspheres and microspheres entrapped in PNIPAM, supporting the idea that PNIPAM does not provide a significant barrier to drug release by itself.

PNIPAM was also tested as a carrier for free gefitinib. At time zero, right after PNIPAM gelation, a full release of gefitinib was detected. This indicates that gefitinib was not entrapped in PNIPAM but rather exuded out with the PBS as PNIPAM phase transitioned. This means that microspheres will be necessary to achieve a sustained release of gefitinib.

The second molecule that was studied for release was the model antibody, IgG. Two distinct particle sizes were studied: 11 ± 7 μm (Set A) and 43 ± 25 μm (Set B) in diameter. Both microsphere sizes were formulated at 7.5 mg initial IgG loading with an external aqueous phase concentration of 33% IgG (w/v). However, for Set A, the encapsulation efficiency and drug loading was high at 88 ± 12% and 0.32 ± 0.05%, respectively. Set B, on the other hand, had a low encapsulation efficiency of 34 ± 11% and drug loading of 0.13 ± 0.03%. As discussed in Chapter 2, this was attributed to the different particle sizes and the competing factors of the drug diffusion out of the sphere versus the rate of drug entrapment from sphere hardening. As shown in Figure 3.9, the release of IgG from PLA microspheres was dependent on the microsphere formulation. Set A had an initial burst release of 13 ± 11% followed by a near linear release over 495 days or over 16 months. Set A is still releasing to this date. Set B also had an initial burst release of 19 ± 13%. Then, a near linear release was achieved over the full release of 284 days or over nine months.

It is hypothesized that the burst releases are due to IgG located on or near the surface of the PLA microspheres. For Set A, the SEM micrograph in Figure 2.18b shows bumps on the surface while Figure 2.18c for Set B has material present at the surface. Following the hypothesis of the precipitation kinetics described in Chapter 2, the bumps in Set A could be attributed to pockets of IgG that were diffusing towards the external aqueous phase and entrapped as the sphere hardened. These bumps are not present on the larger microspheres in Set B because of the longer time for sphere hardening, allowing the IgG to fully diffuse. Instead, the material that is seen via SEM could be residual IgG from the external aqueous phase that was not fully washed off during microsphere formulation. Taking this under consideration, Set B, with more IgG readily

available on the surface, would have a higher initial burst while Set A, with IgG under the polymer surface, would have a smaller initial burst. Note that Figure 3.9 reports the error per day rather than the cumulative error and that there is no statistical difference between the release of Set A and Set B ($p < 0.05$). This is from the high cumulative error that largely derives from the variation in burst releases. To see Figure 3.9 with cumulative error, reference Appendix 16. While the release of IgG from PLA microspheres entrapped in PNIPAM was not evaluated, it is hypothesized that PNIPAM will not severely hinder the release of IgG beyond a few days, as it did for rhodamine B. When tested, PNIPAM fully released free IgG after two days (Appendix 17). Therefore, the control in release will come from tuning the microsphere formulation.

One of the novel characteristics of DREAM BIG Therapy is the idea of different polymer microspheres releasing several chemotherapeutics sequentially. As shown in Figure 3.18, when the release of gefitinib from PLGA and IgG from PLA (Set A, 11 ± 7 μm) in PBS are plotted together, a sequential, step release is achieved. After an initial burst release from IgG-PLA, the release of IgG remains relatively low through day 50. During this window of minimal IgG release, gefitinib completely releases. After day 50, an increase in IgG release is seen and maintained through the end of the study. When Set B (43 ± 25 μm) of IgG-PLA is plotted against the gefitinib release, an overlapping release is achieved (Figure 3.19). Instead of plateauing for 50 days after the initial burst release, IgG steadily releases, coinciding with the release of gefitinib from PLGA microspheres. These two different release types allow flexibility in the choice of therapeutic care. The microsphere sets can be chosen based on whether an overlapping or sequential release is more beneficial, allowing for a personalized health care approach.

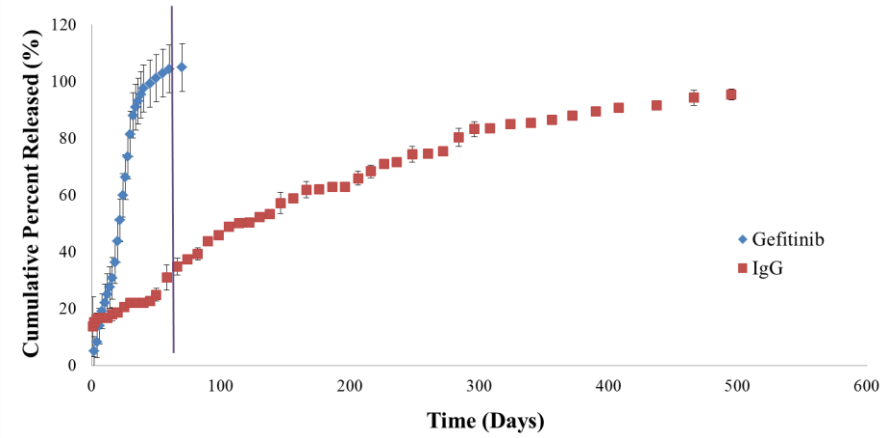

Figure 3.18 The step release of gefitinib from PLGA microspheres and IgG from PLA microspheres in PBS at 37°C and gently shaken, n=3. The line represent where GB release ends and IgG release begins. GB-PLGA was formulated with 1.5 mg GB initial loading and 2800 rpm. IgG-PLA was formulated with 7.5 mg IgG initial loading, 33% IgG (w/v) in the external, aqueous phase, and 2800 rpm.

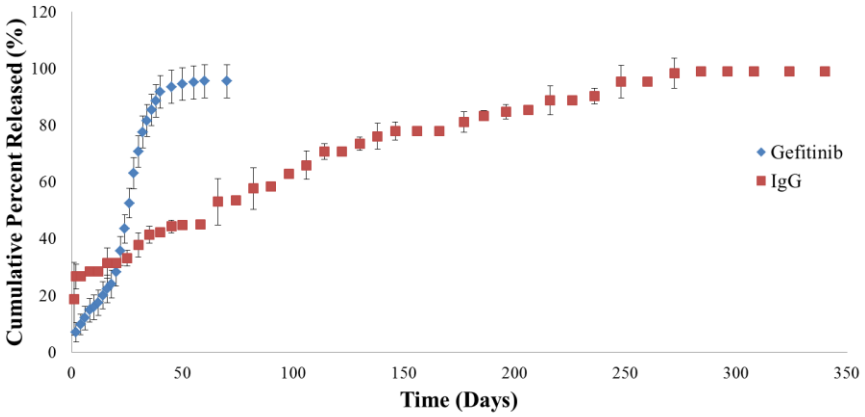

Figure 3.19 The overlapping release of gefitinib from PLGA microspheres and IgG from PLA microspheres in PBS at 37°C and gently shaken, n=3. GB-PLGA was formulated with 1.5 mg GB initial loading and 2800 rpm. IgG-PLA was formulated with 7.5 mg IgG initial loading, 33% IgG in the external, aqueous phase, and 1260 rpm.

As a proof of concept, gefitinib-PLGA and IgG-PLA were placed in the same media to demonstrate a combination release versus the separate releases that were plotted together and

previously described. However, since the release of IgG-PLA was over one year in PBS, an accelerated media was used to shorten the time span of the study. Figure 3.10 shows several different buffers at both acidic and basic pHs that were tested, with the most basic buffer at pH 10 increasing the release rate of IgG from PLA the most. This supports what has been reported in the literature, that pH extremes such as pH 10 and 2 increase the degradation rate of PLA [128-130]. Using these results, GB-PLGA and IgG-PLA were combined in pH 10 buffer solution and their release determined.

As can be seen in Figure 3.11a, gefitinib is fully released in forty days with the bulk of the release occurring between day 26 and day 40. While GB's release in pH 10 is similar to its release in PBS, there are two things to note during this time period. First, GB released to approximately 120%. Secondly, IgG is shown to also be releasing in this time, which is not similar to the release of IgG in PBS. It is hypothesized that the method of detection, UV-vis spectroscopy, is the cause of these two trends. When the combined release is measured, it is possible that the spectrum of gefitinib could interfere and contribute to the IgG spectrum and vice versa. In an attempt to properly baseline the measurements, the release of GB and IgG were measured separately at pH 10 and the contribution of GB to the measurement peak of IgG was removed and vice versa. However, as Figure 3.11a shows, this did not fully correct the baseline. Figure 3.11c shows the release of IgG in pH 10 from the combined release compared to the singular release of IgG in pH 10. It is noted that the combined release has a higher value when compared to the single release, possibly an effect of GB's spectrum. This is further supported when IgG's release slows down after day 40, coinciding with GB no longer releasing. While GB appears to significantly affect the quantification of IgG release, the reverse is not true. As Figure

3.11b shows, the combined and single release of GB from PLGA are approximately the same, with no significant difference between the releases ($p < 0.05$). A better study design would be to repeat this experiment and use a method of detection that could separate the molecules, such as high performance liquid chromatography (HPLC), and then quantify with a UV-vis or mass spectrometer [131].

Interestingly, in this experiment at pH 10, a burst release was not noted for IgG either in combination with GB or singularly. This is contradictory to the preliminary study of IgG release from PLA at pH 10 shown in Figure 3.10. It is hypothesized that this reduction in release is due to the addition of 1 M HCl before the pH 10 solution is removed for measurement. The 1 M HCl was added to increase the solubility of GB, but it appears to have an adverse effect on IgG release. After addition of the 1 M HCl, the pH was approximately 1.1. This is lower than the 3.86 pKa of lactic acid and the isoelectric point for sheep IgG (5-7.2) [132, 133]. In addition, it was reported that fragments of IgG are unstable at a pH less than 5.1 [134]. All of these factors could play a role in why IgG was not measured. Future experiments should use HPLC to avoid this issue.

The last chemotherapeutic-microsphere combination to be studied *in vitro* was lomustine encapsulated in PCL microspheres. Unlike GB-PLGA and IgG-PLA, the release of lomustine from PCL in PBS was not studied long term. This is due to PCL's slow degradation rate, estimated at two to four years depending on the starting molecular weight [122-124]. Therefore, a method capable of accelerating the release of lomustine from PCL was investigated. These options included enzymatic, thermal, and base-promoted hydrolytic degradation [123, 124].

Hydrolytic degradation using 5 M NaOH was chosen due to the simplicity of implementation. In addition, the high temperatures of thermal degradation could deform the polymeric microspheres and enzymes would degrade antibodies such as IgG if a comparison study was conducted, removing these methods from consideration.

Figure 3.13 shows that after two days, a full release of lomustine from PCL microspheres was achieved in 5 M NaOH-DMSO 65-35 (v/v). This is a rough model of release because lomustine degrades in aqueous solutions and has a half-life of 71 minutes in 50 mM PBS [135]. To correct for this degradation, the rate of free lomustine degradation in 5 M NaOH-DMSO was also determined and applied to the release (Figure 3.12b). It is expected that this will produce an overestimate of lomustine degradation when applied to release from microspheres because the entirety of the lomustine is subject to degradation when it is "free" in solution. However, the PCL microspheres could provide a limited protection before becoming completely degraded. This is demonstrated in Figure 3.13, where the release of lomustine from PCL microspheres finished at 130%.

As a control, the release of lomustine from PCL microspheres in PBS was determined over four days. This release followed a similar protocol, with the degradation of free lomustine in PBS determined and used as a correction for lomustine release from the PCL microspheres (Figure 3.12). A negligible release was achieved, approximately 1% over four days.

The aerosolized delivery of PNIPAM to tissue at physiological temperature *ex vivo* was also tested in this chapter. Initial images were taken of an untreated brain and blank PNIPAM sprayed

on the brain to show their limited background contribution (Figure 3.14). The aqueous solution of degradable PNIPAM suspending rhodamine B encapsulated PLGA microspheres was then successfully aerosolized and applied to tissue at physiological temperature. As can be seen in Figure 3.15 and Figure 3.16, the PNIPAM entrapped the microspheres on the surface of the brain and provided a relatively homogenous distribution of the microspheres on the surface. This system conformed to the convoluted surface morphology of the brain, demonstrated by the microspheres that line the junction or fissure between the two cerebral hemispheres. The entrapped rhodamine B encapsulated microspheres were detected without fluorescence when magnified (Figure 3.16c). Additionally, the application of PNIPAM changed the appearance of the exposed brain, from a shiny, mucosal dura in Figure 3.14a to a matte surface appearance shown in Figure 3.16a. Interestingly, the PNIPAM formed a stiff, adherent layer on the surface of the brain, that when removed with tweezers, also removed the top layer of the exposed brain including blood vessels (Figure 3.17). Comparatively, the removal of the top layer of the untreated, exposed brain was difficult and shredded easily. The PNIPAM layer was easily removed when bathed in water slightly below room temperature. This easy removal was expected based on the results of PNIPAM used as an adhesive glue for retinal implants; the PNIPAM adhesion was reversible by lowering the temperature [115].

3.6 Conclusions

The first part of this work focused on determining the release profile of rhodamine B, gefitinib, IgG, and lomustine from microspheres *in vitro*. We determined that the overall release from PLGA microspheres can be tuned from 20 days to 40 days by using either a hydrophilic (rhodamine B) or hydrophobic (gefitinib) compound, respectively. In addition, the release from

PLGA is characterized by a biphasic profile: passive diffusion and then polymer degradation. Particle size was found to effect release rate with smaller microspheres releasing faster due to their larger surface area to volume ratio. When microspheres were entrapped in PNIPAM, it was discovered that the release was only delayed by two to eight days depending on drug properties. Thus, while PNIPAM will delay release to some extent, the microspheres are the main controls for tuning the release profile.

The release of IgG from PLA microspheres exhibited an initial burst release followed by a near linear release until full release was achieved. The burst release and length of release was dependent on microsphere formulation, with the distribution and amount of IgG playing a pivotal role. For larger, lower loaded IgG-PLA microspheres, release can extend as long as 284 days. However, for smaller, higher loaded IgG-PLA microspheres, release can be extended longer than 495 days.

When the release of gefitinib from PLGA and IgG from PLA were plotted together, either a sequential step release or overlapping release could be achieved. This demonstrates the potential of flexibility in the choice of therapeutic care. Therapeutic microsphere sets can be chosen based on whether an overlapping or sequential release is more beneficial, allowing for a personalized health care approach.

A proof of concept was attempted, where gefitinib-PLGA and IgG-PLA were released together in pH 10 buffered solution. While initial results are promising, a limitation in the detection

method was determined and further experimentation will need to use a more precise method, such as HPLC.

The third chemotherapeutic, lomustine, was shown capable of release from PCL in accelerated media, with a full release in two days. In contrast, lomustine release in PBS was negligible over the same time period.

Finally, we found that aqueous, degradable PNIPAM was capable of suspending polymeric microspheres that can be applied in aerosol form to the surface of a brain at physiological temperature. This delivery system displayed the liquid-gel transition due to temperature, forming an adherent layer with entrapped microspheres and conforming to the complex surface morphology of the brain.

4 *In Vivo* Evaluation of Gefitinib Encapsulated PLGA Microspheres Entrapped in PNIPAM

4.1 Background

4.1.1 Motivation

Chapters 2 and 3 focused on formulating and characterizing drug encapsulated polymeric microspheres for glioma therapy. While the microspheres were characterized *in vitro*, their efficacy *in vivo* has not been tested. This chapter will focus on a subcutaneous tumor model that was used to test the gefitinib encapsulated PLGA microspheres *in vivo*. In addition, a selected review of the literature covering *in vivo* results for drug encapsulated microspheres for glioma therapy will be given.

4.1.2 Drug Encapsulated Polymeric Microspheres for Intracranial Tumor Therapy: In Vivo Results

Paclitaxel, 5-FU, carboplatin, BCNU, camptothecin, and vincristine are some examples of chemotherapeutics that have been encapsulated in polymer microspheres for intracranial tumor therapy and tested *in vivo* [25, 26, 32-35, 38, 55, 57, 61, 72, 136]. Studies include both the simplistic subcutaneous tumor model to intracranial tumor models in mice and rats that have progressed to Phase II clinical trials.

An example of a subcutaneous glioma study was reported by Naraharisetti et al. using paclitaxel encapsulated PLGA microspheres [55]. These drug loaded microspheres, formulated either by spray drying or electrohydrodynamic atomization (EHDA), were implanted along the tumor sites of BALB/c nude mice bearing C6 glioma cells subcutaneously. The two different formulation

techniques produced microspheres with unique release kinetics. Microspheres produced by spray drying had a sustained, first-order release over 60 days while the EHDA technique had a pseudo-zero order release for 28 days after an initial burst for the first two days. The spray dried microspheres arrested tumor growth for more than 45 days when applied 6 days after tumor cell inoculation. However, when applied at day 9, the tumor did not respond to treatment due to the large tumor size; the tumor was too large for the drug dosage. The EHDA generated microparticles were applied 14 days after tumor cell inoculation (larger tumor volume) and arrested tumor growth for 10 days after the first injection. However, tumor growth rate increased even after a repeated injection two weeks later of the paclitaxel loaded PLGA microparticles. Overall, during 21 days of treatment, tumor growth was inhibited by 59% and 65% for the spray dried and EHDA microparticles, respectively, in comparison to the blank placebo. However, over longer time points, the spray-dried, slower releasing microspheres were the most effective. In a similar subcutaneous tumor study, Ranganath et al. demonstrated the efficacy of paclitaxel encapsulated PLGA microspheres in alginate beads. After 21 days of treatment, tumor volumes were reduced by 85% and 78% for paclitaxel-PLGA when compared to a blank control and the free drug form of paclitaxel, respectively [24]. As opposed to Naraharisetti et al., Ranganath et al. implanted the drug loaded beads into the tumor itself instead of peripherally at the tumor site.

The small molecule imatinib mesylate was encapsulated by Benny et al. in PLGA microspheres and tested *in vivo,* both subcutaneously and intracranially [45]. Swiss nude and C57/BL mice were subcutaneously inoculated with human U87-MG and GL261 glioblastoma cells, respectively. Tumor volume was suppressed by 79% after 30 days and 88% after 22 days for the GL261 and U87-MG cell line, respectively. The U87-MG cell line was then tested intracranially

in Swiss nude mice. The imatinib mesylate encapsulated PLGA microspheres significantly reduced tumor growth by 79% when compared to blank microspheres 14 days after intratumoral injection.

Camptothecin was also tested intracranially using PLGA microspheres [47, 57, 61]. Ozeki et al. injected camptothecin encapsulated PLGA microspheres suspended in a TGP directly on the brain of Sprague-Dawley rats against C6 glioma cells [47]. At physiological temperature, the TGP underwent a phase transition from a liquid to a gel, holding the microspheres at the tumor site. Localized treatment with camptothecin-PLGA in the TGP increased survival significantly, with one third of the rats surviving more than 60 days compared to a 16 day mean survival for animals with no treatment. The same dosage of free camptothecin dispersed in TGP had a median survival of only 21 days. A follow up study was conducted with the drug delivery system injected after tumor resection [61]. Tumor resection without additional treatments had a median survival of 18.5 days while resection plus camptothecin-PLGA in the TGP had a 24 and 26 day median survival for a 10 and 30 μg camptothecin dose, respectively. The camptothecin-PLGA in the TGP was also applied without tumor resection, resulting in the same median survival. However, only groups with both tumor resection and the drug delivery system demonstrated long-term survivors.

The radiosensitizer 5-fluorouracil has been extensively used for *in vivo* studies, progressing to the point of a Phase II clinical trial [26, 32-36, 72, 136]. In one study, 5-FU encapsulated PMM 2.1.2 microspheres were tested by Fournier et al. against the F98 tumor cell line inoculated intracranially in Fisher rats [35]. The 5-FU microspheres increased the median survival to 34.1 ±

5.6 days compared to the no treatment control at 22.7 ± 3.3 days and a 5-FU solution applied stereotactically at 26.5 ± 2.4 days.

The most common system for 5-FU encapsulated microspheres applied to gliomas consists of stereotactically injected, 5-FU loaded PLGA microspheres as shown in Figure 4.1 [26, 32-34, 36, 72, 136]. Lemaire et al. demonstrated that the stereotactic administration of the 5-FU loaded PLGA microspheres slowed tumor development by a factor of three when compared to a bolus 5-FU solution injected intratumorally for Sprague-Dawley rats bearing C6 glioma cells intracranially [26]. Overall, both protocols increased survival time by ~50% over the controls. However, overall survival was not significantly different between the two therapies, with a 30 ± 1 day and 32 ± 2 days survival for the bolus and microsphere injection, respectively. An interesting result of this experiment is that tumor proliferation was significantly reduced in the vicinity of the stereotactic injection site before regrowth. This led to a multi-site injection protocol, further elucidated in a study using the same system with [^{3}H]5-FU to monitor diffusion in Sprague-Dawley rats [36]. In the tumor bearing rats, the drug encapsulated microspheres were found to diffuse ~ 1.5 mm distance from the injection site and to release 5-FU at a maximum of 3 mm. Multiple injections covering the whole area of the tumor would be needed for the best chance of tumor eradication.

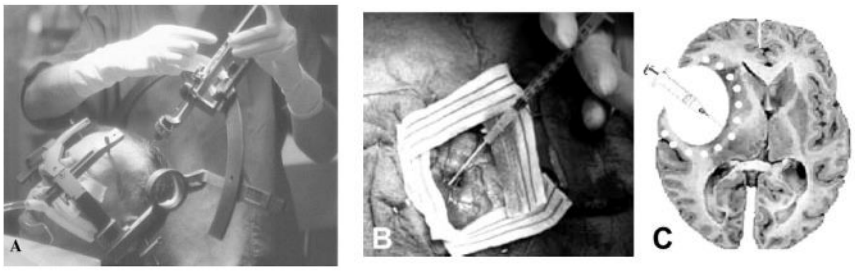

Figure 4.1: The treatment of gliomas with stereotactically injected 5-FU encapsulated PLGA microspheres a) stereotaxic procedure with the frame [34], b) implantation of the microsphere suspension without a frame, and c) multiple sites of injection [33]. Reprinted from Cancer, 100/2, Menei et al., Stereotaxic implantation of 5-fluorouracil-releasing microspheres in malignant glioma, 405-410, 2004, with permission from Wiley. Reprinted from Neurosurgery, 56/2, Menei et al., Local and Sustained Delivery of 5-Fluorouracil from Biodegradable Microspheres for the Radiosensitization of Malignant Glioma: A Randomized Phase II Trial, 242-247, 2005, with permission from Wolters Kluwer.

Additional studies on 5-FU encapsulated PLGA microspheres by Roullin et al. utilized its radiosensitizing potential and applied 36 grays to test therapeutic potential in C6 glioma bearing Sprague-Dawley rats [136]. Two drug loaded microsphere formulations characterized by a fast (7 days for 100% release) and slow release (20 days for 100% release) were explored. The 5-FU loaded microspheres in combination with radiotherapy caused a 47% complete remission rate, while radiotherapy alone and no therapy had an 8% and 0% remission, respectively. The survival for the slow and fast releasing drug loaded microspheres in combination with radiotherapy was 57% and 41%, respectively, while survival without the radiotherapy was 0 and 27%, respectively.

A pilot study conducted by Menei et al. included eight patients with newly diagnosed glioblastoma that were treated with 5-FU encapsulated PLGA microspheres [72]. The drug loaded microspheres were applied along the walls of the tumor resection cavity for a total dosage of either 70 mg or 132 mg. External beam radiotherapy was applied between the second and

seventh day after surgery for a total of 59.4 grays. The dose of 132 mg caused recurrent brain swelling 3 weeks after radiotherapy and required steroid treatment before completing the radiation. One month after implantation, significant levels of 5-FU were present in the cerebral spinal fluid enabling optimal radiosensitization. All patients treated with the 5-FU-PLGA system had a median survival time of 98 weeks at the last evaluation, greater that the 50.6 weeks for resection and radiotherapy alone. The higher dosage had two long term survivors that were in disease remission at 139 and 153 weeks.

To further confirm the potential of the 5-FU encapsulated PLGA microspheres against glioma cells, a Phase I study was conducted by Menei et al. [34]. This study included 10 patients with newly diagnosed, inoperable, malignant gliomas that were dosed one time with 132 mg of encapsulated 5-FU. Different stereotactical injection trajectories (one to seven deposits) were applied dependent on the 3-D conformation of the tumor. The overall median survival was 40 weeks with 2 long-term survivors (71 and 89 weeks). Based on the these promising results, a Phase II trial was conducted [33]. This trial was composed of two treatments groups: in Arm A, 49 patients received 5-FU releasing microspheres (130 mg) with early radiotherapy (59.4 gray) and in Arm B, 46 patients received only early radiotherapy (59.4 gray). All therapies were applied after gross tumor resection. A median overall survival of 15.2 months was achieved in Arm A, approximately 2.9 months longer than radiotherapy (Arm B). However, it did not reach statistical significance. Time to tumor progression was also not significantly different, 6.5 months in Arm A and 6.3 months in Arm B. While this Phase II study shows some potential, it was not designed and powered sufficiently to show a statistically significant result [33].

The multi-injection strategy to treat gliomas was also studied by Emerich et al. using carboplatin encapsulated PLGA microspheres [39]. In a study against RG2 cells in male Fisher rats, the location of microsphere injection played an important role in survival. The rats that received drug loaded microspheres through direct injection into the tumor cavity did not show a significant improvement when compared to the control animals that underwent a tumor resection alone. Direct injection of the highest dose (100 μg carboplatin) increased median survival from 20 days (no treatment) to 36 days while tumor resection alone increased median survival to 30 days. However, animals that were injected along the perimeter of the tumor cavity with carboplatin loaded PLGA microspheres had a higher survival compared to the controls. The 100 μg of encapsulated carboplatin applied along the perimeter increased median survival by 110% with two animals surviving the 180 day duration of the experiment. Additionally, a significant decrease in tumor volume was detected for the perimeter injection when compared to resection alone: 14.8 mm^3 compared to 99.5 mm^3 at day 28 and 50.7 mm^3 versus 99.5 mm^3 at day 38, respectively. Similar studies were conducted by the same group testing BCNU loaded PLGA microspheres injected along or inside the tumor cavity [39]. The results supported the trend demonstrated with the carboplatin loaded PLGA microspheres. PLGA microspheres with 100 μg of encapsulated BCNU injected directly into the tumor cavity had a lower median survival than microspheres injected along the tumor perimeter; a 36% and 61% increase in survival, respectively, compared to tumor resection alone.

In a follow-up study, Emerich et al. studied the effects of repeated peritumoral injection of carboplatin encapsulated PLGA microspheres [38]. Carboplatin loaded particle were injected into 8 sites around the RG2 tumor resection cavity. This initial therapy increased median survival

by 141% over tumor debulking. However, when the same therapy was repeated 20 days later, median survival increased to 219%. One third of the rats studied were long term survivors, greater than 150 days. Histology results demonstrated the complete eradication of the tumor for the double injection. Emerich et al. continued this study by mixing both BCNU and carboplatin encapsulated microspheres together and injecting peritumorally. As shown in Figure 4.2, when mixed together and injected into 8 sites, an increase in median survival compared to tumor debulking was 193-245%. However, when the drugs were injected separately but spatially alternating around the tumor site, the increase in median survival was only 55-77%. This supports the idea that a polypharmacy therapy such as our drug delivery system will supply could further improve survival beyond the traditional application of a single chemotherapeutic. In addition, when our system is applied, it will cover the entirety of the exposed tumor or resection cavity with one application and have a sustained release, removing the need for multiple injections.

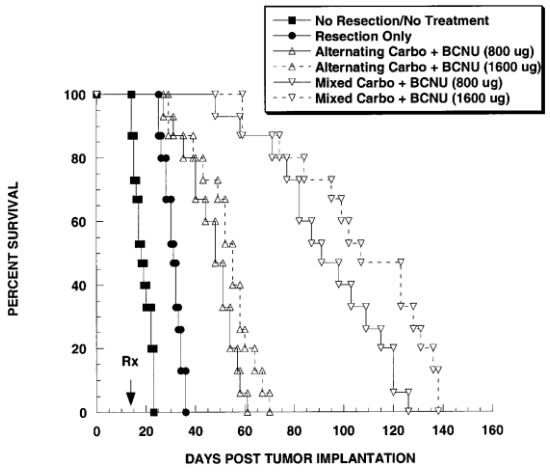

Figure 4.2: The effect of combining carboplatin and BCNU encapsulated PLGA microspheres on survival. Microspheres were either injected separately but spatially alternating around the tumor site or mixed together and delivered as a single suspension after tumor resection [38]. Reprinted from Cell Transplantation, 11/1, Emerich et al., Injection of Chemotherapeutic Microspheres and Glioma IV: Eradicating Tumors in Rats, 47-54, 2002, DOI 10.0000/096020198389771, with permission from Cognizant Communication Corporation.

4.2 Hypothesis

It is hypothesized that:

(1) Free gefitinib applied to C6 glioma cells *in vitro* will have a dosage dependent effect on cell viability

(2) In a subcutaneous tumor model, gefitinib encapsulated PLGA microspheres entrapped in PNIPAM will reduce tumor volume when compared to blank PLGA microspheres entrapped in PNIPAM

4.3 Materials and Methods

4.3.1 Materials

4.3.1.1 Materials for Cell Culture and Gefitinib Testing

Dulbecco's Modified Eagle Medium (DMEM; Invitrogen), fetal bovine Serum (FBS; Optima), L-glutamine (Sigma), antibiotic/antimycotic (A/A; Gibco), dimethyl sulfoxide (DMSO; Sigma), Vybrant MTT cell proliferation assay kit (Invitrogen), and gefitinib (GB; Fisher, free base >99%) were used as received.

4.3.1.2 Materials for C6 Subcutaneous Injection and Treatment

Microspheres and PNIPAM used in this section were formulated or synthesized in Chapter 2 under sterile conditions. The formulations parameters are listed below in Table 4.1. Limulus amebocyte lysate pyrogent plus kit (Lonza), sterile saline (Hospira), and optimal cutting temperature (OCT, Tissue-Tek) were used as received.

Table 4.1 Microsphere formulation parameters for *in vivo* studies

Pilot Study	Polymer Type	Emulsion Type	Impeller Setting (rpm)	Initial Drug Loading (mg)	Other Conditions	Final Drug Loading (%)
1	PLGA	Single	2800	0	3% PVA	0
				1.5	3% PVA	0.09 ± 0.004
2	PLGA	Single	2000	15	2.5 g PLGA, 3% PVA	0.54 ± 0.030

4.3.2 Cell Culture

NIH/3T3 fibroblast cells and C6 glioma cells (gift from R. Rostomily, University Of Washington) were cultured in DMEM supplemented with 10% FBS, 1% L-glutamine, and 1% A/A.

4.3.3 Growth Inhibition of Free Gefitinib on C6 Cells In Vitro

The effect of gefitinib on cells was tested using a 3-(4,5-dimethylthiazol-2-yl)-2,5-diphenytltetrazolium bromide (MTT) cell proliferation assay kit. C6 cells were seeded at 5,000 cells/well on a 48 well plate and allowed to culture for 24 hours. Then, the media was removed and replaced with gefitinib enriched media. The gefitinib enriched media was prepared by first dissolving gefitinib in DMSO and adding to DMEM at 0.1% v/v [137, 138]. The total gefitinib concentrations in DMEM were 0.1, 1, 5, 10, and 20 μM. After 24 hours, the media was removed and replaced with the MTT assay solution for 3-4 hours. This media was then removed and 0.5 mL of DMSO added to the wells. The absorbance values of the wells were measured with a VERSAmax tunable microplate reader at 550 nm. Controls included fresh media (no conditioning) and latex conditioned media containing 0.1% DMSO (v/v). The absorbance values

were normalized to the fresh media as 100% cell viability. All measurements were performed in triplicate with error bars to one standard deviation and analyzed with an unpaired t test.

4.3.4 Gefitinib-PLGA-PNIPAM against a Subcutaneous Glioma Tumor

Animal experiments were approved by the University of Washington Animal Care and Use Committee (IACUC) and followed federal guidelines for laboratory animal use. Blank microspheres were evaluated for cytotoxicity using the elution method and following United States Pharmacopeia and International Organization of Standardization (ISO) guidelines. At least three samples per batch of microspheres were placed in DMEM for 24 hours at either 0.2 g per mL media or 6 cm^2 surface area per mL media. NIH/3T3 cells were exposed to this conditioned media for 48 hours and examined via light microscopy at 12, 24, and 48 hours for any cytotoxic response. GB-PLGA microspheres were not tested as GB would be toxic to cells. Both microspheres and PNIPAM were evaluated for endotoxicity using a standard limulus amebocyte lysate gel clot protocol. Three samples per microsphere set and PNIPAM batch were extracted at a concentration of 0.2 g per mL endotoxin free water or 6 cm^2 surface area per mL endotoxin free water. To pass testing, all samples had to have less than 0.06 EU/mL (EU is endotoxin unit) from the sample extracts.

4.3.4.1 Pilot 1

Six athymic, male, nude mice (6-7 weeks old, Charles River) were subcutaneously injected in the right dorsal flank with 5 X 10^5 C6 cells in a 100 µL volume of DMEM and 1% L-glutamine. The injected cells were allowed to grow and form tumors over 8 days. The animals were randomly divided into two groups of three mice each. The first group received a single, 0.5 mL

subcutaneous injection below the growing tumor of blank PLGA microspheres suspended in PNIPAM at 218 mg dry microspheres per mL PNIPAM (2.5% W_{PNIPAM}/V_{Saline}). The second group also received a single, 0.5 mL subcutaneous injection below the growing tumor of GB-PLGA microspheres suspended in PNIPAM at the same concentration, with the total gefitinib dosage equaling 200 µg GB/mouse. The polymer system was delivered under inhaled isoflurane anesthesia. Note that the first control injection was done by making an incision midline to the tumor, dripping the PNIPAM solution in place, and closing with wound clips. However, due to sample loss, the remaining five samples were done by injection. Tumor volume was calculated by measuring the length (head to tail) and width (side to side) of the tumor and using Equation 4.1. Mice body weight, movement, feeding habits, and overall condition was also monitored. Mice were humanely euthanized by carbon dioxide asphyxia after the tumor reached an average of 20 mm in diameter or earlier due to health issues. Tumors were excised with half of the tumor embedded in OCT and snap frozen before being stored at -80°C and the second half fixed overnight in a zinc fixative at 4°C. For volume measurements, the error bars are given to one standard deviation.

Equation 4.1 Tumor volume

$$Volume(mm^3) = \frac{Length(mm)\ X\ Width(mm)^2}{2}$$

4.3.4.2 Pilot 2

Three athymic, male, nude mice (6-7 weeks old, Charles River) were subcutaneously injected in the right dorsal flank with 5 X 10^5 C6 cells in a 100 µL volume of DMEM and 1% L-glutamine. The injected cells were allowed to grow and form tumors over 7 days. All mice received a single, 0.5 mL, subcutaneous injection at day 7 below the growing tumor of GB-PLGA microspheres suspended in PNIPAM at 83 mg dry microspheres per mL PNIPAM (2.5% W_{PNIPAM}/V_{Saline}). The total gefitinib dosage equaled 450 µg GB/mouse. Note that all material was kept at 4°C prior to injection and the drug delivery system was applied under inhaled isoflurane anesthesia. After injection, the site was rinsed with cold saline to remove any PNIPAM or microspheres from the wound. Tumor volume was calculated by measuring the length (head to tail) and width (side to side) of the tumor and using Equation 4.1. Mice body weight, movement, feeding habits, and overall condition was also monitored. Mice were humanely euthanized by carbon dioxide asphyxia after the tumor reached an average of 20 mm in diameter or earlier due to health issues. Tumors were excised with half of tumor embedded in OCT and snap frozen before being stored at -80°C and the second half fixed overnight in zinc fixative at 4°C. Error bars are given to on one standard deviation for volume measurements

Note that on day 19 post-treatment, the two remaining mice were given one dose of buprenorphine SR (1 mg/mL) at 1.2 mg/kg subcutaneously. This was due to the skin progressively breaking down with ulceration, secondary to the tumor.

4.3.5 Histology Analysis: Hematoxylin and Eosin Stain and Trichrome Stain

Fixed explants were dehydrated with a graded ethanol series and cleared with xylene prior to paraffin embedding. The embedded explants were sectioned with a Leica microtome in 5 μm sections and placed on a glass slide. Prior to staining, slides were baked at 50 °C for 30 minutes before deparaffinization in xylene, rehydration through a graded ethanol series, and washing in distilled water. For Hematoxylin and eosin staining (H&E), slides were soaked in Harris hematoxylin solution for 8-10 minutes, rinsed in tap water, dipped three times in acid alcohol, rinsed again in tap water, placed in Scotts Blue to reduce intensity staining, rinsed in tap water, dipped three times in Eosin, and then dehydrated through a graded series of ethanol and xylene before being cover slipped using Permount (Electron Microscopy Sciences). All media used was obtained through Sigma.

For trichrome staining, slides were placed in Bouin's fixative at 55 °C for 45 minutes, rinsed in water, placed in Weigert's iron hematoxylin for 10 minutes, washed in water, placed in Biebrich scarlet-acid fuchsin for 5 minutes, rinsed in water, placed in phosphomolybdic-phosphotungstic acid solution for 10 minutes, placed in Aniline blue for 3 minutes, rinsed in water, and placed in fresh 1% acetic acid for 1 minute. Finally, slides were dehydrated through a graded series of ethanol and xylene before being cover slipped using Permount (Electron Microscopy Sciences). All media used was obtained through Sigma.

Slides were imaged using a Nikon E800 Upright Microscope equipped with Metamorph software (version 6.0, Molecular Devices).

4.4 Results

4.4.1 Growth Inhibition of Free Gefitinib on C6 Cells In Vitro

To confirm that gefitinib was active against C6 glioma cells, the cells were exposed to varying concentrations of gefitinib and their cell viability measured. Figure 4.3 shows the dose dependent response of the cells to the free drug along with the calculated IC_{50}, the amount of drug needed to inhibit cell viability by 50% *in vitro*. Note that the IC_{50} was calculated based on the cell viability of 0.1, 1, 5, and 10 µM gefitinib.

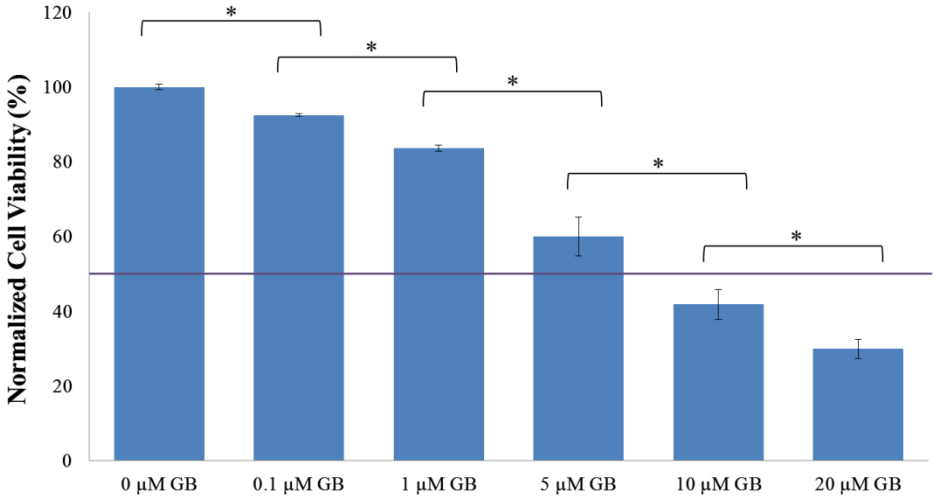

Figure 4.3 Dose dependent response of C6 glioma cells to gefitinib, n=3. The line represents the IC_{50} at approximately 7.9 µM, *p<0.05.

4.4.2 Effect of GB-PLGA-PNIPAM on Subcutaneous Glioma Tumors: Pilot 1

The first *in vivo* pilot studied the effect of a 200 µg dosage of gefitinib encapsulated in PLGA microspheres entrapped in PNIPAM on a subcutaneous glioma tumor versus the control of blank PLGA microspheres in PNIPAM. Figure 4.4 shows the effect of the gefitinib treatment versus

the control on tumor volume growth. Note that the control group only comprises two mice. The third mouse was removed because the tumor grew into the body instead of outwards, resulting with inaccurate tumor volume measurements. During the injection of the gefitinib treatment group, there was a significant issue of PNIPAM gelling in the syringe, preventing a full dose from being delivered. Appendix 18 shows the individual tumor growths and corresponding volume dosing. Table 4.2 lists extent of survival for each mouse with a note that one mouse was euthanized early due to a progressive skin break down with ulceration, secondary to the cancer.

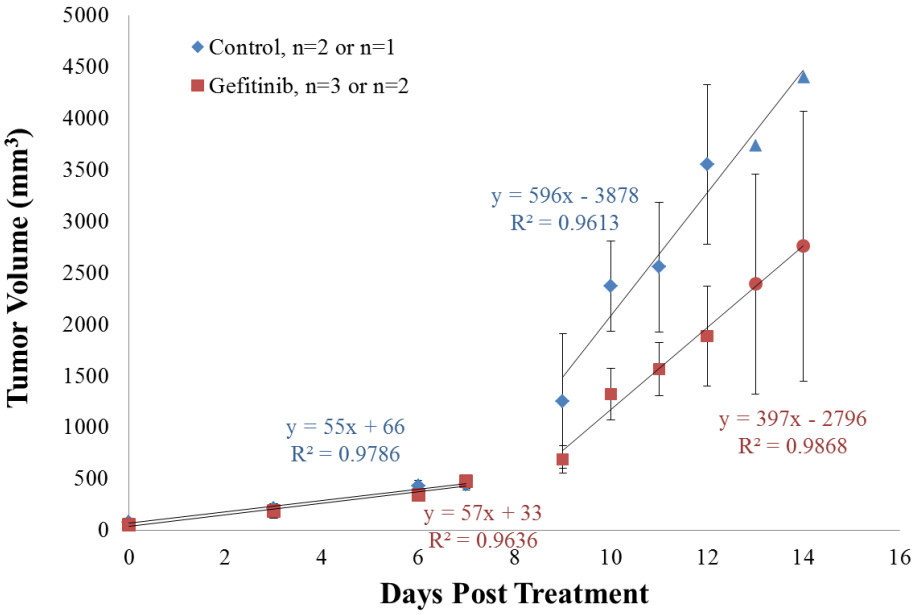

Figure 4.4 The effect of 200 µg gefitinib encapsulated in PLGA microspheres entrapped in PNIPAM on subcutaneous tumor volume growth. For the control group of blank PLGA entrapped in PNIPAM, the group size is 2 mice (diamond) and then one mouse (triangle). For the gefitinib treatment group, the size is three mice (square) and then two mice (circle).

Table 4.2 Extent of survival for Pilot 1

Mouse	Survival (days)
Control 1	12
Control 2	14
Gefitinib 1*	12
Gefitinib 2	14
Gefitinib 3	19

* Mouse was euthanized before maximum tumor diameter was reached

All explanted tumors were examined histologically, using a hematoxylin and eosin (H&E) and trichrome stain. H&E stains cell nuclei blue/black and cytoplasm pink while trichrome stains cell nuclei blue/black, cytoplasm and muscle red, and collagen blue. Representative H&E and trichrome stains of the final tumor explants are shown below in Figure 4.6 and Figure 4.7 for the control and treatment group, respectively. Figure 4.5 shows that the PNIPAM still maintained its thermoresponsiveness after injection, converting back to a liquid and seeping out of the tumor explant after being exposed to a temperature below 32 °C.

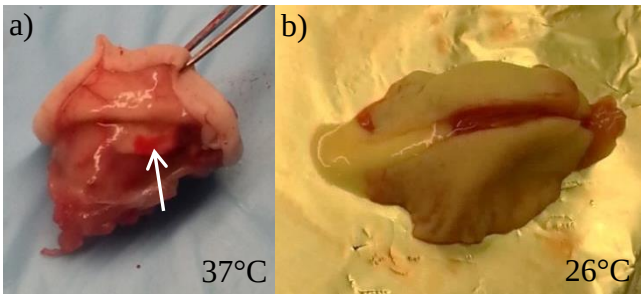

Figure 4.5 Tumor explants from Pilot 1 showing the presence of PNIPAM as a) a gel after 12 days in a mouse and b) a liquid after 14 days in a mouse.

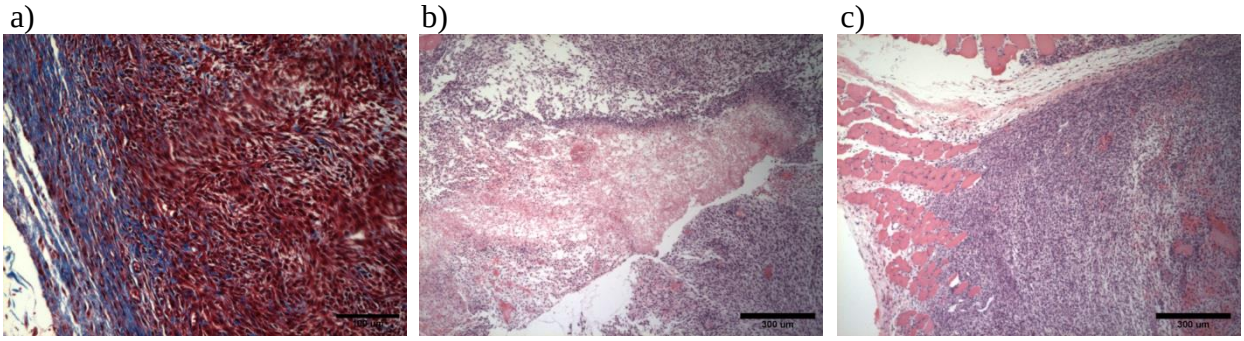

Figure 4.6 Histological staining of a tumor explant from the control group in Pilot 1. a) Trichrome of the tumor (skin side) scale bar 100 µm, b), H&E of the middle of the tumor exhibiting pseudopalisading, and c) H&E showing the tumor invading muscle cells. Tumor was 12 days, post treatment.

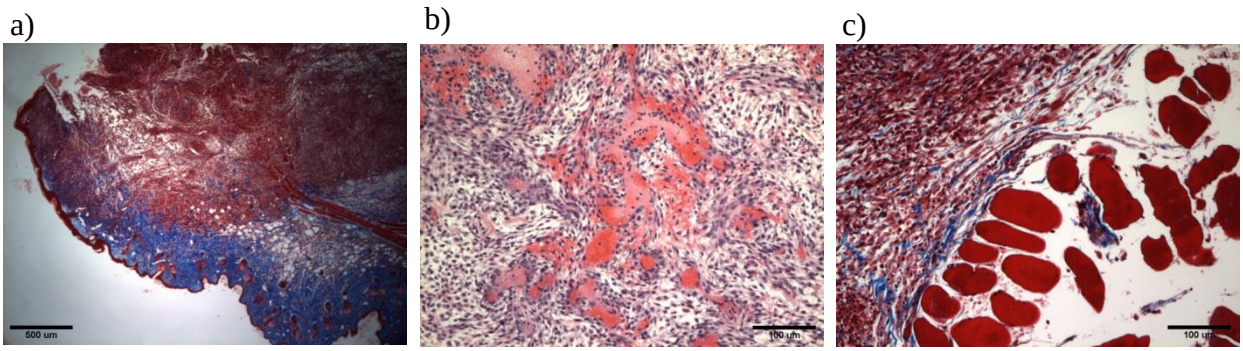

Figure 4.7 Histological staining of tumors explanted from the treatment group in Pilot 1. a) Trichrome of the skin side showing tumor cells growing into the dermis layer, b) H&E showing poorly formed blood vessels, and c) trichrome showing the tumor encroaching on muscle cells. Tumors were 12 days post treatment for a) and 19 days post treatment for b) and c).

4.4.3 Effect of GB-PLGA-PNIPAM on Subcutaneous Glioma Tumors: Pilot 2

As a follow up to Pilot 1, a second pilot study was conducted increasing the gefitinib amount to 450 µg. In this case, a second formulation of GB-PLGA microspheres (Table 4.1) was used to treat three athymic nude mice with a subcutaneous C6 glioma. Due to funding limitations, a control group was not included. Figure 4.8 shows a comparison of the results obtained in Pilot 2 to Pilot 1. While it is not a perfect comparison due to differences in the microsphere formulation and cell media (FBS, cell aliquot), we believe this presents a fair comparison of a control and the

effect of increasing drug dosages. Note that only two mice are included in Pilot 2 even though 3 mice were treated. The third mouse was removed because the tumor grew into the body cavity, preventing accurate tumor volume measurement. Table 4.3 lists the extent of survival for each mouse with a note that both mice were euthanized early due to a progressive skin break down with ulceration, secondary to the cancer.

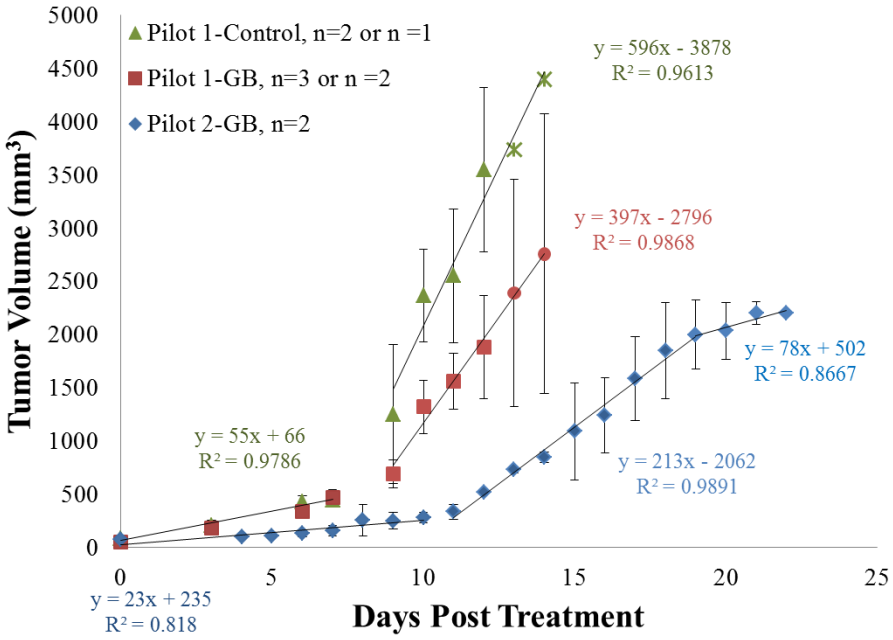

Figure 4.8 The effect of 200 µg gefitinib and 450 µg gefitinib encapsulated PLGA microspheres entrapped in PNIPAM on subcutaneous tumor volume growth. For the Pilot 1 control group of blank PLGA entrapped in PNIPAM, the group size is 2 mice (triangle) and then one mouse (star). For the Pilot 1 gefitinib treatment group, the size is three mice (square) and then two mice (circle). For the pilot 2 gefitinib treatment group, the size is two mice (diamond).

Table 4.3 Extent of survival for Pilot 2

Mouse	Survival (days)
Gefitinib 1*	22
Gefitinib 2*	22

* Mouse was euthanized before maximum tumor diameter was reached

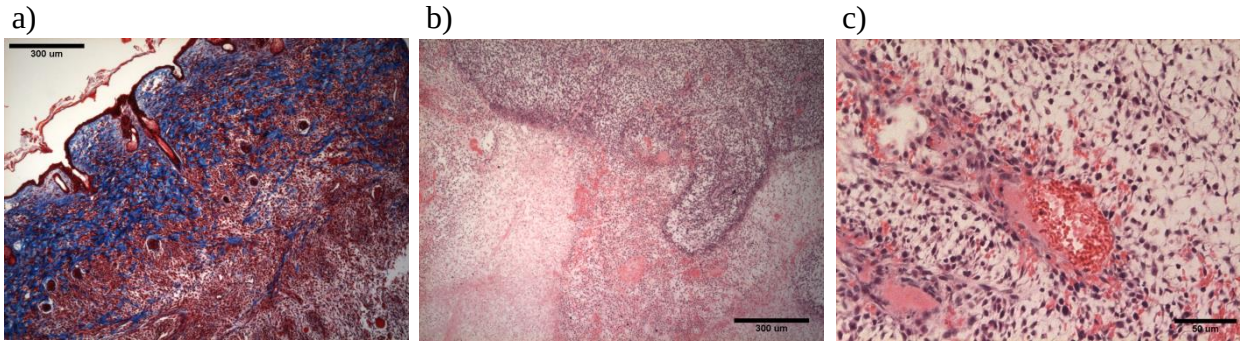

Figure 4.9 Histological staining of tumors explanted from Pilot 2. a) Trichrome of the tumor skin side showing cell invasion b) H&E showing pseudopalisading, and c) H&E showing poorly formed blood vessels. Tumors were 22 days post treatment.

4.5 Discussion

The studies presented in Chapter 4 are focused on the *in vivo* evaluation of gefitinib encapsulated PLGA microspheres against a subcutaneous tumor model in mice. As a preliminary test, the growth inhibition effect of free gefitinib (not encapsulated) on C6 glioma cells was determined *in vitro*. The C6 glioma cell line was chosen because it is a well-known and recognized cell line used for subcutaneous tumor studies [24, 55, 139]. In addition, the C6 cell line has a Biosafety Level 1 rating, low culturing costs, and is reported to express epidermal growth factor receptor (EGFR), the target receptor for gefitinib [139]. As can be seen in Figure 4.3, gefitinib has a dose dependent effect on C6 cell viability, with increasing concentrations of gefitinib causing a decrease in cell viability. The IC_{50} was calculated to be approximately 7.9 µM. While this is high in comparison to a 33 nM IC_{50} for cell lines that express high EGFR activity, we hypothesize

that gefitinib will still have an effect *in vivo* [140]. In the literature, orally applied gefitinib decreased tumor volume in a study against subcutaneous, human non-small lung cancer tumor with an IC_{50} of 7.1 µM [141]. In addition, our gefitinib would be applied locally to the tumor instead of orally, which would increase the local drug concentration and prevent gefitinib from affecting the entire body. Therefore, a pilot animal study using the GB-PLGA-PNIPAM was conducted.

The purpose of the first pilot study was to determine if gefitinib released from PLGA microspheres entrapped in PNIPAM could reduce or prevent tumor growth. The subcutaneous tumor model was chosen because it provides a simplistic and easy to measure model of tumor growth and is a first step for testing of many polymeric microsphere systems [24, 44, 48, 55, 63]. Only gefitinib encapsulated PLGA microspheres, the fastest releasing microspheres, were used to shorten the duration of the experiment and because their release *in vitro* was fully elucidated. A total of 200 µg gefitinib was chosen as a safe, preliminary dosing based on reports of other microsphere systems applied against subcutaneous tumors that ranged from 50 to 500 µg [24, 43, 44, 55].

As seen in Figure 4.4, from day zero through day 7, there is not a noticeable difference between the control group of blank PLGA-PNIPAM and the treatment group of GB-PLGA-PNIPAM, with a tumor volume growth rate of 55 and 57 mm^3/day, respectively. However, after day 9, both groups exhibited a strong increase in tumor volume growth rate. The control group increased to 596 mm^3/day while the treatment group increased to 397 mm^3/day, approximately 33% less than the control. While statistical significance could not be reached because of the low number of

mice per group, this is a positive result demonstrating the potential of our microsphere-PNIPAM system.

A point of interest is that during tumor excision, samples of the microsphere-PNIPAM system were located. Figure 4.5a shows a white gel at 37 °C that we hypothesize to be the microsphere-PNIPAM system. Figure 4.5b shows a tumor explant that was allowed to come to room temperature (26 °C) and then sectioned with PNIPAM seeping out in liquid form. This demonstrates that even after being in the body for 14 days, PNIPAM still maintained its thermoresponsiveness. This is an added benefit for drug delivery purposes, with the microsphere-PNIPAM system allowing for an easy removal by bathing with water below its LCST, 32 °C.

Figure 4.6 and Figure 4.7 show selected histological images of the tumor explants from the control and treatment group, respectively. While differences between the control and treatment groups were not noted, several examples of glioma characteristics are given. In Figure 4.6, tumor invasion is seen, with the cells growing up and into the dermis layer and surrounding and infiltrating muscle cells. Figure 4.6b is an example of pseudopalisading, where dense cellular arrays are arranged around progressive or serpiginous necrotic areas. Figure 4.7 also shows the invasiveness of the tumor cells, with Figure 4.7a showing tumor cells that broke through the dermis layer and caused a rupture in the skin layer. Figure 4.7b is an example of poorly formed blood vessels exhibiting non-circular vessels with poor cell lining. When low magnifications images of the tumors were briefly evaluated by Dr. Kelly McSweeney, pathologist at Beaufort Memorial Hospital, she indicated that all correct markers for gliomas were present, such as necrotic areas, poorly formed vascular growth, and invasive cell growth. It is hypothesized that

with a higher drug dosing and explants that were taken on the same day post treatment, a noticeable different in necrotic area and cell density could be measured.

Several modifications were made throughout this pilot study. Initially, the PLGA-PNIPAM system was to be applied by making an incision alongside the tumor, applying the system on the exposed tumor, and then closing the incision with wound clips. However, when first applied, there was significant sample loss through the incision. Therefore, one control mouse had the system applied with an incision and the remaining five mice had the system applied via subcutaneous injection into the area around the tumor. This method proved robust, capable of applying the full dose without significant sample loss. However, a second issue occurred; the PNIPAM gelled in the syringe, preventing full injection of the drug delivery system. A modest decrease in gelation was achieved by placing the PNIPAM syringe at 4 °C, however, full injection remained difficult. Of the three mice treated with gefitinib, one mouse received 100% of the injection volume, the second mouse 60%, and the third mouse, 50%. These percentages are estimations based on the volume of gelled PNIPAM remaining in the syringe but are not necessarily indicative of the GB-PLGA microsphere amount. The microspheres may have settled and more or less may have been injected as this issue was addressed. It is hypothesized that this gelation occurred from handling the syringe and drug delivery system too early near a heating pad, resulting in an increase in the local temperature around the syringe from body heat, triggering PNIPAM gelation. Future studies will maintain the syringe at 4 °C with minimal handling.

Based on the promising results of the first pilot that demonstrated a 33% decrease in tumor volume growth rate for the GB-PLGA-PNIPAM versus PLGA-PNIPAM, a second pilot study was conducted. The purpose of this second study was to determine if a higher dosage of gefitinib would further decrease the tumor volume growth rate. The total amount of gefitinib was increased from 200 to 450 µg per mouse by using higher drug loaded PLGA microspheres (Table 4.1). These higher drug loaded microspheres also reduced the total amount of microspheres from 218 to 83 mg. This in turn reduced the viscosity of the GB-PLGA-PNIPAM slurry, allowing for easier injection. All mice used in this study were treated with the GB-PLGA-PNIPAM drug delivery system. A control group was not included due to cost limitations.

Figure 4.8 shows that through day ten, the second pilot study had a slightly reduced tumor volume growth rate at 23 mm^3/day compared to Pilot 1 at 55 mm^3/day. When the subcutaneous tumor started to rapidly grow on day 11, two days later than Pilot 1, there is a large decrease in the tumor volume growth rate in comparison to the Pilot 1 control at 212 and 596 mm^3/day, respectively. This is a 64% decrease in tumor volume growth rate. Interestingly, around day 19, there is a plateau in the tumor volume growth rate, decreasing from 212 to 78 mm^3/day. Unfortunately, the study was halted at day 22 due to a skin break down with ulceration, secondary to the cancer on both mice along the needle track of the injection site. While this is described as a common occurrence for subcutaneous tumor studies as described by the University of Washington veterinary staff, we are uncertain if this was a long-term plateau or a temporary trend. It is hypothesized that this could be a long-term plateau because the release of gefitinib from PLGA microspheres increased around day 20 *in vitro* as the microsphere bulk degraded (Figure 3.8). Therefore, more gefitinib would be available to target the tumor and

reduce tumor growth. Future studies should attempt to prevent skin ulceration by either using a smaller needle for injection or injecting farther away from the tumor site. It was also confirmed in Pilot 2 that placing the syringe and GB-PLGA-PNIPAM at 4 °C with minimal handling prior to injection prevented PNIPAM from gelling in the syringe. All mice successfully received a full injection of the drug delivery system.

Sample histology images from Pilot 2 are shown in Figure 4.9. Correct markers for gliomas are present, including invasive cell growth into the skin layer, necrotic areas with pseudopalisading, and poorly formed blood vessels [142].

It should be taken under consideration that the comparisons drawn between Pilot 1 and 2 are "soft" comparisons, with trends taken from the data. Hard comparisons are not possible because the Pilot 1 control used PLGA microspheres formulated under different conditions than Pilot 2 (Table 4.1). In addition, the number of animals per group was low and there were different cell aliquots and cell media lots used between Pilot 1 and 2.

When the results of Pilot 2 are compared to a study using paclitaxel-PLGA microspheres entrapped in an alginate matrix against subcutaneous C6 tumors, similar results were achieved in tumor volume suppression [24]. After 21 days of treatment and dependent on the microsphere formulation, the tumor volumes were reduced by 52 to 85% for the paclitaxel-PLGA-alginate system in comparison to the blank microspheres control. Similarly, our Pilot 2 study reduced tumor volume by 64% compared to the Pilot 1 blank microsphere control on day 7 and 80% on day 14. A comparison at day 21 is not available as the control mice did not survive to that point.

However, it is encouraging to see that the gefitinib-PLGA-PNIPAM is achieving similar results to those reported in the literature and an expanded study with larger animal numbers and control groups would be necessary to achieve statistically significant results.

4.6 Conclusion

The first part of this work was focused on determining the growth inhibition effect of free gefitinib on C6 glioma cells *in vitro*. It was found that gefitinib has a dose dependent effect on C6 glioma cells, with higher concentrations of gefitinib decreasing cell viability. Next, the effect of gefitinib encapsulated PLGA microspheres in PNIPAM was evaluated in a subcutaneous tumor model. In the initial pilot study, the tumor volume growth rate was reduced by 33% for GB-PLGA-PNIPAM when compared to the PLGA-PNIPAM control. When evaluated histologically, the subcutaneous tumors demonstrated the markers characteristic of gliomas including necrotic areas, poorly formed vasculature, and invasive cell growth. A second pilot study was then conducted, more than doubling the amount of gefitinib that was delivered. When compared to the first pilot control, the GB-PLGA-PNIPAM system was found to decrease tumor volume growth rate by 64%. Additionally, the last four days of the study demonstrated a plateau in the tumor volume growth that could be indicative of the tumor entering a long-term, slow growth period due to more gefitinib being released from PLGA microspheres that are bulk degrading. When evaluated histologically, the tumors from Pilot 2 exhibited the same glioma markers as Pilot 1.

Further studies with more animals and controls would be needed to fully elucidate the therapeutic benefits of the GB-PLGA-PNIPAM system. However, based on these two pilot studies, this microsphere-PNIPAM system shows great potential for decreasing tumor growth.

5 Conclusions and Future Directions

The treatment of malignant gliomas is a field under constant study and advancements, with researchers aiming to increase patient life expectancy beyond the current 12-15 month prognosis. While there are several different directions being pursued such as targeted therapies, better imaging and resection techniques, and implantable devices, this dissertation has purposed the use of a topical, slow release, degradable, multi-drug delivery system applied post tumor resection entitled **dr**ug **e**ncapsulated **a**erosolized **m**icrospheres as a **b**iodegradable, **i**ntelligent **g**lioma therapy (DREAM BIG Therapy). The work presented here is focused on the production of drug encapsulated polymeric microspheres and a degradable, thermoresponsive PNIPAM carrier, the drug release of the drug-microspheres-carrier *in vitro,* and the effect of a chemotherapeutic-microsphere-carrier on tumor volume growth *in vivo*. Overall, the results demonstrated the potential of the DREAM BIG Therapy as a glioma treatment.

Initially, blank and drug encapsulated PLGA, PLA, and PCL microspheres were successfully produced using emulsion techniques. By optimizing formulation parameters such as polymer, stabilizer, and drug concentration, encapsulation efficiencies greater than 80% and drug loadings greater than 0.3% were achieved for gefitinib encapsulated PLGA microspheres, IgG encapsulated PLA microspheres, and lomustine encapsulated PCL microspheres. A degradable, linear PNIPAM was also successfully synthesized using ATRP. The molecular weight of 20,000 g/mol demonstrated a temperature dependent, reversible phase transition that was capable of entrapping polymeric microspheres.

The *in vitro* release of gefitinib from PLGA microspheres demonstrated a biphasic release profile over 40 days of passive diffusion and then polymer degradation. A more hydrophilic molecule released from similar spheres had a quicker release of 20 days. The antibody IgG demonstrated a burst release from PLA microspheres followed by a sustained release over 284 or 495 days depending on microsphere size and IgG encapsulation. This suggested the potential for tuning drug release based on microsphere formulation parameters. Lomustine was also capable of release from PCL microspheres when placed in extreme basic conditions. When released in PBS short-term, negligible release was achieved. This drug is expected to release from PCL up to 2-2.5 years. A hypothesized release of gefitinib from PLGA microspheres, IgG from PLA microspheres, and lomustine from PCL microspheres is shown in Figure 5.1.

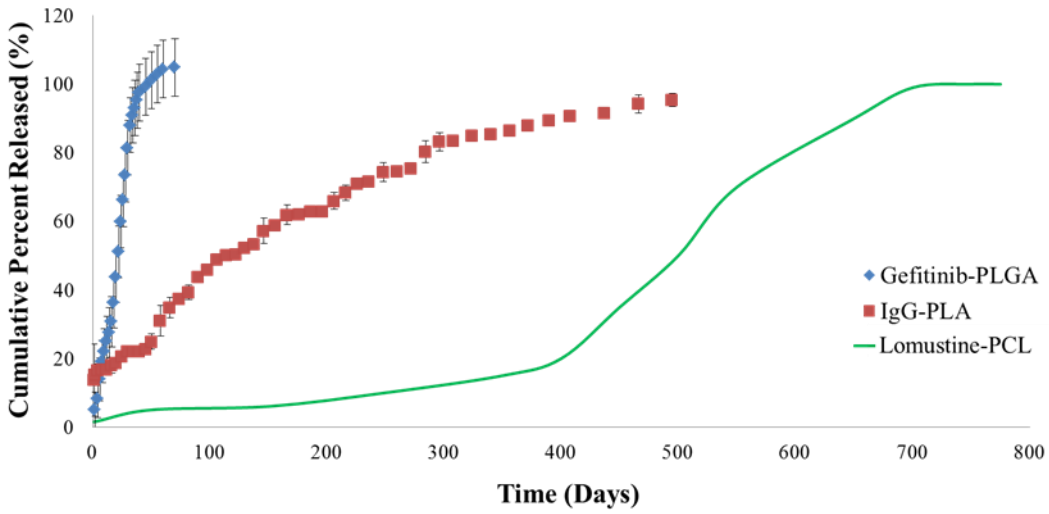

Figure 5.1 A hypothesized combined release of gefitinib, IgG, and lomustine. The release of gefitinib from PLGA and IgG from PLA microspheres was determined in Chapter 3 and the release from lomustine is a hypothetical 2 year release.

The drug-microsphere-PNIPAM system was successfully aerosolized when tested *ex vivo*. The aqueous PNIPAM solution suspended the microspheres and was applied via a spray bottle to tissue at physiological temperature. Microspheres had a uniform distribution that penetrated the convoluted topography of the tissue.

When tested *in vivo*, the gefitinib-PLGA-PNIPAM system reduced the tumor volume growth rate of a subcutaneous glioma when compared to a blank PLGA-PNIPAM control. The trend demonstrated a 33 and 64% decrease in tumor volume growth rate for a dosage of 200 and 450 µg gefitinib, respectively. While these numbers did not reach statistical significance, the pilot studied confirmed the potential of the DREAM BIG Therapy.

Future work would concentrate on encapsulating the chemotherapeutic bevacizumab in PLA microspheres to replace IgG. It is hypothesized that the optimal formulation parameters for IgG will also apply to bevacizumab. The *in vitro* release of bevacizumab-PLA and lomustine-PCL at physiological conditions would also be elucidated and microspheres parameters adjusted as needed to achieve a sequential, step release of the chemotherapeutics.

Based on the promising results demonstrated by the two pilot studies, a fully powered animal study is also suggested. A total of 64 athymic nude mice would be used, with 8 mice per group. The groups would include 1) no treatment, 2) blank PLGA microspheres, 3) blank PLGA microspheres and PNIPAM, 4) PNIPAM, 5) gefitinib in PNIPAM, 6) orally applied “free” gefitinib, 7) gefitinib encapsulated PLGA microspheres and PNIPAM, and 8) gefitinib encapsulated PLGA microspheres and PNIPAM containing gefitinib. While six mice per group

would achieve statistically significant results and allow for mice to be dropped from the study, a 30% better precision and narrowed confidence intervals would be achieved with eight mice per group. Tumor growth rate would be measured and the extent of necrosis in each tumor calculated histologically to determine the effect of each treatment.

Another potential study that could be conducted is a pilot study to determine the extent of drug diffusion released from the polymeric microspheres-PNIPAM system in a rat brain. One of the draw backs of the Gliadel® wafers is the poor penetration of BCNU (carmustine) in the brain. When implanted intracranially, there is a steep concentration gradient between the tissue surrounding the implant and the rest of the brain [5, 143]. For a rat model, a high concentration (~ 1 mM) was found as far away as 5 mm from the implant in the first day [144]. However, this rapidly declined to 1 mm for days 3-14 due to the rapid elimination of the drug, limiting the diffusion of BCNU in the brain. The DREAM BIG Therapy would need to match if not exceed this penetration depth to replace these wafers clinically. A basic outline of this study is as follows: 15 Wistar male rats will have a craniotomy performed with a resection of the occipital or right frontal lobe. Three rats will be in the control group with only a resection performed. The remaining 12 rats will be split evenly into two groups of six, with group 1 having rhodamine B encapsulated PLGA microspheres in PNIPAM applied in the resection cavity at one concentration and group 2 having a higher concentration applied. Rhodamine B will be used to determine the extent of diffusion because it is easily detected fluorescently and was already used as a model drug for detection of polymeric microspheres injected intracranially [44]. At day 10, 20, and 30, two rats from each treated group will be sacrificed along with a rat from the control group. The brains will be removed and sectioned to determine the extent of rhodamine B

diffusion. By taking a progression of samples over 30 days, the rate of diffusion into the surrounding tissue can be determined. Rhodamine B should initially be concentrated at the site of injection. Over time, we expect rhodamine B to be present 0.5 to 2-3 mm away from the injection site [36, 39, 78, 144]. If both the subcutaneous tumor study and the intracranial study yield positive results, then an intracranial tumor model would be the next logical step.

The potential of the DREAM BIG Therapy is that it provides an alternative solution to the treatment of gliomas by using multiple microspheres types with different degradation rates and chemotherapeutics in a thermoresponsive formulation. Multi-staged, sequential drug release could combat tumor regrowth and tumor drug resistance long-term with a single, localized application by the surgeon to the patient. In addition, various polymer-drug combinations could be chosen and applied with the PNIPAM to specifically tailor a treatment based on the cancer's characteristics, allowing for a personalized therapeutic approach. This system is not limited to gliomas, but could also be applied to other cancer types, such as breast and liver cancer. Other applications could include an intramuscular, long term contraceptive or pain reliever.

Appendix 1: Standard curves of a) rhodamine B in PBS at 536 nm, b) rhodamine B in THF-1 M HCl 90-10 (v/v) at 536 nm, c) gefitinib in PBS-1 M HCL 90-10 (v/v) at 333 nm, d) gefitinib in pH 10-1 M HCL 80-20 (v/v) e) gefitinib in THF-1 M HCl 90-10 (v/v) at 333 nm, f) IgG in PBS at 283 nm, g) IgG in pH 10 at 283 nm, h) IgG in pH 6 at 283 nm, i) IgG in pH 4 at 283 nm, j) IgG in PBS-1 M HCL 90-10 (v/v) at 283 nm, k) IgG in 1 M NaOH at 283 nm, l) lomustine in PBS-DMSO 55-45 (v/v) at 396 nm, m) lomustine in 5M NaOH-DMSO 65-35 (v/v) at 344 nm, and n) lomustine in DCM at 396 nm, n=3

a)

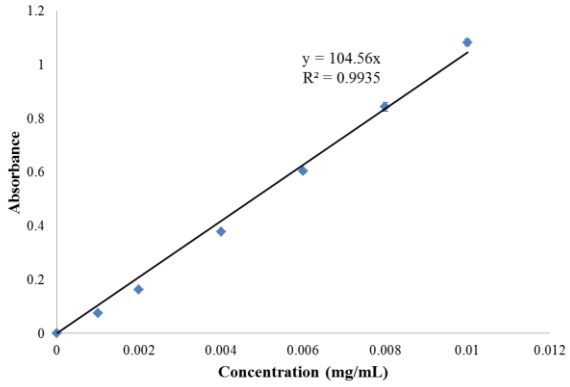

b)

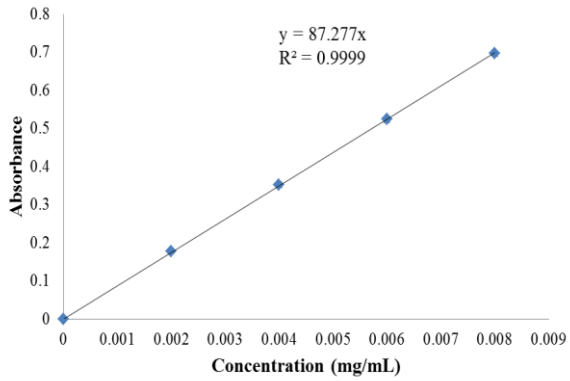

c)

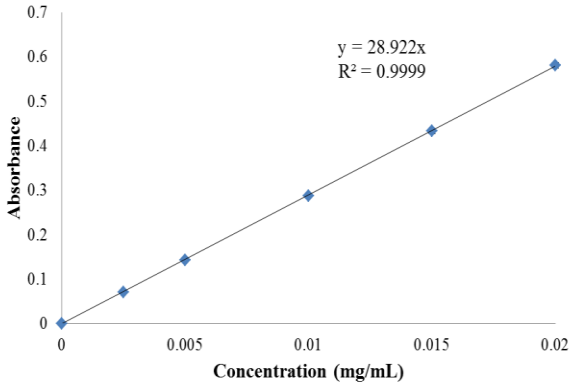

d)

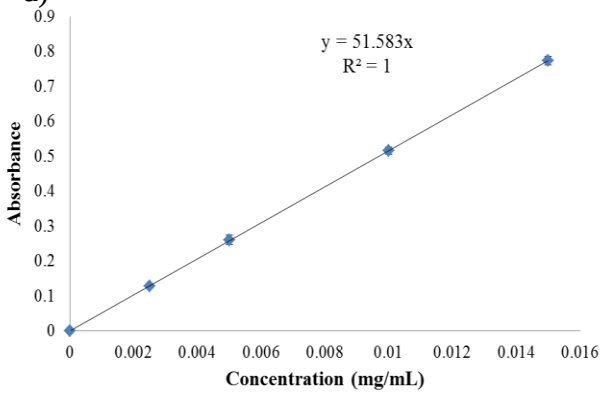

e)

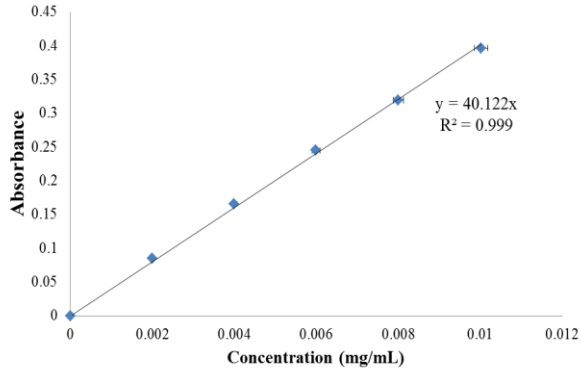

f)

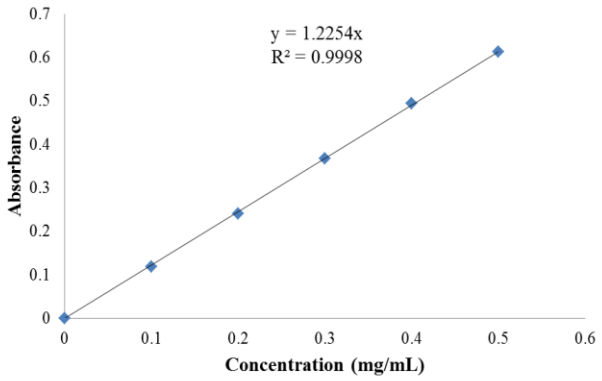

g)

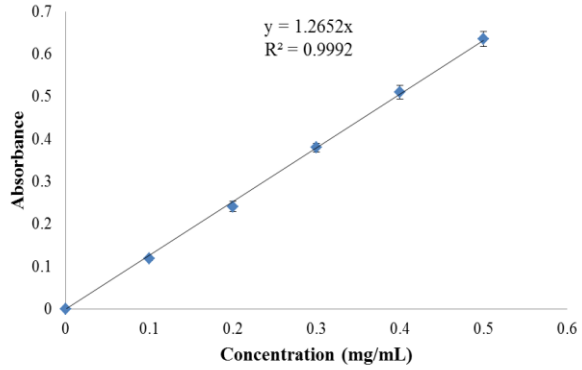
y = 1.2652x
R² = 0.9992
Absorbance
Concentration (mg/mL)

h)

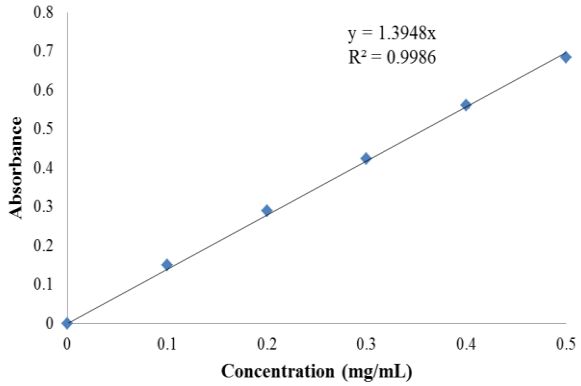
y = 1.3948x
R² = 0.9986
Absorbance
Concentration (mg/mL)

i)

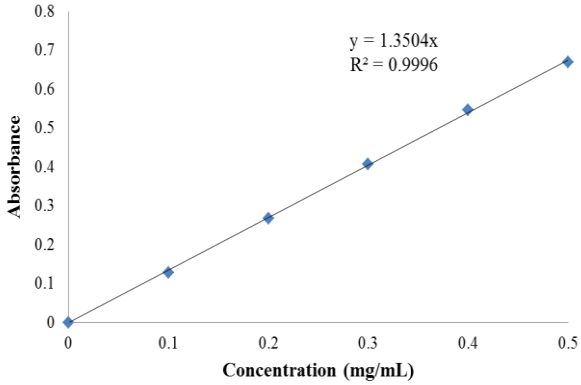
y = 1.3504x
R² = 0.9996
Absorbance
Concentration (mg/mL)

j)

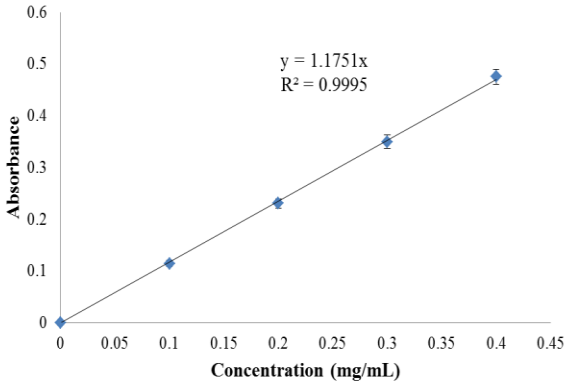
y = 1.1751x
R² = 0.9995
Absorbance
Concentration (mg/mL)

k)

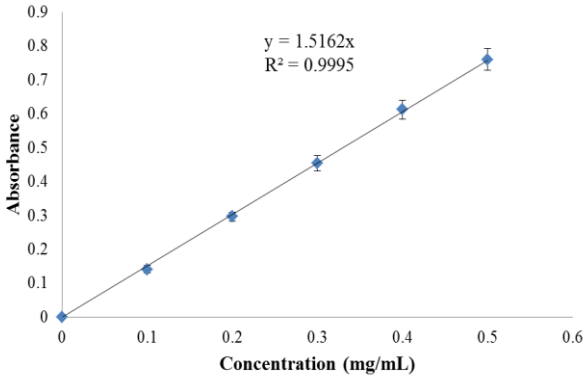
y = 1.5162x
R² = 0.9995
Absorbance
Concentration (mg/mL)

l)

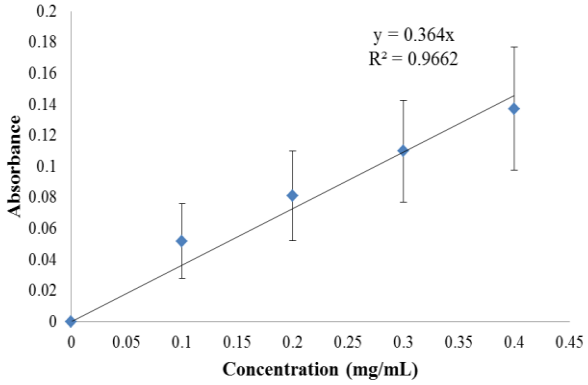
y = 0.364x
R² = 0.9662
Absorbance
Concentration (mg/mL)

m)

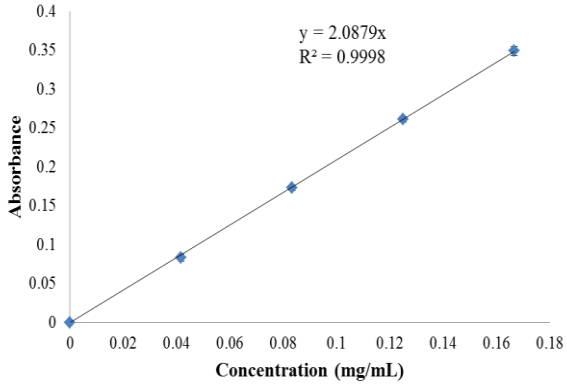
y = 2.0879x
R² = 0.9998
Absorbance
Concentration (mg/mL)
0.4
0.35
0.3
0.25
0.2
0.15
0.1
0.05
0
0 0.02 0.04 0.06 0.08 0.1 0.12 0.14 0.16 0.18

n)

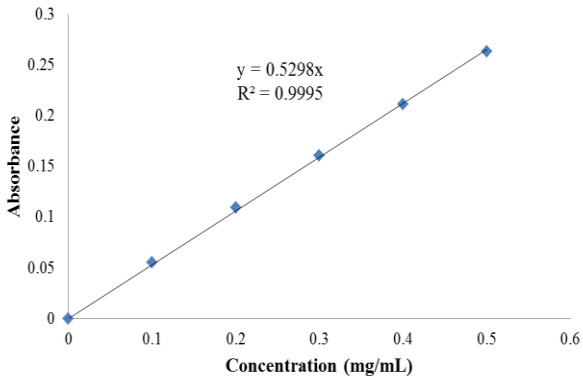
y = 0.5298x
R² = 0.9995
Absorbance
Concentration (mg/mL)
0.3
0.25
0.2
0.15
0.1
0.05
0
0 0.1 0.2 0.3 0.4 0.5 0.6

Appendix 2: Initial microsphere attempts for making PLA microspheres with morphology depedent on impellar type: a) clover leaf impellar, b) four blade imellar, and c) five blade impellar. Note that smaller microspheres are present on the surface because the filtration step was not used during initial formulations.

a)

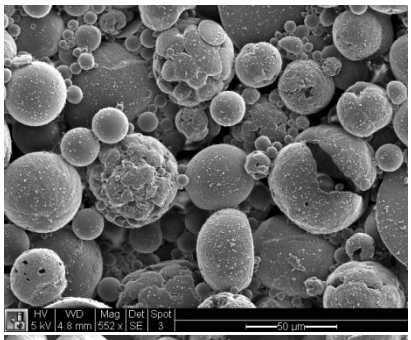

b)

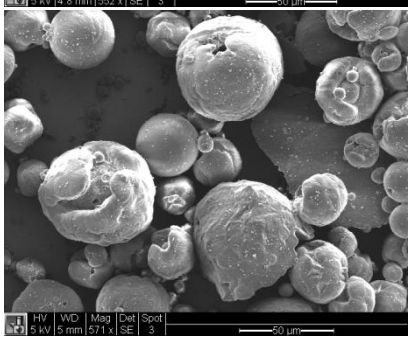

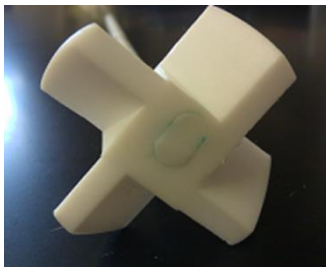

c)

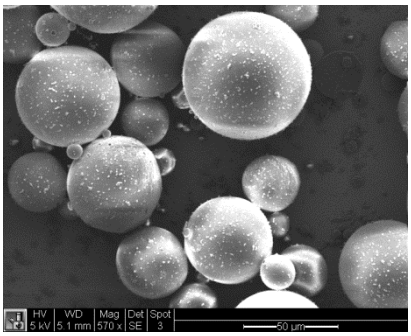

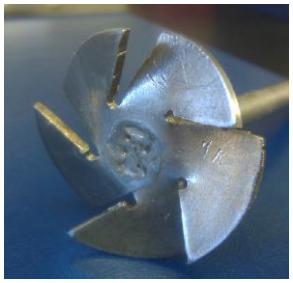

Appendix 3: Encapsulation efficiency values of rhodamine B encapsulated PLGA, PLA, and PCL microspheres

Polymer	Conditions	EE (%)	Std Dev (%)
PLGA	42 µm, 1.5 mg RB	53.1	9.0
	42 µm, 1.5 mg RB, 1 mg RB in W2	275.4	13.0
	23 µm, 1.5 mg RB, 5 mg RB in W2	438.7	15.5
PLA	37 µm, 1.5 mg RB	21.3	6.7
	27 µm, 1.5 mg RB	17.4	5.4
	37 µm, 3 mg RB	20.1	7.6
PCL	52 µm, 1.5 mg RB	12.6	8.1
	51 µm, 1.5 mg RB	8.3	4.4
	52 µm, 3 mg RB	5.5	5.6
	52 µm, 6 mg RB	26.1	5.6
	52 µm, 1.5 mg RB, single emulsion	8.3	5.5
	52 µm, 6 mg RB, single emulsion	13.7	10.9
	51 µm, 1.5 mg RB, single emulsion	6.3	1.5
	52 µm, 1.5 mg RB, 2.25 g PCL, 3% PVA	12.9	8.7
	52 µm, 6 mg RB, 2.25 g PCL, 5% PVA	5.9	3.4
	52 µm, 6 mg RB, 5% PVA, 10 mg RB in W2	69.6	13.9
	52 µm, 12 mg RB, 5% PVA, 10 mg RB in W2	54.1	7.6

Appendix 4: Drug loading values of rhodamine B encapsulated PLGA, PLA, and PCL microspheres

Polymer	Conditions	DL (%)	Std Dev (%)
PLGA	42 µm, 1.5 mg RB	0.08	0.007
	42 µm, 1.5 mg RB, 1 mg RB in W2	0.23	0.010
	23µm, 1.5 mg RB, 5 mg RB in W2	0.78	0.141
PLA	37 µm, 1.5 mg RB	0.04	0.008
	27 µm, 1.5 mg RB	0.03	0.004
	37 µm, 3 mg RB	0.06	0.005
PCL	52 µm, 1.5 mg RB	0.02	0.006
	51 µm, 1.5 mg RB	0.02	0.003
	52 µm, 3 mg RB	0.07	0.039
	52 µm, 6 mg RB	0.14	0.020
	52 µm, 1.5 mg RB, single emulsion	0.01	0.005
	52 µm, 6 mg RB, single emulsion	0.10	0.046
	51 µm, 1.5 mg RB, single emulsion	0.01	0.001
	52 µm, 1.5 mg RB, 2.25 g PCL, 3% PVA	0.07	0.002
	52 µm, 6 mg RB, 2.25 g PCL, 5% PVA	0.11	0.033
	52 µm, 6 mg RB, 5% PVA, 10 mg RB in W2	0.36	0.027
	52 µm, 12 mg RB, 5% PVA, 10 mg RB in W2	0.55	0.168

Appendix 5: Encapsulation efficiency values of gefitinib in PLGA

Polymer	Conditions	EE (%)	Standard Deviation (%)
PLGA	23 µm, 1.5 mg GB, 3% PVA	89.3	2.4
	23 µm, 3 mg GB, 3% PVA	48.7	8.8
	23 µm, 4.5 mg GB, 3% PVA	39.4	3.7
	28 µm, 15 mg GB, 2.5 g PLGA, 3% PVA	82.3	9.1
	19 µm, 1.5 mg GB, 3% PVA	47.0	5.1
	10 µm, 15 mg GB, 2.5 g PLGA	86.5	12.2

Appendix 6: Drug loading values of gefitinib in PLGA

Polymer	Conditions	DL (%)	Standard Deviation (%)
PLGA	23 µm, 1.5 mg GB, 3% PVA	0.11	0.002
	23 µm, 3 mg GB, 3% PVA	0.12	0.004
	23 µm, 4.5 mg GB, 3% PVA	0.21	0.013
	28 µm, 15 mg GB, 2.5 g PLGA, 3% PVA	0.63	0.023
	19 µm, 1.5 mg GB, 3% PVA	0.07	0.005
	10 µm, 15 mg GB, 2.5 g PLGA	0.55	0.026

Appendix 7: Total amount of gefitinib encapsualted in PLGA

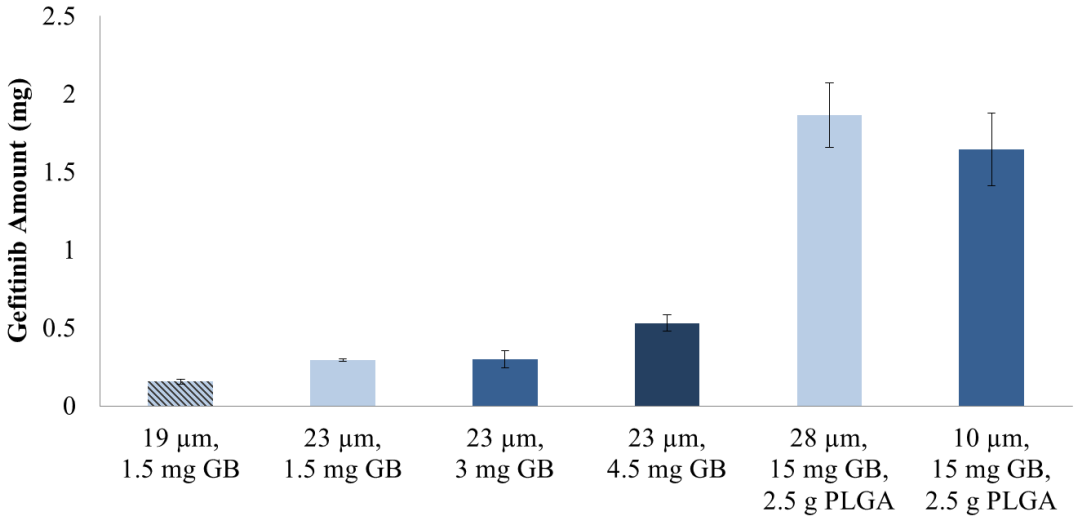

Appendix 8: Encapsulation efficiency values of IgG in PLA

Polymer	Conditions	EE (%)	Std Dev (%)
PLA	11 µm, 3 mg IgG, 3% PVA	17.8	4.1
	11µm, 15 mg IgG, 3% PVA	35.8	8.5
	11 µm, 3 mg IgG, 30 mL W2, 5% PVA	45.7	15.1
	11 µm, 12 mg IgG, 30 mL W2, 5% PVA	29.8	6.3
	11 µm, 3 mg IgG, 30 mL W2, 5% PVA, 5 mg IgG in W2	105.0	10.0
	11 µm, 7.5 mg IgG, 30 mL W2, 5% PVA, 5 mg IgG in W2	45.9	6.4
	11 µm, 7.5 mg IgG, 30 mL W2, 5% PVA, 10 mg IgG in W2	88.4	12.1
	43 µm, 7.5 mg IgG, 30 mL W2, 5% PVA, 10 mg IgG in W2	34.4	10.5
	11 µm, 3 mg IgG, 2 g PLA, 3% PVA	23.3	1.5
	11 µm, 3 mg IgG, 2 g PLA, 3% PVA	24.6	1.9

Appendix 9: Drug loading values of IgG in PLA

Polymer	Conditions	DL (%)	Std Dev (%)
PLA	11 µm, 3 mg IgG, 3% PVA	0.05	0.01
	11 µm, 15 mg IgG, 3% PVA	0.23	0.03
	11 µm, 3 mg IgG, 30 mL W2, 5% PVA	0.07	0.02
	11 µm, 12 mg IgG, 30 mL W2, 5% PVA	0.24	0.06
	11 µm, 3 mg IgG, 30 mL W2, 5% PVA, 5 mg IgG in W2	0.13	0.01
	11 µm, 7.5 mg IgG, 30 mL W2, 5% PVA, 5 mg IgG in W2	0.19	0.03
	11 µm, 7.5 mg IgG, 30 mL W2, 5% PVA, 10 mg IgG in W2	0.32	0.05
	43 µm, 7.5 mg IgG, 30 mL W2, 5% PVA, 10 mg IgG in W2	0.13	0.03
	11 µm, 3 mg IgG, 2 g PLA, 3% PVA	0.04	0.00
	11 µm, 3 mg IgG, 2 g PLA, 3% PVA	0.24	0.02

Appendix 10: Total amount of IgG encapsualted in PLA

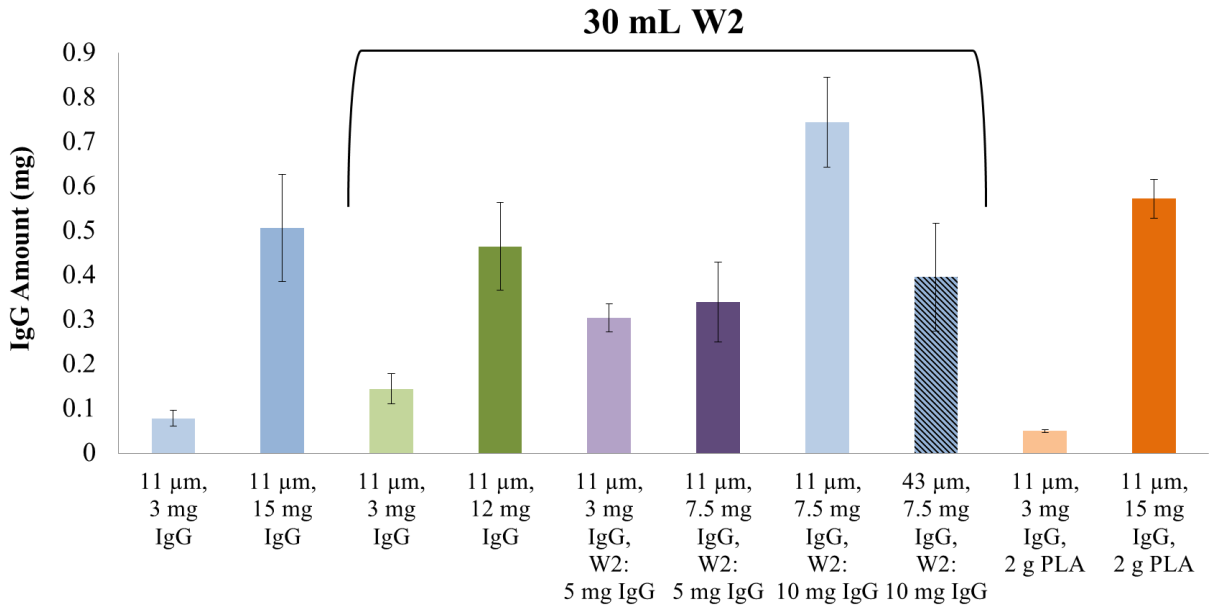

Appendix 11: Encapsulation efficiency values of LMT encapsulated in PCL

Polymer	Conditions	EE (%)	Std Dev (%)
PCL	31 µm, 1.5 mg LMT, 3% PVA	18.1	0.7
	31 µm, 3 mg LMT, 3% PVA	12.6	0.4
	31 µm, 6 mg LMT, 3% PVA	17.6	2.8
	31 µm, 9 mg LMT, 3% PVA	15.6	1.2
	31 µm, 15 mg LMT, 3% PVA	18.0	1.8
	31 µm, 15 mg LMT, 5 mg in W2, 3% PVA	24.2	2.4
	31 µm, 3 mg LMT, 30 mL W2, 5% PVA	34.0	3.3
	31 µm, 15 mg LMT, 30 mL W2, 5% PVA	34.1	1.1
	31 µm, 3 mg LMT, 30 mL W2, 5% PVA, 5 mg LMT in W2	291.2	36.3
	31 µm, 15 mg LMT, 30 mL W2, 5% PVA, 5 mg LMT in W2	101.6	11.5
	31 µm, 3 mg LMT, 2.5 g PCL, 5% PVA	22.0	2.1
	31 µm, 15 mg LMT, 2.5 g PCL, 5% PVA	21.1	7.2
	3560 rpm, 3 mg LMT, 3% PVA	13.2	2.8

Appendix 12: Drug loading values of LMT encapsulated in PCL

Polymer	Conditions	DL (%)	Std Dev (%)
PCL	31 µm, 1.5 mg LMT, 3% PVA	0.05	0.007
	31 µm, 3 mg LMT, 3% PVA	0.08	0.004
	31 µm, 6 mg LMT, 3% PVA	0.20	0.007
	31 µm, 9 mg LMT, 3% PVA	0.26	0.015
	31 µm, 15 mg LMT, 3% PVA	0.47	0.019
	31 µm, 15 mg LMT, 5 mg in W2, 3% PVA	0.63	0.052
	31 µm, 3 mg LMT, 30 mL W2, 5% PVA	0.09	0.011
	31 µm, 15 mg LMT, 30 mL W2, 5% PVA	0.58	0.050
	31 µm, 3 mg LMT, 30 mL W2, 5% PVA, 5 mg LMT in W2	0.84	0.125
	31 µm, 15 mg LMT, 30 mL W2, 5% PVA, 5 mg LMT in W2	1.54	0.081
	31 µm, 3 mg LMT, 2.5 g PCL, 5% PVA	0.08	0.005
	31 µm, 15 mg LMT, 2.5 g PCL, 5% PVA	0.39	0.032
	3560 rpm, 3 mg LMT, 3% PVA	0.08	0.005

Appendix 13: Total amount of LMT encapsulated in PCL. Unless otherwise stated, all formulations are at 2800 rpm.

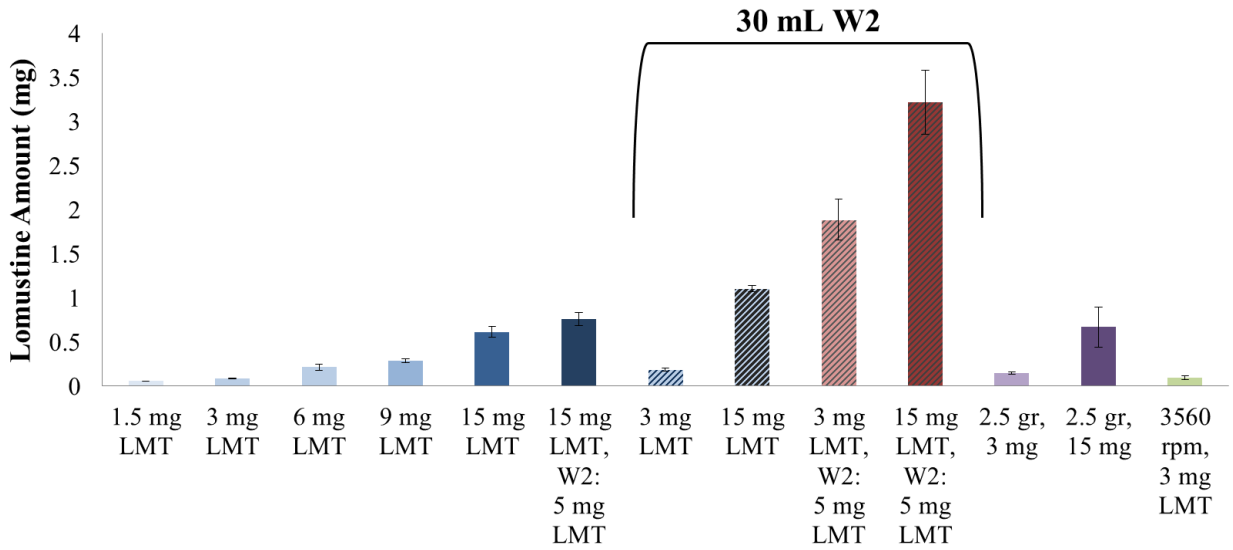

Appendix 14: Time points for measurements in the *in vitro* drug release.

***In vitro* Release Type**	**Drug**	**Particle Size (μm)**	**Days Measured**
Microspheres in PBS	Rhodamine B	23 ± 8	2, 4, 6, 8, 10, 12, 14, 16, 18, 20, 22, 24, 26, 28, 30, 32, 36, 40, 50, 60, 70
		44 ± 17	2, 4, 6, 8, 10, 12, 14, 18, 22, 26, 30, 34, 42, 50, 60, 70
	Gefitinib	19 ± 8	2, 4, 6, 8, 10, 12, 14, 16, 18, 20, 22, 24, 26, 28, 30, 32, 34, 36, 38, 40, 45, 50, 52, 54, 56, 58, 60, 65, 70
		23 ± 8	2, 4, 6, 8, 10, 12, 14, 16, 18, 20, 22, 24, 26, 28, 30, 32, 34, 36, 38, 40, 45, 50, 52, 54, 56, 58, 60, 65, 70
	IgG	11 ± 7	1, 2, 4, 8, 12, 16, 20, 25, 30, 35, 40, 45, 50, 58, 66, 74, 82, 90, 98, 106, 114, 122, 130, 138, 146, 156, 166, 177, 186, 196, 206, 216, 226, 236, 248, 260, 272, 284, 296, 308, 324, 340, 356, 372, 390, 408, 437, 466, 495
		43 ± 25	1, 2, 4, 8, 12, 16, 20, 25, 30, 35, 40, 45, 50, 58, 66, 74, 82, 90, 98, 106, 114, 122, 130, 138, 146, 156, 166, 177, 186, 196, 206, 216, 226, 236, 248, 260, 272, 284, 296, 308, 324, 340
	Lomustine	31 ± 12	1, 2, 3, 4
Microspheres in pH 10	IgG	11 ± 7	1, 2, 4, 8, 12, 16
Microspheres in pH 6	IgG	11 ± 7	1, 2, 5, 8
Microspheres in pH 4	IgG	11 ± 7	1, 2, 5, 8, 12, 16
Combined microspheres in pH 10	IgG and Gefitinib	IgG: 11 ± 7 GB: 19 ± 8	1, 2, 5, 8, 12, 16, 20, 26, 33, 40, 47, 54, 79, 104
Microspheres in 5 M NaOH-DMSO	Lomustine	31 ± 12	1, 2, 3, 4
Microspheres in PNIPAM in PBS	Rhodamine B	23 ± 8	2, 4, 6, 8, 10, 12, 14, 16, 18, 20, 22, 24, 26, 28, 30, 32, 34, 36, 38, 40
		44 ± 17	2, 4, 6, 8, 10, 12, 14, 16, 18, 20, 22, 24, 26, 28, 30, 32, 34, 36, 38, 40
	Gefitinib	19 ± 8	2, 4, 6, 8, 10, 12, 14, 16, 18, 20, 22, 24, 26, 28, 30, 32, 34, 36, 38, 40, 45, 50, 55, 60, 70
		23 ± 8	2, 4, 6, 8, 10, 12, 14, 16, 18, 20, 22, 24, 26, 28, 30, 32, 34, 36, 38, 40, 45, 50, 55, 60, 70

Appendix 15: *In vitro* release of rhodamine B from PLGA microspheres (44 ± 17 µm) in PBS and microspheres entrapped in PNIPAM and suspended in PBS at 37°C and gently shaken, n=3.

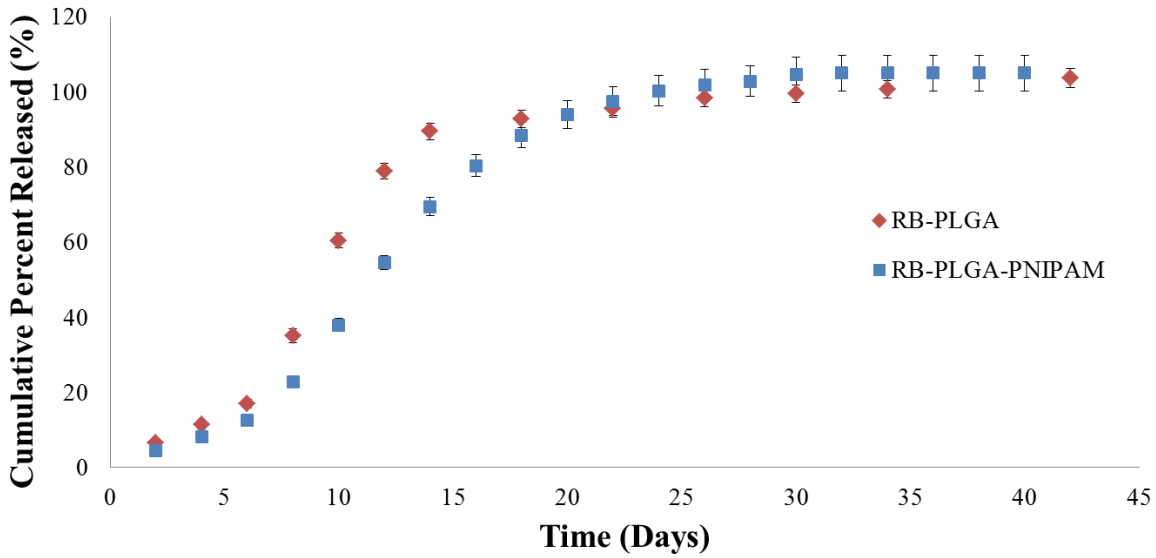

Appendix 16: *In vitro* release of IgG from PLA microspheres with cumulative error, n=3.

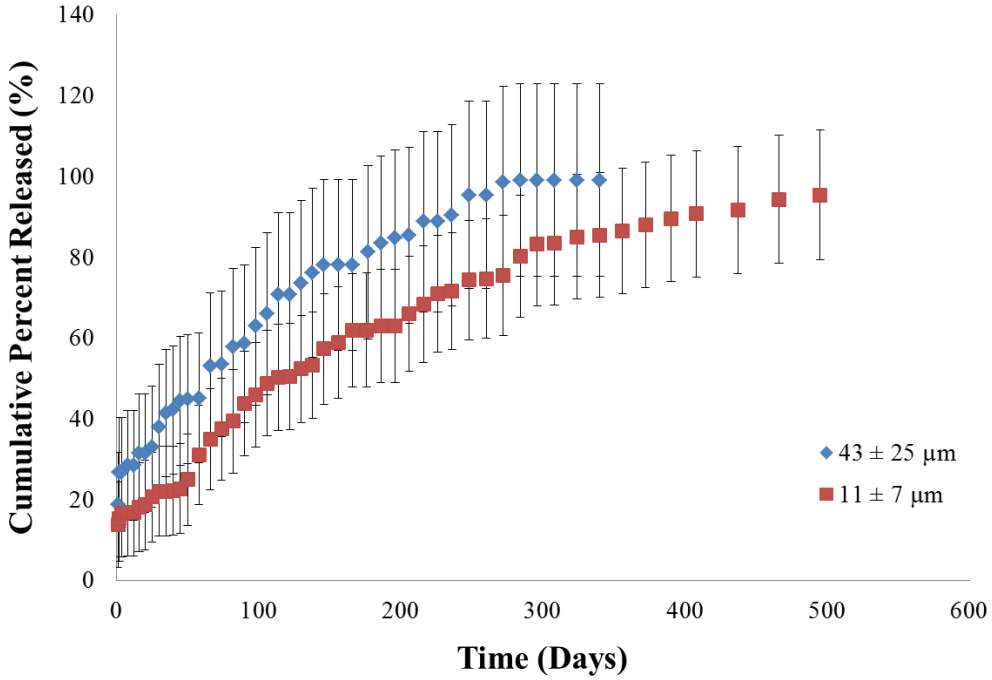

Appendix 17: *In vitro* release of free IgG from PNIPAM, n=3.

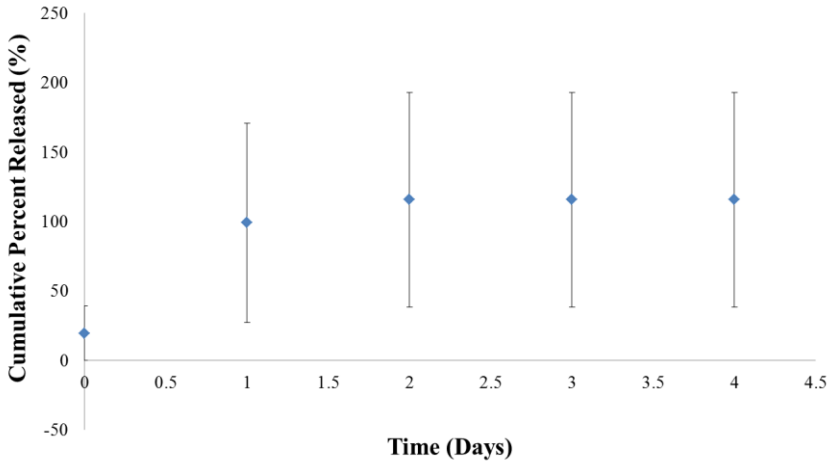

Appendix 18: Individual tumor measurements of Pilot Study 1. A complete dose is a full 0.5 mL volume injected, with total of 200 µg gefitinib encapsulated in PLGA microspheres suspended in PNIPAM. The control was blank PLGA microspheres in PNIPAM. The percentages given are estimates based on volume remaining in the syringe; however, microspheres may not have been equally dispersed in solution due to gelation.

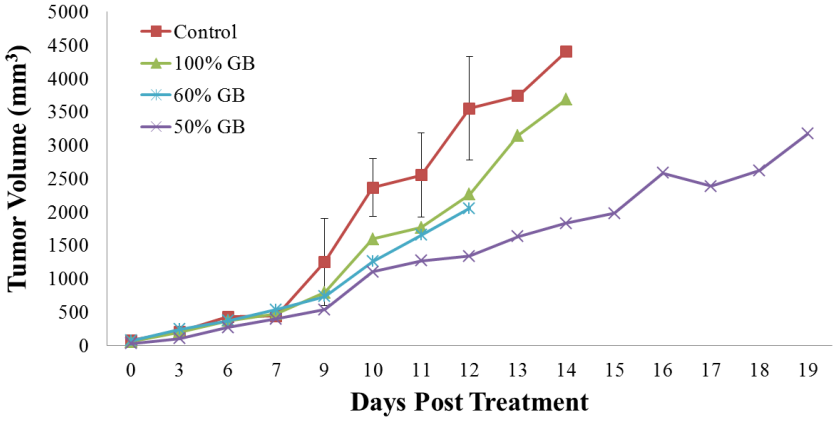

Appendix 19: Vertebrate Animals

The subcutaneous tumor model protocol involving vertebrate animals have been approved by the University of Washington Institutional Animal Care and Use Committee (IACUC) under protocol 3043-01 (PI: Dr. Buddy Ratner). All animal studies will be completed in a facility managed by the University of Washington Department of Comparative Medicine, which is accredited by the Association for Assessment of Laboratory Animal Care (AALAC).

6 References

[1] Howlader N, N. A., Krapcho M, Neyman N, Aminou R, Altekruse SF, Kosary CL, Ruhl J, Tatalovich Z, Cho H, Mariotto A, Eisner MP, Lewis DR, Chen HS, Feuer EJ, Cronin KA (eds), April 2012 "SEER Cancer Statistics Review, 1975-2009 (Vintage 2009 Populations)," http://seer.cancer.gov/csr/1975_2009_pops09/ </csr/1975_2009_pops09/>

[2] 2015, "Cancer Facts & Figures 2015," American Cancer Society, ed.Atlanta, GA.

[3] Holland, E. C., 2000, "Glioblastoma multiforme: The terminator," Proceedings of the National Academy of Sciences of the United States of America, 97(12), pp. 6242-6244.

[4] Van Meir, E. G., Hadjipanayis, C. G., Norden, A. D., Shu, H. K., Wen, P. Y., and Olson, J. J., 2010, "Exciting New Advances in Neuro-Oncology The Avenue to a Cure for Malignant Glioma," Ca-a Cancer Journal for Clinicians, 60(3), pp. 166-193.

[5] Buonerba, C., Di Lorenzo, G., Marinelli, A., Federico, P., Palmieri, G., Imbimbo, M., Conti, P., Peluso, G., De Placido, S., and Sampson, J. H., 2011, "A comprehensive outlook on intracerebral therapy of malignant gliomas," Crit Rev Oncol Hematol, 80(1), pp. 54-68.

[6] National Cancer Institute, 2009, "What You Need To Know About Brain Tumors."

[7] Hochberg, F. H., and Pruitt, A., 1980, "Assumptions in the radiotherapy of glioblastoma," Neurology, 30(9), pp. 907-911.

[8] Athanassiou, H., Synodinou, M., Maragoudakis, E., Paraskevaidis, M., Verigos, C., Misailidou, D., Antonadou, D., Saris, G., Beroukas, K., and Karageorgis, P., 2005, "Randomized phase II study of temozolomide and radiotherapy compared with radiotherapy alone in newly diagnosed glioblastoma multiforme," J Clin Oncol, 23(10), pp. 2372-2377.

[9] Dang, W. B., Daviau, T., Ying, P., Zhao, Y., Nowotnik, D., Clow, C. S., Tyler, B., and Brem, H., 1996, "Effects of GLIADEL(R) wafer initial molecular weight on the erosion of wafer and release of BCNU," Journal of Controlled Release, 42(1), pp. 83-92.

[10] Westphal, M., Hilt, D. C., Bortey, E., Delavault, P., Olivares, R., Warnke, P. C., Whittle, I. R., Jaaskelainen, J., and Ram, Z., 2003, "A phase 3 trial of local chemotherapy with biodegradable carmustine (BCNU) wafers (Gliadel wafers) in patients with primary malignant glioma," Neuro Oncol, 5(2), pp. 79-88.

[11] Attenello, F. J., Mukherjee, D., Datoo, G., McGirt, M. J., Bohan, E., Weingart, J. D., Olivi, A., Quinones-Hinojosa, A., and Brem, H., 2008, "Use of Gliadel (BCNU) wafer in the surgical treatment of malignant glioma: A 10-year institutional experience," Annals of Surgical Oncology, 15(10), pp. 2887-2893.

[12] Alam, M. I., Beg, S., Samad, A., Baboota, S., Kohli, K., Ali, J., Ahuja, A., and Akbar, M., 2010, "Strategy for effective brain drug delivery," European Journal of Pharmaceutical Sciences, 40(5), pp. 385-403.

[13] Groothuis, D. R., 2000, "The blood-brain and blood-tumor barriers:
A review of strategies for increasing drug
delivery," Neuro Oncol, 2(1), pp. 45-59.

[14] Orive, G., Ali, O. A., Anitua, E., Pedraz, J. L., and Emerich, D. F., 2010, "Biomaterial-based technologies for brain anti-cancer therapeutics and imaging," Biochimica Et Biophysica Acta-Reviews on Cancer, 1806(1), pp. 96-107.

[15] Bredel, M., and Zentner, J., 2002, "Brain-tumour drug resistance: the bare essentials," Lancet Oncology, 3(7), pp. 397-406.

[16] Wolinsky, J. B., Colson, Y. L., and Grinstaff, M. W., 2012, "Local drug delivery strategies for cancer treatment: Gels, nanoparticles, polymeric films, rods, and wafers," Journal of Controlled Release, 159(1), pp. 14-26.
[17] American Cancer Society, 2013, "Brain and Spinal Cord Tumors in Children."
[18] Clarke, J., Butowski, N., and Chang, S., 2010, "Recent Advances in Therapy for Glioblastoma," Archives of Neurology, 67(3), pp. 279-283.
[19] Sawyer, A. J., Piepmeier, J. M., and Saltzman, W. M., 2006, "New methods for direct delivery of chemotherapy for treating brain tumors," Yale J Biol Med, 79(3-4), pp. 141-152.
[20] Guerin, C., Olivi, A., Weingart, J. D., Lawson, H. C., and Brem, H., 2004, "Recent advances in brain tumor therapy: local intracerebral drug delivery by polymers," Investigational New Drugs, 22(1), pp. 27-37.
[21] Allhenn, D., Boushehri, M. A. S., and Lamprecht, A., 2012, "Drug delivery strategies for the treatment of malignant gliomas," International Journal of Pharmaceutics, 436(1-2), pp. 299-310.
[22] Bidros, D. S., and Vogelbaum, M. A., 2009, "Novel Drug Delivery Strategies in Neuro-Oncology," Neurotherapeutics, 6(3), pp. 539-546.
[23] Zhang, D. Y., Tian, A., Xue, X. X., Wang, M., Qiu, B., and Wu, A. H., 2012, "The Effect of Temozolomide/Poly(lactide-co-glycolide) (PLGA)/Nano-Hydroxyapatite Microspheres on Glioma U87 Cells Behavior," International Journal of Molecular Sciences, 13(1), pp. 1109-1125.
[24] Ranganath, S. H., Kee, I., Krantz, W. B., Chow, P. K. H., and Wang, C. H., 2009, "Hydrogel Matrix Entrapping PLGA-Paclitaxel Microspheres: Drug Delivery with Near Zero-Order Release and Implantability Advantages for Malignant Brain Tumour Chemotherapy," Pharmaceutical Research, 26(9), pp. 2101-2114.
[25] Pradilla, G., Wang, P. P., Gabikian, P., Li, K., Magee, C. A., Walter, K. A., and Brem, H., 2006, "Local intracerebral administration of paclitaxel with the Paclimer (R) delivery system: toxicity study in a canine model," Journal of Neuro-Oncology, 76(2), pp. 131-138.
[26] Lemaire, L., Roullin, V. G., Franconi, F., Venier-Julienne, M. C., Menei, P., Jallet, P., Le Jeune, J. J., and Benoit, J. P., 2001, "Therapeutic efficacy of 5-fluorouracil-loaded microspheres on rat glioma: a magnetic resonance imaging study," Nmr in Biomedicine, 14(6), pp. 360-366.
[27] Elkharraz, K., Faisant, N., Guse, C., Siepmann, F., Arica-Yegin, B., Oger, J. M., Gust, R., Goepferich, A., Benoit, J. P., and Siepmann, J., 2006, "Paclitaxel-loaded microparticles and implants for the treatment of brain cancer: Preparation and physicochemical characterization," International Journal of Pharmaceutics, 314(2), pp. 127-136.
[28] Zhang, H., and Gao, S., 2007, "Temozolomide/PLGA microparticles and antitumor activity against Glioma C6 cancer cells in vitro," International Journal of Pharmaceutics, 329(1-2), pp. 122-128.
[29] Zhang, Y. H., Yue, Z. J., Zhang, H., Tang, G. S., Wang, Y., and Liu, J. M., 2010, "Temozolomide/PLGA microparticles plus vatalanib inhibits tumor growth and angiogenesis in an orthotopic glioma model," European Journal of Pharmaceutics and Biopharmaceutics, 76(3), pp. 371-375.
[30] Gil-Alegre, M. E., Gonzalez-Alvarez, I., Gutierrez-Pauls, L., and Torres-Suarez, A. I., 2008, "Three weeks release BCNU loaded hydrophilic-PLGA microspheres for interstitial chemotherapy: Development and activity against human glioblastoma cells," Journal of Microencapsulation, 25(8), pp. 561-568.

[31] Chen, W., and Lu, D. R., 1999, "Carboplatin-loaded PLGA microspheres for intracerebral injection: formulation and characterization," Journal of Microencapsulation, 16(5), pp. 551-563.
[32] Menei, P., BoisdronCelle, M., Croue, A., Guy, G., and Benoit, J. P., 1996, "Effect of stereotactic implantation of biodegradable 5-fluorouracil-loaded microspheres in healthy and C6 glioma-bearing rats," Neurosurgery, 39(1), pp. 117-123.
[33] Menei, P., Capelle, L., Guyotat, J., Fuentes, S., Assaker, R., Bataille, B., Francois, P., Dorwling-Carter, D., Paquis, P., Bauchet, L., Parker, F., Sabatier, J., Faisant, N., and Benoit, J. P., 2005, "Local and sustained delivery of 5-fluorouracil from biodegradable microspheres for the radiosensitization of malignant glioma: A randomized phase II trial," Neurosurgery, 56(2), pp. 242-247.
[34] Menei, P., Jadaud, E., Faisant, N., Boisdron-Celle, M., Michalak, S., Fournier, D., Delhaye, M., and Benoit, J. P., 2004, "Stereotaxic implantation of 5-fluorouracil-releasing microspheres in malignant glioma - A phase I study," Cancer, 100(2), pp. 405-410.
[35] Fournier, E., Passirani, C., Montero-Menei, C., Colin, N., Breton, P., Sagodira, S., Menei, P., and Benoit, J. P., 2003, "Therapeutic effectiveness of novel 5-fluorouracil-loaded poly(methylidene malonate 2.1.2)-based microspheres on F98 glioma-bearing rats," Cancer, 97(11), pp. 2822-2829.
[36] Roullin, V. G., Deverre, J. R., Lemaire, L., Hindre, F., Venier-Julienne, M. C., Vienet, R., and Benoit, J. P., 2002, "Anti-cancer drug diffusion within living rat brain tissue: an experimental study using [H-3](6)-5-fluorouracil-loaded PLGA microspheres," European Journal of Pharmaceutics and Biopharmaceutics, 53(3), pp. 293-299.
[37] Reza, M. S., and Whateley, T. L., 1998, "Iodo-2 '-deoxyuridine (IUdR) and (125)IUdR loaded biodegradable microspheres for controlled delivery to the brain," Journal of Microencapsulation, 15(6), pp. 789-801.
[38] Emerich, D. F., Winn, S. R., and Bartus, R. T., 2001, "Injection of chemotherapeutic microspheres and glioma IV: Eradicating tumors in rats," Cell Transplantation, 11(1), pp. 47-54.
[39] Emerich, D. F., Winn, S. R., Hu, Y. H., Marsh, J., Snodgrass, P., LaFreniere, D., Wiens, T., Hasler, B. P., and Bartus, R. T., 2000, "Injectable chemotherapeutic microspheres and glioma I: Enhanced survival following implantation into the cavity wall of debulked tumors," Pharmaceutical Research, 17(7), pp. 767-775.
[40] Emerich, D. F., Winn, S. R., Snodgrass, P., LaFreniere, D., Agostino, M., Wiens, T., Xiong, H., and Bartus, R. T., 2000, "Injectable chemotherapeutic microspheres and glioma II: Enhanced survival following implantation into deep inoperable tumors," Pharmaceutical Research, 17(7), pp. 776-781.
[41] Fournier, E., Passirani, C., Colin, N., Breton, P., Sagodira, S., and Benoit, J. P., 2004, "Development of novel 5-FU-loaded poly(methylidene malonate 2.1.2)-based microspheres for the treatment of brain cancers," European Journal of Pharmaceutics and Biopharmaceutics, 57(2), pp. 189-197.
[42] Boisdroncelle, M., Menei, P., and Benoit, J. P., 1995, "Preparation and Characterization of 5-Fluorouracil-Loaded Microparticles as Biodegradable Anticancer Drug Carriers," Journal of Pharmacy and Pharmacology, 47(2), pp. 108-114.
[43] Benny, O., Duvshani-Eshet, M., Cargioli, T., Bello, L., Bikfalvi, A., Carroll, R. S., and Machluf, M., 2005, "Continuous delivery of endogenous inhibitors from poly (lactic-co-glycolic acid) polymeric microspheres inhibits glioma tumor growth," Clinical Cancer Research, 11(2), pp. 768-776.

[44] Benny, O., Kim, S. K., Gvili, K., Radzishevsky, I. S., Mor, A., Verduzco, L., Menon, L. G., Black, P. M., Machluf, M., and Carroll, R. S., 2008, "In vivo fate and therapeutic efficacy of PF-4/CTF microspheres in an orthotopic human glioblastoma model," Faseb Journal, 22(2), pp. 488-499.
[45] Benny, O., Menon, L. G., Arid, G., Goren, E., Kim, S. K., Stewman, C., Black, P. M., Carroll, R. S., and Machluf, M., 2009, "Local Delivery of Poly Lactic-co-glycolic Acid Microspheres Containing Imatinib Mesylate Inhibits Intracranial Xenograft Glioma Growth," Clinical Cancer Research, 15(4), pp. 1222-1231.
[46] Chandy, T., Das, G. S., and Rao, G. H. R., 2000, "5-fluorouracil-loaded chitosan coated polylactic acid microspheres as biodegradable drug carriers for cerebral tumours," Journal of Microencapsulation, 17(5), pp. 625-638.
[47] Ozeki, T., Hashizawa, K., Kaneko, D., Imai, Y., and Okada, H., 2010, "Treatment of rat brain tumors using sustained-release of camptothecin from poly(lactic-co-glycolic acid) microspheres in a thermoreversible hydrogel," Chem Pharm Bull (Tokyo), 58(9), pp. 1142-1147.
[48] Arai, T., Benny, O., Joki, T., Menon, L. G., Machluf, M., Abe, T., Carroll, R. S., and Black, P. M., 2010, "Novel local drug delivery system using thermoreversible gel in combination with polymeric microspheres or liposomes," Anticancer Res, 30(4), pp. 1057-1064.
[49] Hussain, M., Beale, G., Hughes, M., and Akhtar, S., 2002, "Co-delivery of an antisense oligonucleotide and 5-fluorouracil using sustained release poly (lactide-co-glycolide) microsphere formulations for potential combination therapy in cancer," Int J Pharm, 234(1-2), pp. 129-138.
[50] Emerich, D. F., Winn, S. R., and Bartus, R. T., 2001, "Injection of chemotherapeutic microspheres and glioma III: Parameters to optimize efficacy," Cell Transplantation, 11(1), pp. 35-45.
[51] Song, T. T., Yuan, X. B., Sun, A. P., Wang, H., Kang, C. S., Ren, Y., He, B., Sheng, J., and Pu, P. Y., 2009, "Preparation of Injectable Paclitaxel Sustained Release Microspheres by Spray Drying for Inhibition of Glioma In Vitro," Journal of Applied Polymer Science, 115(3), pp. 1534-1539.
[52] Lin, R., Shi Ng, L., and Wang, C. H., 2005, "In vitro study of anticancer drug doxorubicin in PLGA-based microparticles," Biomaterials, 26(21), pp. 4476-4485.
[53] Xie, J. W., Marijnissen, J. C. M., and Wang, C. H., 2006, "Microparticles developed by electrohyd ro dynamic atomization for the local delivery of anticancer drug to treat C6 glioma in vitro," Biomaterials, 27(17), pp. 3321-3332.
[54] Xie, J. W., Tan, R. S., and Wang, C. H., 2008, "Biodegradable microparticles and fiber fabrics for sustained delivery of cisplatin to treat C6 glioma in vitro," Journal of Biomedical Materials Research Part A, 85A(4), pp. 897-908.
[55] Naraharisetti, P. K., Ong, B. Y. S., Xie, J. W., Lee, T. K. Y., Wang, C. H., and Sahinidis, N. V., 2007, "In vivo performance of implantable biodegradable preparations delivering Paclitaxel and Etanidazole for the treatment of glioma," Biomaterials, 28(5), pp. 886-894.
[56] Li, K. W., Dang, W. B., Tyler, B. M., Troiano, G., Tihan, T., Brem, H., and Walter, K. A., 2003, "Polilactofate microspheres for paclitaxel delivery to central nervous system malignancies," Clinical Cancer Research, 9(9), pp. 3441-3447.
[57] Ozeki, T., Kaneko, D., Hashizawa, K., Imai, Y., Tagami, T., and Okada, H., 2012, "Improvement of survival in C6 rat glioma model by a sustained drug release from localized PLGA microspheres in a thermoreversible hydrogel," International Journal of Pharmaceutics, 427(2), pp. 299-304.

[58] Rhines, L. D., Sampath, P., DiMeco, F., Lawson, H. C., Tyler, B. M., Hanes, J., Olivi, A., and Brem, H., 2003, "Local immunotherapy with interleukin-2 delivered from biodegradable polymer microspheres combined with interstitial chemotherapy: a novel treatment for experimental malignant glioma," Neurosurgery, 52(4), pp. 872-879; discussion 879-880.
[59] Beer, S. J., Hilfinger, J. M., and Davidson, B. L., 1997, "Extended release of adenovirus from polymer microspheres: potential use in gene therapy for brain tumors," Adv Drug Deliv Rev, 27(1), pp. 59-66.
[60] Beer, S. J., Matthews, C. B., Stein, C. S., Ross, B. D., Hilfinger, J. M., and Davidson, B. L., 1998, "Poly(lactic-glycolic) acid copolymer encapsulation of recombinant adenovirus reduces immunogenicity in vivo," Gene Therapy, 5(6), pp. 740-746.
[61] Ozeki, T., Kaneko, D., Hashizawa, K., Imai, Y., Tagami, T., and Okada, H., 2012, "Combination Therapy of Surgical Tumor Resection with Implantation of a Hydrogel Containing Camptothecin-Loaded Poly(lactic-co-glycolic acid) Microspheres in a C6 Rat Glioma Model," Biological & Pharmaceutical Bulletin, 35(4), pp. 545-550.
[62] Zhang, Y. H., Zhang, H., Liu, J. M., and Yue, Z. J., 2011, "Temozolomide/PLGA microparticles: a new protocol for treatment of glioma in rats," Medical Oncology, 28(3), pp. 901-906.
[63] Dong, J., Zhou, G. H., Tang, D. F., Chen, Y. M., Cui, B. Q., Dai, X. L., Zhang, J. S., Lan, Q., and Huang, Q., 2012, "Local delivery of slow-releasing temozolomide microspheres inhibits intracranial xenograft glioma growth," Journal of Cancer Research and Clinical Oncology, 138(12), pp. 2079-2084.
[64] Hanes, J., Sills, A., Zhao, Z., Suh, K. W., Tyler, B., DiMeco, F., Brat, D. J., Choti, M. A., Leong, K. W., Pardoll, D. M., and Brem, H., 2001, "Controlled local delivery of interleukin-2 by biodegradable polymers protects animals from experimental brain tumors and liver tumors," Pharm Res, 18(7), pp. 899-906.
[65] Hsu, W., Lesniak, M. S., Tyler, B., and Brem, H., 2005, "Local delivery of interleukin-2 and adriamycin is synergistic in the treatment of experimental malignant glioma," Journal of Neuro-Oncology, 74(2), pp. 135-140.
[66] Freiberg, S., and Zhu, X., 2004, "Polymer microspheres for controlled drug release," International Journal of Pharmaceutics, 282(1-2), pp. 1-18.
[67] Edlund, U., and Albertsson, A. C., 2002, "Degradable polymer microspheres for controlled drug delivery," Degradable Aliphatic Polyesters, 157, pp. 67-112.
[68] Park, J. H., Ye, M. L., and Park, K., 2005, "Biodegradable polymers for microencapsulation of drugs," Molecules, 10(1), pp. 146-161.
[69] Vilos, C., and Velasquez, L. A., 2012, "Therapeutic Strategies Based on Polymeric Microparticles," Journal of Biomedicine and Biotechnology.
[70] Hu, L., Zhang, H., and Song, W., "An overview of preparation and evaluation sustained-release injectable microspheres," J Microencapsul.
[71] Makadia, H. K., and Siegel, S. J., "Poly Lactic-co-Glycolic Acid (PLGA) as Biodegradable Controlled Drug Delivery Carrier," Polymers (Basel), 3(3), pp. 1377-1397.
[72] Menei, P., Venier, M. C., Gamelin, E., Saint-Andre, J. P., Hayek, G., Jadaud, E., Fournier, D., Mercier, P., Guy, G., and Benoit, J. P., 1999, "Local and sustained delivery of 5-fluorouracil from biodegradable microspheres for the radiosensitization of glioblastoma - A pilot study," Cancer, 86(2), pp. 325-330.

[73] Menei, P., Daniel, V., Montero-Menei, C., Brouillard, M., Pouplard-Barthelaix, A., and Benoit, J. P., 1993, "Biodegradation and brain tissue reaction to poly(D,L-lactide-co-glycolide) microspheres," Biomaterials, 14(6), pp. 470-478.
[74] Veziers, J., Lesourd, M., Jollivet, C., Montero-Menei, C., Benoit, J. P., and Menei, P., 2001, "Analysis of brain biocompatibility of drug-releasing biodegradable microspheres by scanning and transmission electron microscopy," Journal of Neurosurgery, 95(3), pp. 489-494.
[75] Ratner, B. D., 2004, Biomaterials science : an introduction to materials in medicine, Elsevier Academic Press, Amsterdam ; Boston.
[76] Rahane, S. B., Floyd, J. A., Metters, A. T., and Kilbey, S. M., 2008, "Swelling behavior of multiresponsive poly(methacrylic acid)-block-poly (N-isopropylacrylamide) brushes synthesized using surface-initiated photoiniferter-mediated photopolymerization," Advanced Functional Materials, 18(8), pp. 1232-1240.
[77] Tran, V. T., Benoit, J. P., and Venier-Julienne, M. C., 2011, "Why and how to prepare biodegradable, monodispersed, polymeric microparticles in the field of pharmacy?," International Journal of Pharmaceutics, 407(1-2), pp. 1-11.
[78] Yemisci, M., Bozdag, S., Cetin, M., Soylemezoglu, F., Capan, Y., Dalkara, T., and Vural, I., 2006, "Treatment of malignant gliomas with mitoxantrone-loaded poly (lactide-co-glycolide) microspheres," Neurosurgery, 59(6), pp. 1296-1302; discussion 1302-1293.
[79] Berkland, C., Kim, K., and Pack, D. W., 2003, "PLG microsphere size controls drug release rate through several competing factors," Pharmaceutical Research, 20(7), pp. 1055-1062.
[80] Araki, T., Yashima, H., Shimizu, K., Aomori, T., Hashita, T., Kaira, K., Nakamura, T., and Yamamoto, K., "Review of the treatment of non-small cell lung cancer with gefitinib," Clin Med Insights Oncol, 6, pp. 407-421.
[81] 2013, "Full Prescribing Information: Avastin," Genentech, Inc.
[82] Zhuang, L., Gao, J., Zeng, Y., Yu, F., Zhang, B., Li, M., Derendorf, H., and Liu, C., "HPLC method validation for the quantification of lomustine to study pharmacokinetics of thermosensitive liposome-encapsulated lomustine containing iohexol for CT imaging in C6 glioma rats," Eur J Drug Metab Pharmacokinet, 36(2), pp. 61-69.
[83] Mehrotra, A., Nagarwal, R. C., and Pandit, J. K., "Lomustine loaded chitosan nanoparticles: characterization and in-vitro cytotoxicity on human lung cancer cell line L132," Chem Pharm Bull (Tokyo), 59(3), pp. 315-320.
[84] Loftsson, T., and Fridriksdottir, H., 1990, "Degradation of Lomustine (Ccnu) in Aqueous-Solutions," International Journal of Pharmaceutics, 62(2-3), pp. 243-247.
[85] Muller, F., Riesenberg, H., Hirnle, P., Gehl, H. B., Duwel, P., and Gorner, M., "[Complete remission of multiple brain metastases of non-small cell lung cancer induced by gefitinib monotherapy]," Strahlenther Onkol, 187(12), pp. 826-830.
[86] Yuan, Y., Tan, C., Li, M., Shen, H., Fang, X., Hu, Y., and Ma, S., 2012, "Activity of pemetrexed and high-dose gefitinib in an EGFR-mutated lung adenocarcinoma with brain and leptomeningeal metastasis after response to gefitinib," World J Surg Oncol, 10, p. 235.
[87] Ceresoli, G. L., Cappuzzo, F., Gregorc, V., Bartolini, S., Crino, L., and Villa, E., 2004, "Gefitinib in patients with brain metastases from non-small-cell lung cancer: a prospective trial," Ann Oncol, 15(7), pp. 1042-1047.
[88] National Cancer Institute, 2012, "Lomustine," http://www.cancer.gov/cancertopics/druginfo/lomustine.

[89] Roy, P. G., P.; Nayek, A.; Samanta, A., 2012, "Preparation of Gefitinib Loaded Polycaprolactone Microcapsule for Controlled Release Drug Delivery System," International Journal of Pharmacology and Pharmaceutical Technology, 1(2), pp. 57-61.
[90] Kaur, J., and Tikoo, K., 2013, "p300/CBP dependent hyperacetylation of histone potentiates anticancer activity of gefitinib nanoparticles," Biochimica Et Biophysica Acta-Molecular Cell Research, 1833(5), pp. 1028-1040.
[91] Li, F. H., B.; Liu, Y.; Leonard, B.; Griffith, M, 2012, "Controlled Release of Bevacizumab Through Nanospheres for Extended Treatment of Age-Related Macular Degeneration," The Open Ophthalmology Journal, 6, pp. 64-58.
[92] Pan, C. K., Durairaj, C., Kompella, U. B., Agwu, O., Oliver, S. C. N., Quiroz-Mercado, H., Mandava, N., and Olson, J. L., 2011, "Comparison of Long-Acting Bevacizumab Formulations in the Treatment of Choroidal Neovascularization in a Rat Model," Journal of Ocular Pharmacology and Therapeutics, 27(3), pp. 219-224.
[93] Abrishami, M., Ganavati, S. Z., Soroush, D., Rouhbakhsh, M., Jaafari, M. R., and Malaekeh-Nikouei, B., 2009, "Preparation, Characterization, and in Vivo Evaluation of Nanoliposomes-Encapsulated Bevacizumab (Avastin) for Intravitreal Administration," Retina-the Journal of Retinal and Vitreous Diseases, 29(5), pp. 699-703.
[94] Benita, S., Benoit, J. P., Puisieux, F., and Thies, C., 1984, "Characterization of Drug-Loaded Poly(D,L-Lactide) Microspheres," Journal of Pharmaceutical Sciences, 73(12), pp. 1721-1724.
[95] Davis, S. S., 1984, Microspheres and drug therapy : pharmaceutical, immunological, and medical aspects, Elsevier ;
Sole distributors for the USA and Canada, Elsevier Science Pub. Co., Amsterdam ; New York New York, NY, USA.
[96] Trzebicka, B., Robak, B., Trzcinska, R., Szweda, D., Suder, P., Silberring, J., and Dworak, A., 2013, "Thermosensitive PNIPAM-peptide conjugate - Synthesis and aggregation," European Polymer Journal, 49(2), pp. 499-509.
[97] Plamper, F. A., Steinschulte, A. A., Hofmann, C. H., Drude, N., Mergel, O., Herbert, C., Erberich, M., Schulte, B., Winter, R., and Richtering, W., 2012, "Toward Copolymers with Ideal Thermosensitivity: Solution Properties of Linear, Well-Defined Polymers of N-Isopropyl Acrylamide and N,N-Diethyl Acrylamide," Macromolecules, 45(19), pp. 8021-8026.
[98] Siegwart, D. J., Bencherif, S. A., Srinivasan, A., Hollinger, J. O., and Matyjaszewski, K., 2008, "Synthesis, characterization, and in vitro cell culture viability of degradable poly(N-isopropylacrylamide-co-5,6-benzo-2-methylene-1,3-dioxepane)-based polymers and crosslinked gels," Journal of Biomedical Materials Research Part A, 87A(2), pp. 345-358.
[99] Galperin, A., Long, T. J., Garty, S., and Ratner, B. D., 2013, "Synthesis and fabrication of a degradable poly(N-isopropyl acrylamide) scaffold for tissue engineering applications," Journal of Biomedical Materials Research Part A, 101A(3), pp. 775-786.
[100] Berkland, C., King, M., Cox, A., Kim, K., and Pack, D. W., 2002, "Precise control of PLG microsphere size provides enhanced control of drug release rate," Journal of Controlled Release, 82(1), pp. 137-147.
[101] Berkland, C., Kipper, M. J., Narasimhan, B., Kim, K. K., and Pack, D. W., 2004, "Microsphere size, precipitation kinetics and drug distribution control drug release from biodegradable polyanhydride microspheres," Journal of Controlled Release, 94(1), pp. 129-141.

[102] Wu, J., Kong, T., Yeung, K. W., Shum, H. C., Cheung, K. M., Wang, L., and To, M. K., "Fabrication and characterization of monodisperse PLGA-alginate core-shell microspheres with monodisperse size and homogeneous shells for controlled drug release," Acta Biomater.
[103] Mark, J. E., 1996, Physical properties of polymers handbook, AIP Press, Woodbury, N.Y.
[104] Middleton, J. C., and Tipton, A. J., 2000, "Synthetic biodegradable polymers as orthopedic devices," Biomaterials, 21(23), pp. 2335-2346.
[105] Huatan, H., Collett, J. H., and Attwood, D., 1995, "The microencapsulation of protein using a novel ternary blend based on poly(epsilon-caprolactone)," J Microencapsul, 12(5), pp. 557-567.
[106] Kim, B. K., Hwang, S. J., Park, J. B., and Park, H. J., 2005, "Characteristics of felodipine-located poly(epsilon-caprolactone) microspheres," J Microencapsul, 22(2), pp. 193-203.
[107] Youan, B. B., Benoit, M. A., Baras, B., and Gillard, J., 1999, "Protein-loaded poly(epsilon-caprolactone) microparticles. I. Optimization of the preparation by (water-in-oil)-in water emulsion solvent evaporation," J Microencapsul, 16(5), pp. 587-599.
[108] Auras, R. A., Lim, L. T., Selke, S. E. M., and Tsuji, H., Poly(lactic acid): Synthesis, Structures, Properties, Processing, and Applications, Wiley.
[109] 2007, "Gefitinib," I. Santa Cruz Biotechnology, ed.Santa Cruz.
[110] Romio, A. P., Sayer, C., Araujo, P. H. H., Al-Haydari, M., Wu, L. B., and da Rocha, S. R. P., 2009, "Nanocapsules by Miniemulsion Polymerization with Biodegradable Surfactant and Hydrophobe," Macromolecular Chemistry and Physics, 210(9), pp. 747-751.
[111] Hu, H. R., Wang, H. T., and Du, Q. G., 2012, "Preparation of pH-sensitive polyacrylic acid hollow microspheres and their release properties," Soft Matter, 8(25), pp. 6816-6822.
[112] Leimann, F. V., Cardozo, L., Sayer, C., and Araujo, P. H. H., 2013, " Poly(3-hydroxybutyrate-co-3- hydroxyvalerate) nanoparticles prepared by a miniemulsion/solvent evaporation technique. Effect of phbv molar mass and concentration," Brazilian Journal of Chemical Engineering, 30(2), pp. 369-377.
[113] Luo, Y. W., and Zhou, X. D., 2004, "Nanoencapsulation of a hydrophobic compound by a miniemulsion polymerization process," Journal of Polymer Science Part a-Polymer Chemistry, 42(9), pp. 2145-2154.
[114] Canavan, H. E., Cheng, X. H., Graham, D. J., Ratner, B. D., and Castner, D. G., 2006, "A plasma-deposited surface for cell sheet engineering: Advantages over mechanical dissociation of cells," Plasma Processes and Polymers, 3(6-7), pp. 516-523.
[115] Tunc, M., Cheng, X. H., Ratner, B. D., Meng, E., and Humayun, M., 2007, "Reversible thermosensitive glue for retinal implants," Retina-the Journal of Retinal and Vitreous Diseases, 27(7), pp. 938-942.
[116] Guan, Y., and Zhang, Y. J., 2011, "PNIPAM microgels for biomedical applications: from dispersed particles to 3D assemblies," Soft Matter, 7(14), pp. 6375-6384.
[117] Ayano, E., Karaki, M., Ishihara, T., Kanazawa, H., and Okano, T., "Poly (N-isopropylacrylamide)-PLA and PLA blend nanoparticles for temperature-controllable drug release and intracellular uptake," Colloids Surf B Biointerfaces, 99, pp. 67-73.
[118] Soppimath, K. S., Aminabhavi, T. M., Dave, A. M., Kumbar, S. G., and Rudzinski, W. E., 2002, "Stimulus-responsive "smart" hydrogels as novel drug delivery systems," Drug Development and Industrial Pharmacy, 28(8), pp. 957-974.
[119] Bikram, M., and West, J. L., 2008, "Thermo-responsive systems for controlled drug delivery," Expert Opinion on Drug Delivery, 5(10), pp. 1077-1091.

[120] "Buffer Reference Center," http://www.sigmaaldrich.com/life-science/core-bioreagents/biological-buffers/learning-center/buffer-reference-center.html.
[121] Reddy, C. N., Prasad, P., Sreedhar, N.Y., 2011, "Voltammetric Behavior of Gefitinib and its Adsorptive Stripping Voltammetric Determination in Pharmaceutical Formulations and Urine Samples," International Journal of Pharmacy and Pharmaceutical Sciences, 3(3), pp. 141-145.
[122] Woodruff, M. A., and Hutmacher, D. W., 2010, "The return of a forgotten polymer-Polycaprolactone in the 21st century," Progress in Polymer Science, 35(10), pp. 1217-1256.
[123] Lam, C. X. F., Savalani, M. M., Teoh, S. H., and Hutmacher, D. W., 2008, "Dynamics of in vitro polymer degradation of polycaprolactone-based scaffolds: accelerated versus simulated physiological conditions," Biomedical Materials, 3(3).
[124] Htay, A. S., Teoh, S. H., and Hutmacher, D. W., 2004, "Development of perforated microthin poly(epsilon-caprolactone) films as matrices for membrane tissue engineering," Journal of Biomaterials Science-Polymer Edition, 15(5), pp. 683-700.
[125] Kumar, N., 2011, Handbook of Neurological Examination, Prentice-Hall of India, New Delhility.
[126] Domb, A. J., and Jain, J. P., Biodegradable Polymers in Clinical Use and Clinical Development, Wiley, Hoboken, NJ.
[127] Plata Bedmar, A., and Araguás Araguás, L., 2002, Detection and prevention of leaks from dams, A.A. Balkema, Lisse ; Exton, PA.
[128] Alexis, F., 2005, "Factors affecting the degradation and drug-release mechanism of poly(lactic acid) and poly[(lactic acid)-co-(glycolic acid)]," Polymer International, 54(1), pp. 36-46.
[129] Belbella, A., Vauthier, C., Fessi, H., Devissaguet, J. P., and Puisieux, F., 1996, "In vitro degradation of nanospheres from poly(D,L-lactides) of different molecular weights and polydispersities," International Journal of Pharmaceutics, 129(1-2), pp. 95-102.
[130] de Jong, S. J., Arias, E. R., Rijkers, D. T. S., van Nostrum, C. F., Kettenes-van den Bosch, J. J., and Hennink, W. E., 2001, "New insights into the hydrolytic degradation of poly(lactic acid): participation of the alcohol terminus," Polymer, 42(7), pp. 2795-2802.
[131] Sirard, T., 2012, "Fundamentals of HPLC," Waters Corporation.
[132] Na, D. H., Murty, S. B., Lee, K. C., Thanoo, B. C., and DeLuca, P. P., 2003, "Preparation and stability of poly(ethylene glycol) (PEG)ylated octreotide for application to microsphere delivery," AAPS PharmSciTech, 4(4), p. E72.
[133] Clauss, M. A., and Jain, R. K., 1990, "Interstitial Transport of Rabbit and Sheep Antibodies in Normal and Neoplas Tic Tissues," Cancer Research, 50(12), pp. 3487-3492.
[134] Calmettes, P., Cser, L., and Rajnavolgyi, E., 1991, "Temperature and Ph-Dependence of Immunoglobulin-G Conformation," Archives of Biochemistry and Biophysics, 291(2), pp. 277-283.
[135] Seidegard, J., Gronquist, L., Tuvesson, H., and Gunnarsson, P. O., 2009, "Increased degradation rate of nitrososureas in media containing carbonate," In Vitro Cellular & Developmental Biology-Animal, 45(1-2), pp. 32-34.
[136] Roullin, V. G., Mege, M., Lemaire, L., Cueyssac, J. P., Venier-Julienne, M. C., Menei, P., Gamelin, E., and Benoit, J. P., 2004, "Influence of 5-fluorouracil-loaded microsphere formulation on efficient rat glioma radiosensitization," Pharmaceutical Research, 21(9), pp. 1558-1563.
[137] La Monica, S., Galetti, M., Alfieri, R. R., Cavazzoni, A., Ardizzoni, A., Tiseo, M., Capelletti, M., Goldoni, M., Tagliaferri, S., Mutti, A., Fumarola, C., Bonelli, M., Generali, D.,

and Petronini, P. G., 2009, "Everolimus restores gefitinib sensitivity in resistant non-small cell lung cancer cell lines," Biochem Pharmacol, 78(5), pp. 460-468.
[138] Mukohara, T., Engelman, J. A., Hanna, N. H., Yeap, B. Y., Kobayashi, S., Lindeman, N., Halmos, B., Pearlberg, J., Tsuchihashi, Z., Cantley, L. C., Tenen, D. G., Johnson, B. E., and Janne, P. A., 2005, "Differential effects of gefitinib and cetuximab on non-small-cell lung cancers bearing epidermal growth factor receptor mutations," J Natl Cancer Inst, 97(16), pp. 1185-1194.
[139] Grobben, B., De Deyn, P. P., and Slegers, H., 2002, "Rat C6 glioma as experimental model system for the study of glioblastoma growth and invasion," Cell and Tissue Research, 310(3), pp. 257-270.
[140] Wakeling, A. E., Guy, S. P., Woodburn, J. R., Ashton, S. E., Curry, B. J., Barker, A. J., and Gibson, K. H., 2002, "ZD1839 (Iressa): An orally active inhibitor of epidermal growth factor signaling with potential for cancer therapy," Cancer Research, 62(20), pp. 5749-5754.
[141] Koizumi, F., Shimoyama, T., Taguchi, F., Saijo, N., and Nishio, K., 2005, "Establishment of a human non-small cell lung cancer cell line resistant to gefitinib," International Journal of Cancer, 116(1), pp. 36-44.
[142] Watanabe, M., Yamada, Y., Kato, H., Imai, H., Nakano, H., Araki, T., and Shiraishi, T., 2002, "Malignant phyllodes tumor of the prostate: Retrospective review of specimens obtained by sequential transurethral resection," Pathology International, 52(12), pp. 777-783.
[143] Fleming, A. B., and Saltzman, W. M., 2002, "Pharmacokinetics of the carmustine implant," Clinical Pharmacokinetics, 41(6), pp. 403-419.
[144] Fung, L. K., Shin, M., Tyler, B., Brem, H., and Saltzman, W. M., 1996, "Chemotherapeutic drugs released from polymers: Distribution of 1,3-bis(2-chloroethyl)-1-nitrosourea in the rat brain," Pharmaceutical Research, 13(5), pp. 671-682.